2010

Gamma ray burst redshift catalog and applications

Limin Xiao
Louisiana State University and Agricultural and Mechanical College, lxiao1@tigers.lsu.edu

GAMMA RAY BURST REDSHIFT CATALOG AND APPLICATIONS

A Dissertation

Submitted to the Graduate Faculty of the
Louisiana State University and
Agricultural and Mechanical College
in partial fulfillment of the
requirements for the degree of
Doctor of Philosophy

in

The Department of Physics and Astronomy

by
Limin Xiao
B.S., University of Science and Technology of China, 2005
August, 2010

For Mom and Dad

致我亲爱的爸爸妈妈！

Acknowledgments

I would like to thank my adviser Bradley Schaefer for his support, guidance, and infinite patience throughout this research and my time at LSU. I would also like to thank Robert Hynes, Joel Tohline, Juhan Frank, and Gabriela Gonzlez for their questions and discussions. In addition, thank you to astronomy faculty members Geoff Clayton, and Arlo Landolt. I would also like to thank Andrew Collazzi and Ashley Pagnotta for their useful suggestions and discussions of my research.

I would like to thank my colleagues, especially Changwei Huang, Wanli Xu, Yuan Zhang for their companionship and support throughout graduate school. I would also like to thank the professors and students in the Fermi GBM team for exposing me to new fields and different ways of looking at my research, in particular Rob Preece and Adam Goldstein.

I would like to thank the astrophysics professors at the University of Science and Technology of China who introduced me to astrophysics, especially my undergraduate advisor Fuzhen Cheng and graduate student Cheng Li for initiating my observational astrophysics research. Finally, I would like to thank my parents and my boyfriend Xiaojie Hao for all their support and encouragement as I have pursued my dreams.

This work has been supported by the NASA Earth and Space Science Fellowship.

Table of Contents

List of Tables

List of Figures

Abstract

The measurement of redshifts for gamma-ray bursts (GRBs) is an important issue for the study of the high redshift universe and cosmology. We developed a program to estimate the redshifts for GRBs from the original light curves and spectra, aiming to get redshifts for bursts without spectroscopic or photometric redshifts. We derive the luminosity indicators from the light curves and spectra of each burst, including the lag time between low and high photon energy light curves, the variability of the light curve, the peak energy of the spectrum, the number of peaks in the light curve, and the minimum rise time of the peaks. These luminosity indicators can each be related directly to the luminosity, and we combine their independent luminosities into one weighted average. Then with our combined luminosity value, the observed burst peak brightness, and the concordance redshift-distance relation, we can derive the redshift for each burst. We test the accuracy of our method on 107 bursts with known spectroscopic redshift, which shows that our error bars are good and our estimates are not biased. This method was then applied to all *Swift* long GRBs, and a complete *Swift* long GRB redshift catalog was constructed. Our redshift catalog and catalog of luminosity indicators has many applications in the demographic studies. An investigation of long lag GRBs was made to test the hypothesis that most long lag GRBs are from our local supercluster. An unbiased GRB luminosity function evolution was estimated, and the constraint on the massive star formation rate was made. We also imported the calculation code of luminosity indicators and redshift into the *Fermi* GBM data analysis software RMFIT, with which the all the luminosity indicators and the redshift can be calculated within half an hour after the raw data are generated from the pipeline.

1. Introduction

1.1 GRB History and Current Status

Gamma-Ray Bursts (GRBs) are brief flashes of gamma-radiation coming from random points on the sky. When a GRB flashes, it is the brightest source in the Gamma Ray sky. As the Gamma Ray radiation can be easily absorbed by the earth atmosphere, GRBs cannot be detected by the instruments on the ground. Until now, thousands of GRBs have been detected by Gamma Ray detectors in space. The current detection rate of GRBs are roughly two to three per week, with their times and directions being completely random and isotropic with no repetition. GRBs are not produced in any repeatable mechanism, and for each of the GRBs they happen only once, hence the explosion of GRBs are completely unpredictable. Their durations range from fractions of a second up to minutes, followed by a long-lived afterglow in longer wavelengths. The photon energy of their spectral peak (E_{peak}) ranges from tens of keV to well over a MeV, so they are truly bursts of gamma-rays. With the redshift of 0.008 to 8.2, we know that they are from billions of light years away from earth, and their are huge amount of energy involved in the forming of GRBs.

GRBs were originally discovered in the late 1960s with the Vela satellites. Vela satellites were a group of satellites developed by the United States to monitor compliance with the 1963 Partial Test Ban Treaty by the Soviet Union. The satellites were launched and operated in pairs with two identical satellites on opposite sides of a circular orbit so that it would be able to cover the whole sky. On board of the Vela satellites, there are X-ray, Gamma ray and neutron detectors as well as a variety of optical and EMP detectors. During the operation of Vela Satellites, events that triggered the detectors but were clearly not signatures of nuclear detonations were carefully filed away for the future studies. In 1969, an event recorded by

Vela 4a, b was discovered while looking over the Vela 4 data prior to the launch of Vela 5. This event was recorded on July 2, 1967, and it also triggered the Vela 3 satellites which were still operating. This event appeared to be a cosmic gamma ray burst, but the direction of the source was not able to be determined accurately due to the fair timing resolution at the trigger. It was believed as the first "Gamma-Ray Burst". With the later Vela satellites which have better timing resolution, the deduced direction of these gamma ray events rule out the sun and the earth as orbits. These gamma ray events were then published in (Klebesadel et al., 1973).

To explain the existing of these GRBs, many progenitor models were proposed, most of which were pointed to the sources within our Milky Way Galaxy. These models were not able to be tested without much observational features obtained from the GRBs. In 1991, with the launch of the Compton Gamma Ray Observatory and its on board instrument Burst and Transient Source Experiment (BATSE), thousands of GRBs were detected, with their position resolution to a few degree level. The distribution of these GRB positions on the sky, as shown in Figure 1.1, shows no tendency towards either the plane or the center of the Galaxy. It is completely isotropic, without any bias towards any particular direction in the space. This discovery was a strong evidence towards GRBs being cosmological distance sources, and excludes most Milky Way models, however, some of the Milky Way models, which are constrained to an extremely close distance, were still consistent with this distribution.

On April 22, 1995, a "Great Debate" was held by Robert Nemiroff at the Smithsonians Natural History Museum, with the topic on the distance scale to Gamma-Ray Bursts. The debate was between Bohdan Paczynski and Donald Q. Lamb. Paczynski started from the distribution of BATSE, and listed the sky distribution of possible progenitor mechanisms at different distances, e.g. inner solar system, planetary and galactic halo objects, sources from nearby galaxies, and extragalactic radio sources. With none of these distributions accounts for the BATSE result, he concluded that the only two possible distance left are

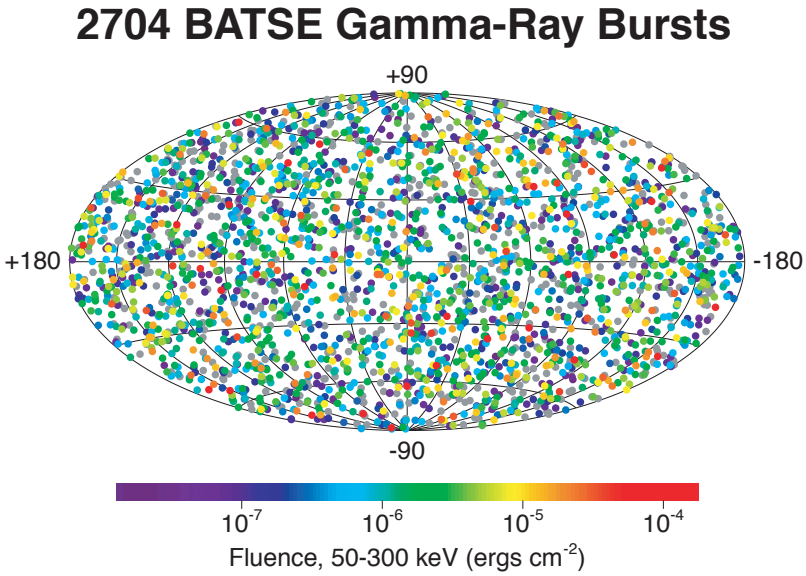

Figure 1.1 Sky distribution of 2704 BATSE GRBs. The distribution is isotropic, without bias towards any particular region of the sky.

within 100 parsec or above 1 Gigaparsec. In this case the cosmological distance was strongly favored, but was not proven. In Lamb's opinion, GRBs are originate from the high velocity neutron stars in the galactic corona. Actually, the magnetic neutron stars model was the most preferred one before BATSE era, with a strong evidence of Cyclotron lines detected in the GRB spectrum. Similar line has been seen in the spectra of accretion-powered pulsars, which are known to be magnetic neutron stars. Magnetic neutron stars in the Galactic corona appear able to produce cyclotron lines, , while these lines is a difficult problem for cosmological models. Besides the Cyclotron lines, Lamb pointed out several other arguments supporting the high-velocity neutron star model, e.g. a distribution plot from 1005 bursts from a Galactic corona of high velocity neutron stars in comparison of BATSE GRB sky distribution, evidence that high velocity neutron stars can produce burst-like behavior: soft gamma-ray repeaters, evidence that high-velocity neutron stars produce an event like GRBs: 1979 March 5 gamma-ray transient, the lack of bright optical counterparts, etc. One weak point for the high-velocity neutron star model is that repeating is naturally expected to

account for the number of GRBs detected every year, which is not seen in the BATSE result. And a disadvantage on cosmological distance models is the huge amount of energy ejected during the burst.

With both the high-velocity neutron star model and the cosmological distance star idea have strong evidence as well as inevitable troubles, the progenitor model problem has not been solved after the debate. This situation continues until 1997, when the first X-ray and optical afterglow detected for a Gamma-Ray Burst (GRB970228, detected by BeppoSAX, an ItalianDutch satellite for X-ray astronomy). After the GRB optical afterglow faded, a distant host galaxy was revealed from the deep imaging of the William Herschel Telescope. A few months later, another GRB detected by BeppoSAX, GRB970508, was localized within hours of the triggered and observed in X-ray, optical and radio wavelength (Costa et al., 1997; van Paradijs et al., 1997; Frail et al., 1997). The spectrum of the afterglow revealed a redshift of $z = 0.835$, which means the GRB is at a distance of about 6 billion light years from the Earth. Both of these evidences proved that GRBs are from a cosmological distance, and the controversy about the GRB distance ended.

Although GRBs were successfully placed at the cosmological distance, the huge amount of energy released from a GRB within seconds to minutes is still a mystery to us. Combining the brightness and the distance of a GRB, an extremely energetic source is needed. Assuming the gamma-ray explosion is spherical, the total energy ejected from a GRB would be on the order of the total rest mass energy of the Sun, which is the energy released if we convert the Sun entirely into radiation. No known process is able to produce this amount of energy during such a short time scale. One alternative model was proposed, suggesting that GRBs are highly focused explosions which are produced in an extra high relativistic jet which travels near the speed of light. With this model, the total energy required in a GRB explosion is released by a factor of a few hundred. With a jet break time detected in the optical afterglow

of several GRBs hours to days after the trigger, this relativistic jet model was confirmed (Sari et al., 1999).

Various dedicated instruments and spacecraft have been flown by NASA. In November 2004, NASA launched a dedicated GRB satellite named *Swift*. It has three instruments onboard: Burst Alert Telescope (BAT), X-ray Telescope (XRT) and UV/Optical Telescope (UVOT), which allows *Swift* to observe a GRB and its afterglows in gamma-ray, X-ray, ultraviolet, and optical wavebands together. BAT is a wide-field gamma-ray detector that detects and positions the burst within seconds, and then slew the entire spacecraft so that the narrow-field X-ray and UV/optical telescopes are imaging the burst within about one minute. Ground-based telescopes are also notified within seconds of the beginning of the burst and slew to start their own detailed observations. As such, *Swift* has allowed the burst community to get impressively complete 'panchromatic' light curves and spectra from the start of the burst until the end of the afterglow. During its first five years of operation, *Swift* has triggered more than 500 GRBs. The distribution of the 500 GRBs also shows an isotropic feature, which is not surprising. It will keep working for the foreseeable future.

Fermi, formerly known as GLAST (Gamma-Ray Large Area Space Telescope), was launched June 11th, 2008. It is another NASA major mission for observations of high energy gamma rays. Its main instrument, the Large Area Telescope (LAT), will provide unprecedented sensitivity to gamma rays in the energy range of $\sim$ 20 MeV to $\sim$ 300 GeV. The GLAST Burst Monitor (GBM) complements the LAT in its observations of transient sources and is sensitive to X-rays and gamma rays with energies between 8 keV and 25 MeV. The combination of the GBM and the LAT provides a powerful tool for studying gamma-ray bursts, particularly for time-resolved spectral studies over a very large energy band. The detection rate of *Fermi* GBM is around $2 - 3$ per week, and during the first two years of operation, about 200 GRBs have been triggered by GBM. The detection rate of LAT is

relatively fewer. All *Swift* and *Fermi* data are open to public, and can be downloaded from the legacy ftp site [1].

For a long time in the past, there was a huge debate about whether these GRBs are located in our galaxy or at cosmological distance. In 1997, the first X-ray, optical, and radio counterparts of bursts was detected , and the redshifts of these bursts were measured. With the launch of *Swift* in late 2004, the accurate positions of GRBs can be measured and then distributed to the community quickly through the Gamma-ray bursts Coordinates Network (GCN) Circulars, and more optical and infrared follow-ups can be performed. Currently, more than 100 GRBs have been reported with spectroscopic redshifts ranging from 0.008 (GRB980425) to 8.2 (GRB090423). With the spectroscopic/photometric redshift measured, the energy from the GRBs is then calculated to be typically within the range $10^{49} - 10^{53}$ergs.

The redshift distribution of long GRBs with redshifts from optical spectroscopy (z_{spec}) has a 90% range of $0.5 < z < 5$. Before *Swift* the typical redshift was $z \sim 1$, while *Swift* is more sensitive and 'sees' further with an average of $z \sim 2.3$. These averages are based on only the minority of bursts with spectroscopic redshfits. For *Swift*, only $\sim 30\%$ of its GRBs have been reported with spectroscopic or photometric redshifts. Various strong selection effects work to distort the observed distribution from the real underlying distribution. For example, redshifts from host galaxies are only likely for $z \lesssim 2$ as more distant galaxies are too faint for discovery or spectroscopic measures. Also, GRBs with $z > 7$ are strongly selected against as they will be invisible in the optical band due to the Lyman break being redshifted to the far red. In principle, *Swift* can detect GRBs out to $z \sim 20$ should there be any bursts out there. The real upper limit on z is the epoch of the first star formation, as bursts come from massive stars within a few million years after their birth, and this is apparently somewhere around $z \sim 10$. Detailed calculations of star formation models says that $\sim 10\%$ of *Swift* bursts should have $z > 5$, and $5\% - 10\%$ have $z > 7$ (Bromm & Loeb , 2006).

[1] ftp://legacy.gsfc.nasa.gov

So we expect $> 5\%$ of *Swift* bursts to be at $z > 7$, which is a very exciting prospect. These GRBs will then become the farthest objects ever seen. As such, their light carries great amounts of information about the earliest Universe. The information comes from the bursts themselves, such as their numbers (giving the star formation rate) and their maximum redshift (giving the epoch of the first star formation), from absorptions in the optical light from the afterglows as they are absorbed by intervening gas clouds (giving the ionization state of the Universe from the Gunn-Peterson troughs) as well as the metallicity from the absorption lines, from sub-arc-second positions of the afterglows (giving a confident place to discover $z > 7$ galaxies), and also from the brightness of the bursts (giving the Hubble diagram as dependent on the nature of the Dark Energy). Modern cosmology has flourished in the past decade, but, as always, deep and important questions remain. Here are the highlights of many of the primary questions now confronting cosmologists: What is the nature of the Dark Energy? When did the first stars form? When was the Universe re-ionized? What are the first galaxies like? How does the star formation history of our Universe change with redshift? When were the heavy elements sprayed back into the gases of the Universe? GRBs can provide a tool to answer all of these fundamental and front-line questions. But for this strong promise to be realized, we need to know the redshifts of these GRBs.

1.2 GRB Observation

1.2.1 GRB Prompt Emission

By plotting the fluence as a function of energy, we will be able to obtain the fluence of a GRB. The peak of the spectrum shows us a typical photon energy value in the GRB explosion. Most of the photons from the prompt emission of GRBs fall in the energy range of a few keV to MeV, and most of the spectrum of the prompt emission is a broken power law, which consists of a shallow power law (with an index of ~ 1) at low energies and a sharp power

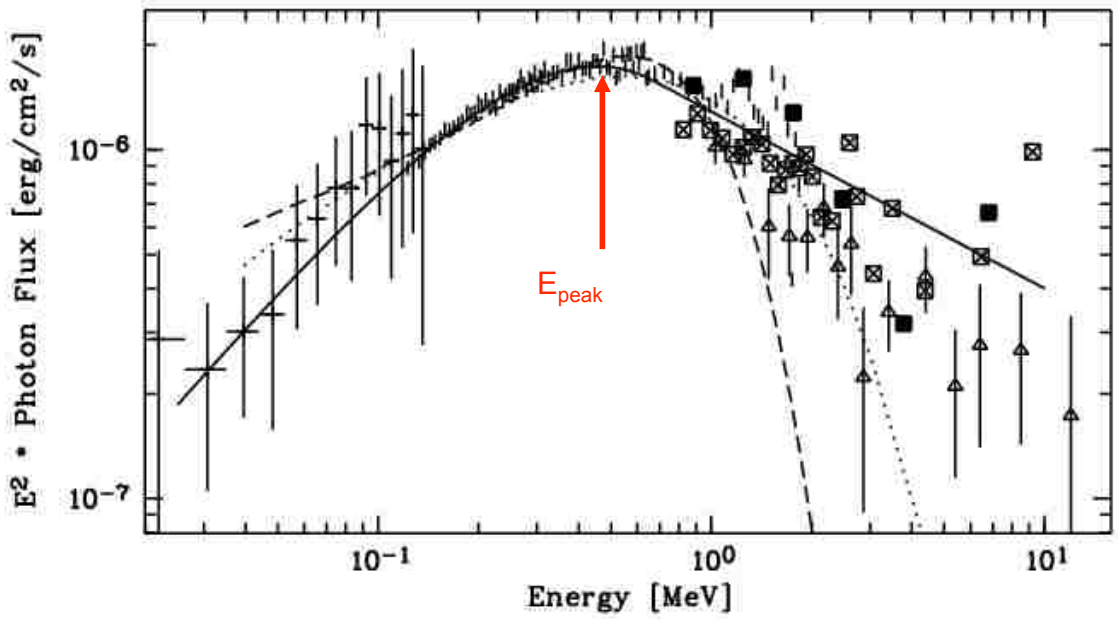

Figure 1.2 GRB spectrum and E_{peak}

law (with an index of ~ 2) at high energies. Various models have been proposed to fit GRB spectra, including a simple power law model, broken power law, broken power law with two breaks, smoothly broken power law, comptonized power law model, etc. The most commonly used spectral model is the one proposed by Band et al. (1993), with which a peak photon energy E_{peak}, a low energy power law index α and a high energy power law index β are used as the parameters. The spectrum and E_{peak} is shown in Figure 1.2.

If we plot out the photon flux as a function of time during the burst, we will be able to obtain the light curve of the GRB. Figure 1.3 shows a few examples of GRB light curves. A few parameters are used to characterize the light curve of a GRB, e.g. rise time of a pulse, decay time of a pulse, pulse width, time duration of the whole light curve, etc. The light curves of the detected GRBs are very chaotic, with a duration ranging from milliseconds up to tens of minutes. A lot of work has been done in the past to study the shape of GRB light curves and to classify GRBs with their shapes, but all failed. Conventionally, the duration of a GRB is measured by T_{90}, which is defined as the time interval over which the middle 90%

of the total background-subtracted counts are observed. The T_{90} distribution of GRBs in log space shows a bimodel distribution feature, with a minimum at around 2 s, and two peaks at around 0.3 s and 30 s. As a result, our detected GRBs are divided into two distinct goups: bursts with $T_{90} > 2$s are classified as long GRBs and those with $T_{90} < 2$s as short GRBs. Normally, short GRBs have a larger hardness ratio (measured by the hard (50-100 keV) to soft (25-50 keV) fluence ratio) than long GRBs, so the two types are also called "long soft bursts" and "short hard bursts". Another parameter which is always used to distinguish different type of GRBs are called 'hardness ratio', which is calculated as the fluence ratio between the hard and soft light curves. The hardness ratio of short GRBs are generally larger than those of long GRBs, which means that short GRBs are generally 'harder' than the long GRBs. As a result, these two classes are also notified as short hard GRBs and long soft GRBs.

Both the T_{90} and hardness ratio were measured in the observer rest frame. Due to the redshifts of GRBs, their time duration have been dilated, with different GRBs at different redshifts having different time dilation effect. In the BATSE era, only a few GRBs have their redshifts measured, so the time dilation effect cannot be excluded. With the launch of *Swift*, a large fraction of GRB redshift was measured from the spectral analysis of the afterglow, and we will be able to make the correction on the T_{90}, and obtain a GRB rest frame time duration histogram. The histogram is shown in Figure 1.4. The distribution also shows a bimodal function of T_{90}, with a minimum at 0.56 second and two peaks at ~ 0.2 second and $30 - 40$ second. The bimodal function is not as significant as that in the BATSE T_{90} distribution plot, because *Swift* has a lower short GRB detection rate, and the short GRBs has a lower rate of spectroscopic redshift measured, as compared with the long GRBs.

Recently, a third group has been observed (Norris & Bonnell, 2006), which has a short hard spike followed by long soft extended emissions. If the short spike and the long extended emission are plotted separately on the hardness ratio versus T_{90} plot, it will obviously showing

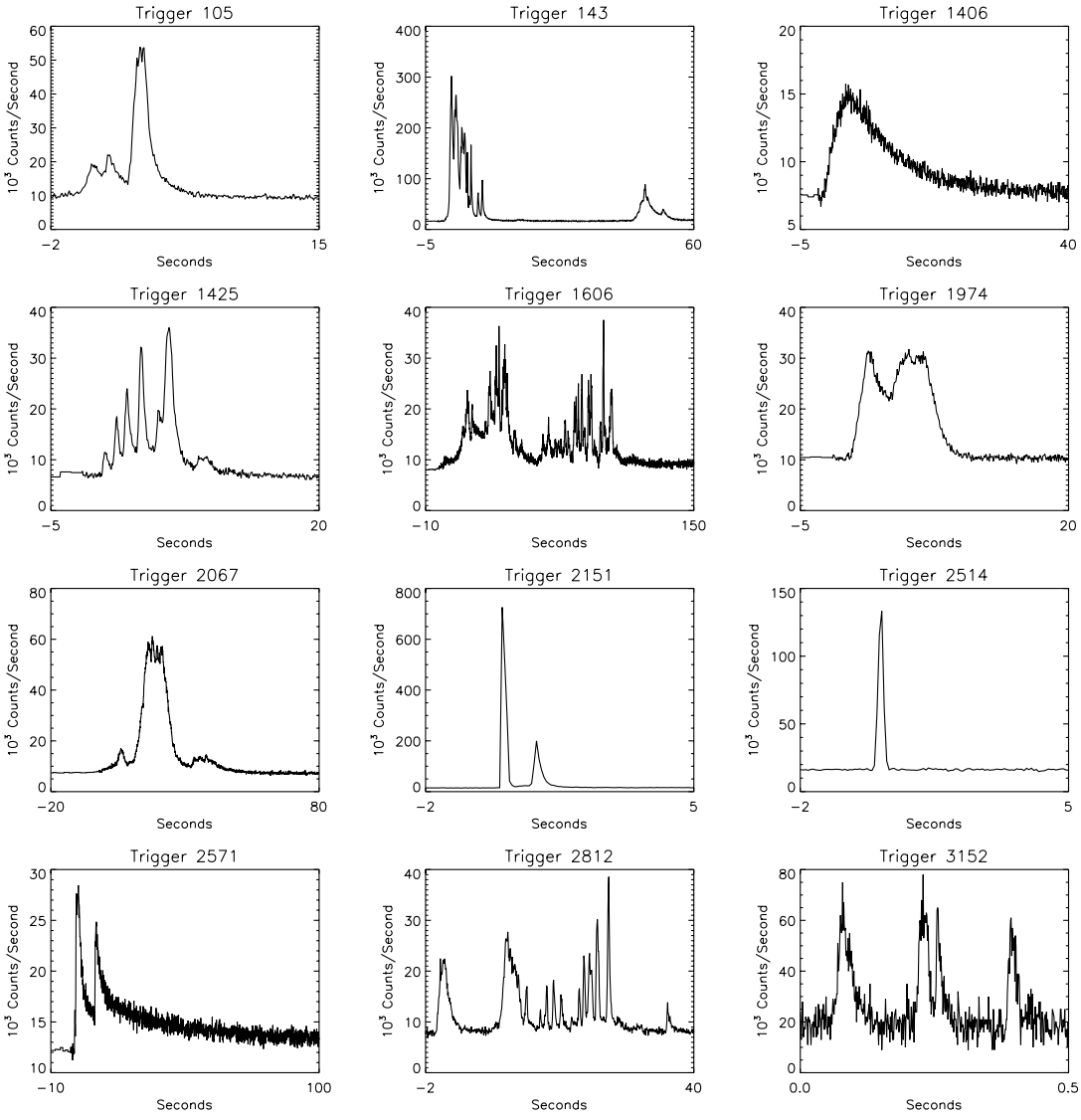

Figure 1.3 A few examples of GRB light curves. Credit: J.P. Norris (NASA/GSFC)

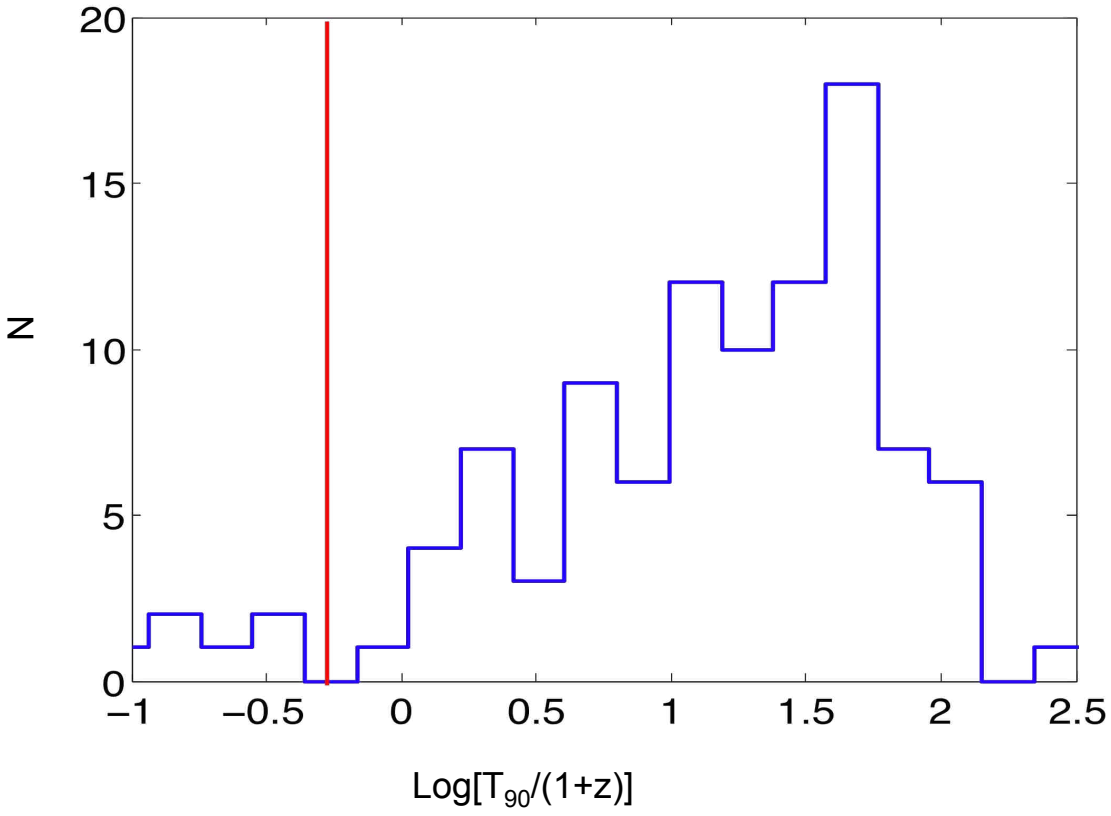

Figure 1.4 Distribution of T_{90} in GRB rest frame for *Swift* GRBs with spectroscopic redshift measured. A bimodal feature is shown in this plot, with a minimum at 0.56 second, and two peaks at ~ 0.2 second and $30 - 40$ second.

that the short spike falls into the short hard region, while the extended tail falls into the long soft region.

In the *BATSE* sample, short hard bursts constitute $\sim 30\%$ of the total, and this number have been decreased to $\sim 10\%$ in the *Swift* sample. Short bursts tend to have prompt burst energy much smaller than that of long bursts, which restricts us from detecting short hard bursts at high redshift, and it might be the most important reason why they have been found at lower redshift than typical long bursts. With the discovery of counterparts of the bursts recently, there is no evidence showing short hard bursts in active star formation regions.

1.2.2 GRB Follow-up Observations

The first X-ray, optical and radio band afterglow of GRBs were made in 1997 (Costa et al., 1997; van Paradijs et al., 1997; Frail et al., 1997). After the launch of *Swift*, the on-board XRT is able to make the X-ray afterglow detection just a few seconds after the trigger. A large sample of GRB X-ray afterglow has been made. A typical X-ray afterglow assumes the form of a power-law with three break points. The power law decay would then be separated to four different power-law segments. These three break points appear between $10^2 - 10^4$ seconds. Various flares are superposed on these power-law decays, which makes different segments difficult to be distinguished. A typical GRB X-ray afterglow is shown in Figure 1.5.

Another on-board instrument of the *Swift* satellite is UVOT, which is used to make follow-up observations in UV and optical band. The response time for UVOT is also less than 100 seconds, which allows it to detect the optical afterglow before it faded too faint. Besides UVOT, a lot of groups around the world are using their ground telescopes to make the follow-up observations. A large sample of optical afterglow light curve has been made from the observations of different groups, and a large fraction of the GRBs have their redshifts measured from the spectral analysis of the afterglow or the GRB host galaxies (Xiao &

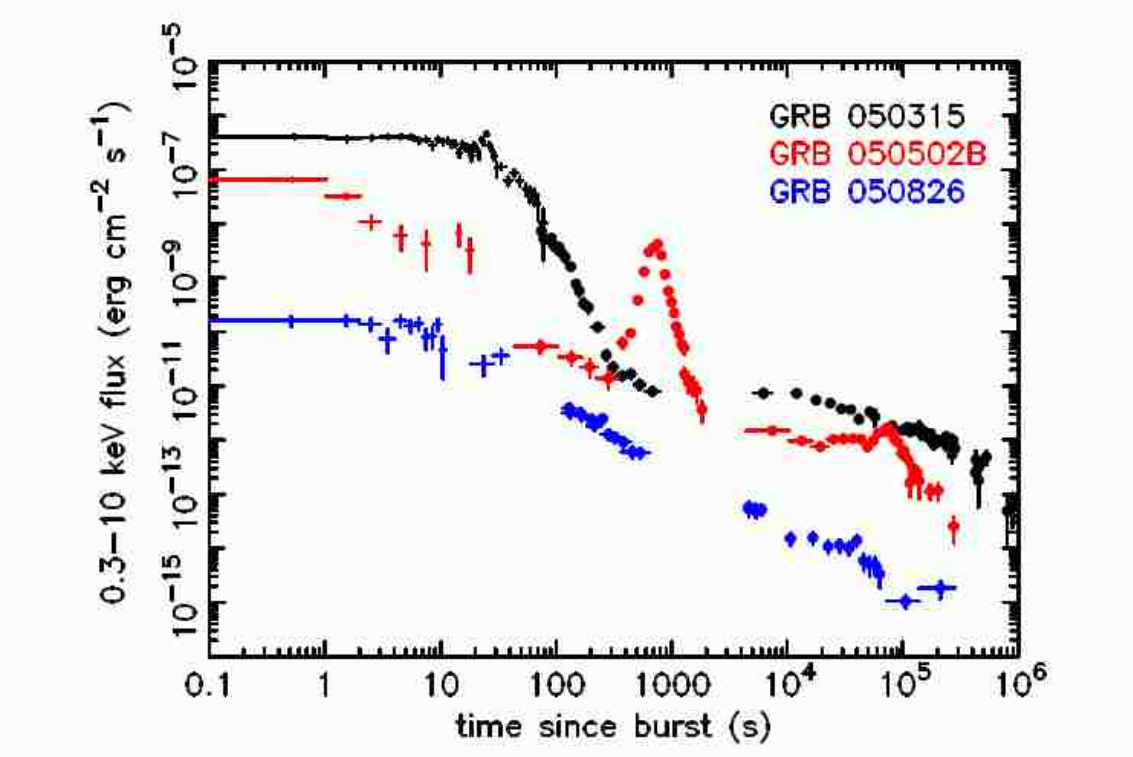

Figure 1.5 X ray afterglow of GRB, from which we can specify different power law segments, break points between these segments and flares superposed on them. Credit: O'Brien et al. (2006)

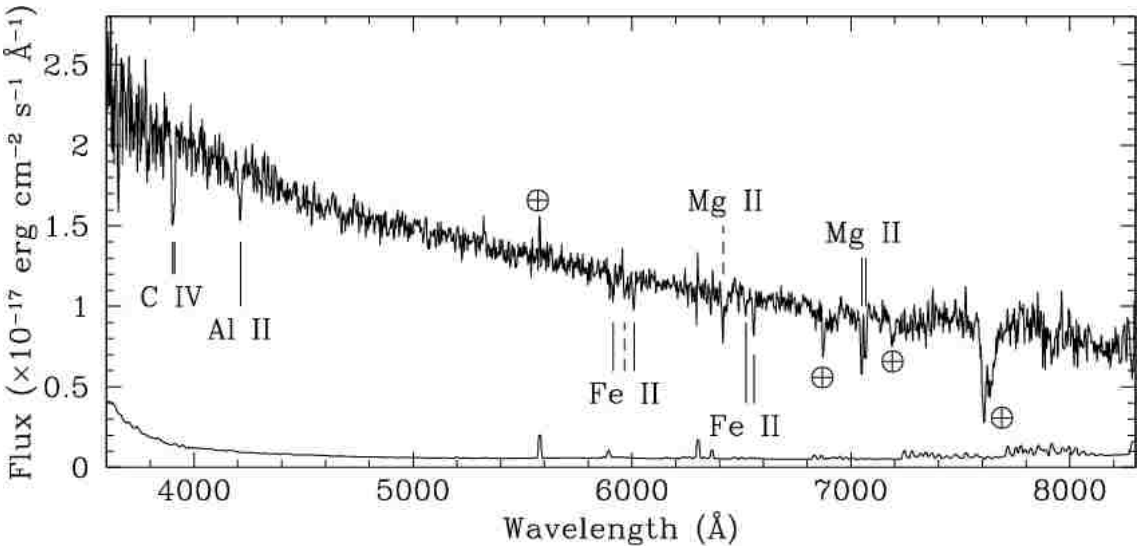

Figure 1.6 Optical afterglow spectrum of a GRB.

Schaefer, 2010). The spectrum of optical afterglow of a GRB is also a power-law as it is produced. However, after traveling through layers of gas and dusts, the fluence of the power law spectrum is mostly absorbed by the nearby star-forming region, and interstellar medium filled with gas and metals will imprint their spectral features on the spectrum, which is used for the redshift measurements. A typical spectrum of GRB optical afterglow in shown in Figure 1.6. Another feature in the optical afterglow is the jet break shown in the light curve. By having a significant break in the afterglow light curve hours to days after the trigger time, it is confirmed that GRBs are not formed from a isotropic explosion, but from a relativistic jet with a Lorentz factor of $\sim 100 - 1000$. It also helped constrain the total energy emitted from the GRB explosion to be within $\sim 10^{53}$ ergs. Figure 1.7 shows an example of a GRB optical afterglow light curve, from which we can clearly specify two segment of power law decay and a significant jet break. The detection of jet break time is not only a strong evidence to confirm the relativistic jet model of a GRB as we stated, and the jet break time is also of important use in the GRB luminosity relations, which we will talk in details in the next section.

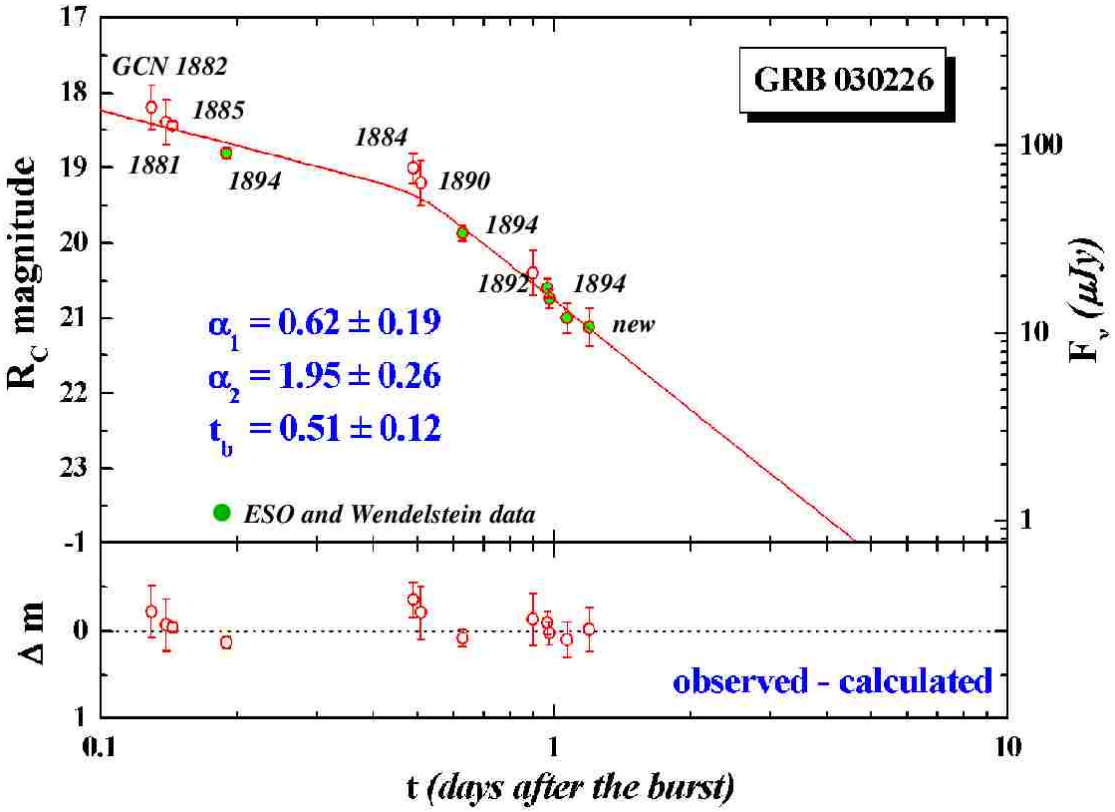

Figure 1.7 Optical afterglow light curve of a GRB, from which we can specify two segment of power law decay, and a significant jet break.

1.3 GRB Theory

Long GRBs are found in star-forming regions, suggesting that they might be related to the death of massive stars, and to the explosion of supernovae (SNe). There is some direct evidence connecting long GRBs and SNe (Type Ic), including the observed pairs of GRB980425 and SN98bw, GRB030329 and SN2003dh, and late red bumps in the light curves of several GRBs (Galama et al., 1998; Stanek et al., 2003; Price et al., 2003). It is believed that GRBs are generated from core collapse Supernovae. However, the rate of GRBs is one per 3×10^5 yr per galaxy (Podsiadlowski et al., 2004), which is $\sim 1/3000$ the rate of SNe, so only a small fraction of supernovae have the conditions required to produce a burst of gamma rays. The reason for this is that to produce a GRB, one do not only need a core collapse supernovae, it is also required to deliver a focused jet with large amount of energy far away from the progenitor star. The jet must escape the host star without losing much of its energy. The time period for the escape is a few to tens of seconds for the jet, and if the jet is interrupted or change its orientation significantly during this time, it will degrades to subrelativistic energies and the producing of GRBs will fail.

The association of long GRBs and supernovae as well as the fact that their host galaxies are rapidly star-forming offer very strong evidence that long gamma-ray bursts are associated with massive stars. The generally accepted progenitor model for long GRBs is the collapsar model. This model starts with a very massive, low metallicity, fast rotating star. The massive star is able to fuse material in the center all the way to iron, and at the point when it is not able to generate energy by fusion, it start collapse, and immediately forms a black hole. Materials around the core then rains down towards the center, and the high angular momentum then drives them into a high density accretion disk. While for the short GRBs, they are shown to be in the less star forming regions, the progenitor star of the relativistic jet might be different. A popular progenitor model for short GRBs involves the

collision of two neutron stars in a tight binary system (with inspiral caused by the emission of gravitational waves), with a resulting ultra-relativistic jet creating the observed burst of gamma radiation. A system of two compact object will slowly lose their energy due to the gravitational radiation and the two neutron stars will spiral closer and closer to each other. To some point that they are close enough, tidal forces will rip the neutron stars apart, and a large amount of energy will be released before the matter plunge into a single black hole. This whole process is extremely fast and can be complete within seconds. Due to the small samples of short hard GRBs, especially those with measured spectroscopic redshift, it has been difficult to confirm this model. It is believed that the twisting of magnetic fields in the accretion disk collimates the outflow along the rotation axis of the central object, so that when conditions are suitable, a jet will emerge from each face of the accretion disk. Materials in the accretion disk falls into the black hole continuously, which drives a pair of relativistic jet out along the rotation axis towards the pole of the star, and pummel all the way to the stellar surface. As the density of the stellar materials decreases, the leading shock accelerates all the way to the surface, and by the time it reaches the surface of the star, it will be traveling with a Lorentz factor of $100 - 1000$. It breaks out into the space, and much of its energy will be released into the form of Gamma-Ray Bursts. Figure 1.8 shows the collapse of the core of a rapidly rotating high mass Wolf-Rayet star and the break out of the relativistic Gamma ray burst jet after it is launched from the center of the Wolf-Rayet star.

It is believed that the Gamma ray prompt emission and longer wavelength afterglows of GRBs are produced from the material collisions in the relativistic jet. Different packages of materials with slightly different travel velocity in the relativistic jet will interact as inner collisions. The collision of the two shells immediately heat the matter, which convert the huge amount of kinetic energy into the random motion of particles. The physical mechanism that produced the observed Gamma ray photons is still under debate, but the most accepted ones are the synchrotron radiation, which produce high energy photons as a particle traveling

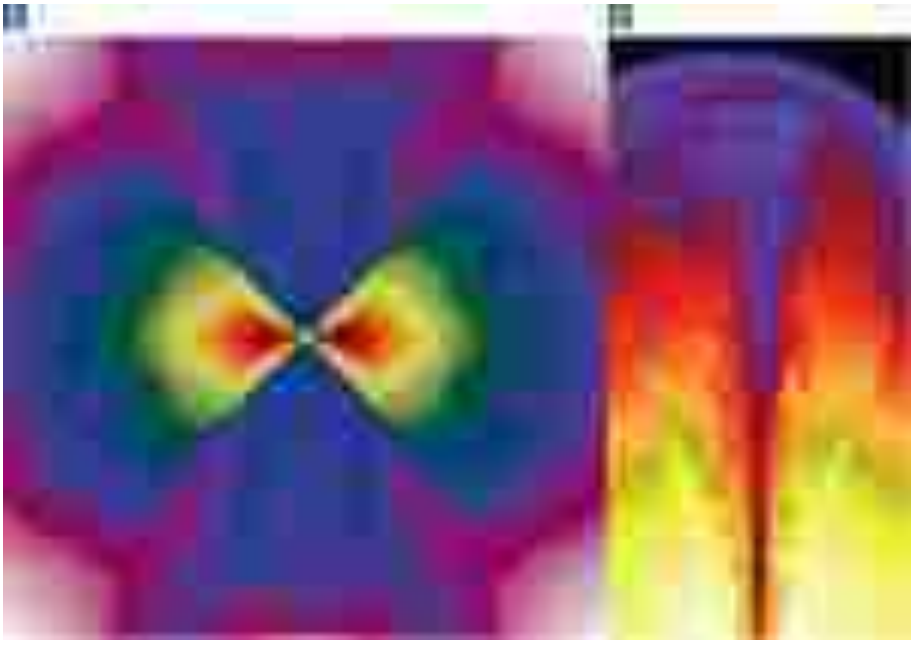

Figure 1.8 Collapse of the core of a rapidly rotating 14 Solar Mass Wolf-Rayet star and the break out of the relativistic Gamma ray burst jet.

in a high magnetic field, or inverse Compton scattering, where low energy photons produced in the thermal spectrum are scattered to higher energies by relativistic electrons (Rees & Mészáros , 1992, 1994). The internal collision to produce the GRB and the external collision to produce the afterglow in longer wavelengths is shown in Figure 1.9 Models for long GRBs must generate energies as high as 10^{51}ergs, and a relativistic flow with jet opening angles $1^\circ < \theta < 20^\circ$ and Lorentz factors of $100 - 1000$. The model described above is the most popular one, but it is not able to be confirmed by the observational features yet. Various alternative models exist, which are also able to produce a GRB from a relativistic jet. The energy in the jet can either be carried by kinetic energy of baryons expanding at relativistic velocities or by Poynting flux driven by the magnetic and rotational energies of collapsing stellar core (Usov, 1992, 1994).

After the prompt emission, all the materials ejected will coalesce into a single shell traveling outwards, and when the shell of materials hit the surrounding interstellar gas, then

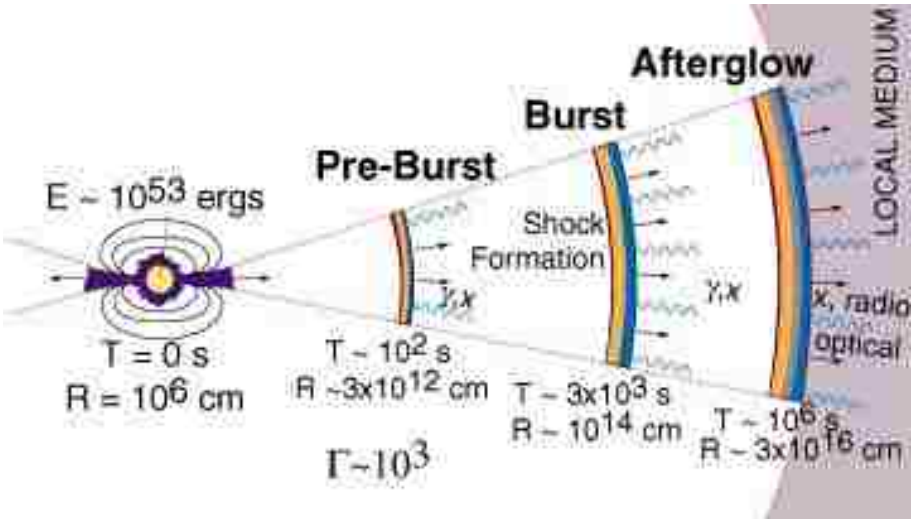

Figure 1.9 Blast wave model of GRB. From this model, GRBs are generated by the internal collisions between different packages of materials in the relativistic jet, and the afterglow of GRBs are generated by the external collisions between the coalesced package of material in the relativistic jet and the surrounding interstellar gas. Credit: unknown.

interstellar gas will be heated to very high temperature, although how it happens is still poorly understood. Materials in the shell would be relativistally moving outwards in a strong local magnetic field. The particles will be accelerated in the magnetic field, which cause them to radiate through synchrotron radiation.

1.4 GRB as Cosmology Tool

At the 5th Huntsville GRB Symposium, two groups put forward relations whereby the luminosity of a burst can be determined from properties of the burst's light curve. The first relation gives the time lag between hard and soft photons (τ_{lag}) as being inversely proportional with the burst isotropic peak luminosity (L), as calibrated with eight GRBs with spectroscopic redshifts (Norris et al., 2000). In the second relation, the variability of the burst light curve (V, taken as the normalized RMS scatter of the light curve about a smoothed light curve) was found to be correlated with the burst L for the same sample of GRBs with known redshifts (Fenimore & Ramirez-Ruiz, 2000). With this, high luminosity

bursts appear spiky with near-zero lags, while low luminosity bursts appear smooth with long lags. The reality of both relations was proven when a large sample of BATSE bursts was shown to have the predicted lag-variability relation. Since then, five other luminosity relations have been discovered, four of which had been predicted on the basis of theoretical arguments before they were empirically confirmed (Lloyd-Ronning et al., 2002; Schaefer, 2002; Schaefer et al., 2003b). These relations involve the photon energy of the spectral peak (E_{peak}), the minimum rise time in the light curve (τ_{RT}), and the number of peaks in the light curve (N_{peak}). These relations yield either the isotropic peak luminosity (L), the isotropic energy emitted in gamma rays ($E_{\gamma,iso}$), or the energy emitted in gamma rays after correction for the beaming of the jet (E_{γ}). Thus, with the luminosity of GRBs simply calculated from the observed parameters of the light curve, GRBs became standard candles (or standardizable candles) and could, in principle, be used for many purposes in cosmology.

The Hubble diagram is a plot of luminosity distance versus redshift, with the slope giving the expansion history of the universe. As the expansion history depends on the amount of mass in our universe (both normal and dark matter) as well as the Dark Energy, the measurement of the universe's expansion history is a good way to understand the properties of the Dark Energy. Type Ia supernovae are now playing an important role in the Hubble diagram work, which gives accurate distance and redshift measurements up to redshift of ~ 1.7 (Riess et al., 2004). However, different cosmological models (concordance cosmology, the best-fit cosmology from the supernovae "golden sample" with w(z) = -1.31+1.48z, and alternatives like Weyl gravity, Chaplygin gas, etc.) show small differences at low redshift region ($z < 1.5$), which could easily get hidden by systematic errors and makes it hard to distinguish them. In contrast, in the high redshift ($z > 3$), these cosmological models differ a lot, as shown in Figure 1.10. GRBs are a standard candles which can extend the Hubble diagram work to redshifts of 8.2. Given the luminosity relations mentioned above, the luminosity of a GRB can be calculated from its light curve and spectrum features, and with

the measured brightness of the GRB, the distance can be calculated. For those bursts with an independent redshift calculated from spectroscopic studies of the afterglow or the host galaxy, a Hubble diagram can be constructed. This expanded GRB Hubble diagram goes up to redshift of 8.2. The 1σ scatter σ_μ of the GRBs about the concordance cosmological model is 0.65 mag in the distance moduli. Comparing with the 0.36 mag for supernovae (Perlmutter et al. 1999) or 0.29 mag for supernovae "gold sample" (Riess et al., 2004), we see that a single GRB has an accuracy that is ~ 2.1 times worse than that of a single supernova. However, as stated above, the models with small differences at z = 1 will have large difference at z = 6. For example, the difference between the concordance cosmology and the best-fit cosmology from "gold sample" differs by -0.03 mag at z = 0.5, 0.04 mag at z = 1, 0.15 mag at z = 1.7, 0.44 mag at z = 3, and 1.00 mag at z = 6, as a result, a single z = 1.7 SN with $\sigma_\mu = 0.30$ mag can distinguish between the two models at a 0.5σ level, whereas a z = 6.6 GRB with $\sigma_\mu = 0.65$ mag can distinguish the two models at a 1.5σ level. Due to the long lever arm in the HD, a single high redshift GRB is three times better than a single maximal-redshift SN.

A 69 GRB Hubble diagram has been made by (Schaefer, 2007), with bursts prior to July, 2006. There have been ~ 70 more GRBs with measured spectroscopic redshifts since then, and I have a full catalog of all parameters needed (all luminosity indicators calculated, peak flux and fluence values, and spectroscopic redshifts). This increase in number of GRBs is critical for three reasons. The first reason is simply that a doubling of the number of GRBs will substantially improve the accuracy on the constraints for the fitted cosmological parameters. The second reason is that the new sample bursts will provide an independent sample against which the results from the first sample can be compared. The third reason is that the many new *Swift* bursts can be combined with the 31 *Swift* bursts (from the 69-GRB Hubble diagram) to make a large homogenous sample. This is in contrast to the current case where GRBs in the Hubble diagram come from six satellites and the largest contributor only

gives 45% of the sample. In such a case, there is always a worry that the differing energy bands, the various procedures for deriving E_{peak} (peak energy in the spectrum) and other luminosity indicators might cause systematic offsets in the calibrations of the luminosity relations.

As long GRBs are thought to be formed by the collapsing of fast-rotating massive stars with a very short main sequence lifetime, their occurrance must happen in close time and position association with star formation. As such, the rate of GRBs should be proportional to the star formation rate, or more certainly, the massive star formation rate. The various other methods for measuring the star formation rates (and its variation with redshift) all are measuring the massive star formation rate, plus they have severe problems with the extinction of optical and ultraviolet (in the galaxy rest frame) light. With GRBs out to redshift larger than 7, we will be able to measure the massive star formation rate as a function of redshift out to $z > 7$ with no extinction problems.

1.5 This Work

In my thesis, I will present my measurement on all the luminosity indicator values, and my derived luminosity relations. The GRB redshift measurement based on these luminosity relations will be introduced, and the calculated redshift values for all GRBs with spectroscopic redshift and all *Swift* long GRBs will be presented. I will also introduce the project of importing my program into the *Fermi* GBM data analysis software RMFIT, and a trial test on a few *Fermi* GRBs with spectroscopic redshift is then presented. A few applications of my redshift catalog and my catalog of luminosity indicators will be presented in the last section.

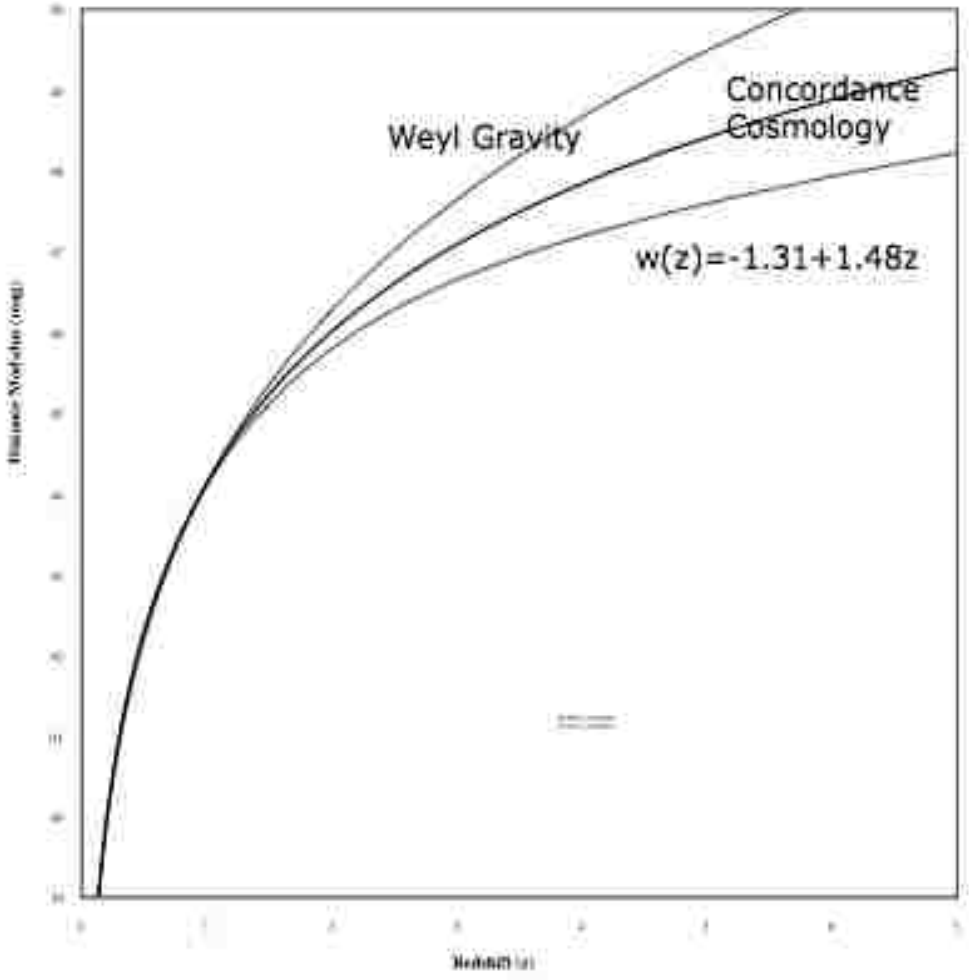

Figure 1.10 Comparison of different cosmological models in the Hubble diagram. From the plot we see that the best fitting model from the 'gold' sample of Supernovae shows a significant offset from the concordance cosmological model, and Weyl Gravity shows also shows a significant different from either of these two.

2. GRB Luminosity Indicators and Relations

2.1 GRB Luminosity Indicators

For long GRBs, it has been proved that some of the parameters from the light curve or the spectrum are related to the luminosity of the burst. These parameters are called luminosity indicators. So far, many single and multiple luminosity indicators have been proposed, and in my work, I choose five well-understood ones. These indicators are the spectral lag (τ_{lag}), variability (V), peak energy in the spectrum (E_{peak}), minimum rise time (τ_{RT}), and number of peaks (N_{peak}) of the light curve. Details of these indicators and corresponding relations are described below.

(1) The spectral lag, τ_{lag}, is the delay time between the soft and hard light curves of a burst. By shifting the hard and soft light curves of a GRB and calculating the cross correlation between them, we are able to get a cross-correlation versus offset plot. The offset corresponding with the peak value of the cross-correlation is the lag time we need. The $\tau_{lag} - L$ relation was first proposed by (Norris et al., 2000), and is a simple consequence of the conservation of energy in the shock material.

(2) The variability, V, a quantitative measure of 'spikiness' in the light curve, has a fairly scattered correlation with the luminosity (Fenimore & Ramirez-Ruiz, 2000). It can be obtained by calculating the normalized variance of the original light curve around the smoothed light curve. The calculation of V is as shown in (Schaefer, 2007):

$$V =< [(C - C_{smooth})^2 - \sigma_C^2]/C_{smooth,max}^2 > \tag{2.1}$$

where C is the count per time bin in the background subtracted light curve, with an uncertainty of σ_C. C_{smooth} is the count in the smoothed light curve, with a box-smoothing width

to be 30% of T_{up}, as the time duration of the burst T_{up} is calculated as the summation of the time with the light curve brighter than 10% of its peak flux. $C_{smooth,max}$ is the peak value of C_{smooth}.

(3) E_{peak} is the photon energy at which the νF_ν spectrum is brightest. By fitting the GRB spectrum with a smoothly broken power law (Band et al., 1993) as

$$\Phi(E) = \begin{cases} A\ E^{\alpha}\ e^{-(2+\alpha)E/E_{peak}} & \text{if } E \leq [(\alpha-\beta)/(2+\alpha)]E_{peak} \\ B\ E^{\beta} & \text{otherwise} \end{cases} \tag{2.2}$$

the peak energy E_{peak} and corresponding parameters α (the asymptotic power law index for photon energies below the break) and β (the power law index for photon energies above the break) can be obtained. Here Φ is the differential photon spectrum (dN/dE) as a function of the photon energy (E). A GRB spectrum can also be fit with a power-law with exponential cutoff model:

$$dN/dE = A\ E^{\alpha} e^{-(2+\alpha)E/E_{peak}} \tag{2.3}$$

with E_{peak} and α values obtained from the fitting parameters. Here A and B are normalizing constants to indicate the brightness and constructed to ensure the continuity of the model spectrum.

(4) The minimum rise time in the light curve, τ_{RT}, was proposed for use in a luminosity relation by (Schaefer, 2002). The minimum rise time of a burst is taken to be the shortest time over which the light curve rises by half the peak flux of the pulse. Normally, the minimum rise time of a pulse is measured by taking the shortest time for the light curve to rise by 1/2 of the pulse, and the minimum of the whole light curve is taken as the smallest minimum rise time of multiple pulses, if there is any.

(5) N_{peak} is defined as the number of peaks in the light curve. With C_{max} as the overall maximum of the background-subtracted light curve, we define a peak to be a local maximum that rises higher than $C_{max}/4$ and is also separated from all other peaks by a local minimum that is at least $C_{max}/4$ below the local lower peak.

2.2 Improving GRB Luminosity Indicator Measurements

2.2.1 Spectral Lag

The spectral lag, τ_{lag}, is the delay time between the soft and hard light curves of a burst. By convention, we use the soft and hard energy bands to be those of BATSE channels 1 and 3, or *Swift* channels 2 and 4, covering roughly 25-50 keV and 100-350 keV. For τ_{lag}, by shifting the hard and soft light curves of a GRB, and calculating the cross correlation between them, we are able to get a cross-correlation versus offset plot. The offset corresponding with the peak value of the cross-correlation is the lag time we need. The calculation is simple and easy for bright bursts, while for those faint ones, since the plot has significant scatters, the offset with the peak correlation (i.e. τ_{lag}) is hard to evaluate under these noisy conditions. To find the offset when the cross-correlation achieves its peak value, we need to make a reasonable fit to the peak region of the cross correlation. As the shape and scatter of the plot varies from burst to burst, we cannot simply fit it with some specific function. If we fit it with a parabola, then any asymmetry in the cross correlation (as is often seen) will incorrectly shift the peak in the model by an amount depending on the range of offset included in the fit. And if we fit it with a high-order polynomial function, then the high-order terms will be unstable as they are trying to follow noise and regions far from the peak. What we did was to fit the cross correlation by polynomials with different orders (normally from 3 to 9), and choose the one which fits best in the very central region (around the peak) of the curve. Two examples are shown in Figure 2.1.

A bootstrap procedure was previously used to calculate the uncertainties on the τ_{lag} (Norris 2002). In our work, we are using a simple propagation method. The uncertainties on the cross-correlation amplitude points are calculated by simply evaluating the RMS scatters of these data points around the fitted curves. We are then able to generate the uncertainties for each of the fitting parameters, and the coefficient errors. Then the uncertainty for our

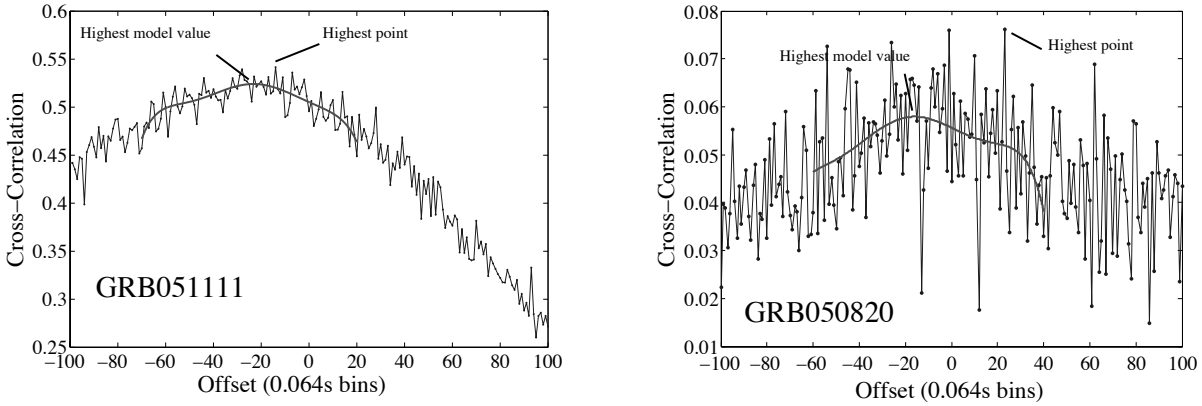

Figure 2.1 τ_{lag} calculation – Cross-Correlation versus Offset plots. The left panel is the plot for GRB051111, which is a moderately bright burst without much noise in the light curve. But we can see that although the curve is relatively smooth, the peak region is quite 'broad' so that we still need an accurate fitting of the curve, especially for the central region of the curve. Had we simply taken the offset of the highest measured cross-correlation, we would have the peak at -14 bins (with τ_{lag} equal to 0.90 seconds), with this value being determined by noise in the cross correlation. Instead, we fitted a 7-order polynomial (smooth curve) and found a peak at -23.1 bins (with τ_{lag} equal to 1.48 seconds), and this model fit is avoiding most of the random noise in the cross correlation. Note, for our choice of bands, the lag will be negative in bins but expressed as positive in time. The right panel is for GRB050820, which is a noisy burst. There is much scatter in the cross-correlation versus offset plot, from which we cannot determine the position of the peak without making a fit around the peak region. In this case, the highest cross correlation is at +23 bins (corresponding to a negative lag of -1.47 seconds), with the model fit (a 7-order polynomial also) providing a more reasonable peak at -15.7 bins (τ_{lag} = 1.00 seconds).

τ_{lag} value, $\sigma_{\tau_{lag}}$, is generated by propagation of the uncertainties on the fitting parameters and the coefficients.

2.2.2 Minimum Rise Time

The minimum rise time in the light curve, τ_{RT}, was proposed for use in a luminosity relation by (Schaefer, 2002). The minimum rise time of a burst is taken to be the shortest time over which the light curve rises by half the peak flux of the pulse. In practice, especially for faint bursts with large Poisson noise, the rate difference between two close bins might be larger than half of the peak flux. As a result, we have to smooth the light curve before we calculate the rise time. The problem is then that if we smooth it too little, the apparent fastest rise time might be dominated by the Poisson noise, resulting in a too-small rise time, and if we smooth it too much, the smoothing effect will dominate, resulting in a rise time near the smoothing time bin.

As the light curves vary greatly among different bursts, there is no specific box smoothing width that can satisfy a majority of bursts. Instead, we vary the box smoothing width from 0 bins (that is, no binning) up to a relatively large number, say 50 bins, and for each of these smoothing widths, we generate a smoothed lightcurve from which a minimum rise time can be calculated. Of course, some of these light curves are over-smoothed and some are under-smoothed. In a minimum rise time versus smoothing width plot, we will have a monotonically rising curve, as shown in Figure 2.2. Although the shape of the curve varies amongst bursts, for most of the bursts there will be a region where the curve appears flat, or with a slightly increasing slope, which we call a plateau. It is easy to explain the existence of the plateau: in this region, the smoothing is enough that Poisson noise is negligible in determining the minimum rise times, while the smoothing is not so much that it determines the minimum rise time. On a plot of minimum rise time versus smoothing width, we can identify three regions: a fast rising region where the Poisson noise dominates, a nearly flat

plateau region where we are seeing the real minimum rise time, following by another rising region for large box smoothing widths where the smoothing is dominating. We can make use of this plateau region by extrapolating it back to the zero-smoothing case (where the box smoothing width is zero), as shown in Figure 2.2. The intercept on the y-axis corresponds with the minimum rise time where the smoothing is effectively zero. With the extrapolation, we are sidestepping the regime where the Poisson noise dominates. As a result, the value of the intercept is just the minimum rise time we need, not affected by either the Poisson noise effect or the smoothing effect.

For some of the extremely faint bursts, the Poisson noise dominant region and the smoothing effect dominant region will overlap with each other, and we are unable to find a plateau in the minimum rise time versus smooth width plot, for which the extrapolation cannot be made. Thus, our technique does not produce τ_{RT} values for the faintest bursts.

The uncertainty of the minimum rise time is calculated by simple propagation from the fitting parameters and the uncertainties on each individual point on the minimum rise time versus smoothing width plot. The uncertainties on each of the individual point are dominated by the noise on each original data points in the light curve. The noise on the peak flux will affect our criteria, by some factor of $\sigma_C/\max(\mathrm{C})$, where C is the rate, and σ_C is the uncertainty of the rate. In addition to that, random noise will affect our determination, i.e. the real rise time between two data points may be larger/smaller than half of the peak flux. This effect is also reflected in our criteria, by a factor of $\sim 2 \times \sigma_C/\max(\mathrm{C})$. As a result, for determine the uncertainties on each of the individual rise time on RT-smoothing width plot, we can change our criteria from 0.5 by a factor of $2.25 \times \sigma_C/\max(\mathrm{C})$, and record how much the resulted minimum rise time values changes. The uncertainties on the fitting parameters and the minimum rise time value can then be calculated from propagation.

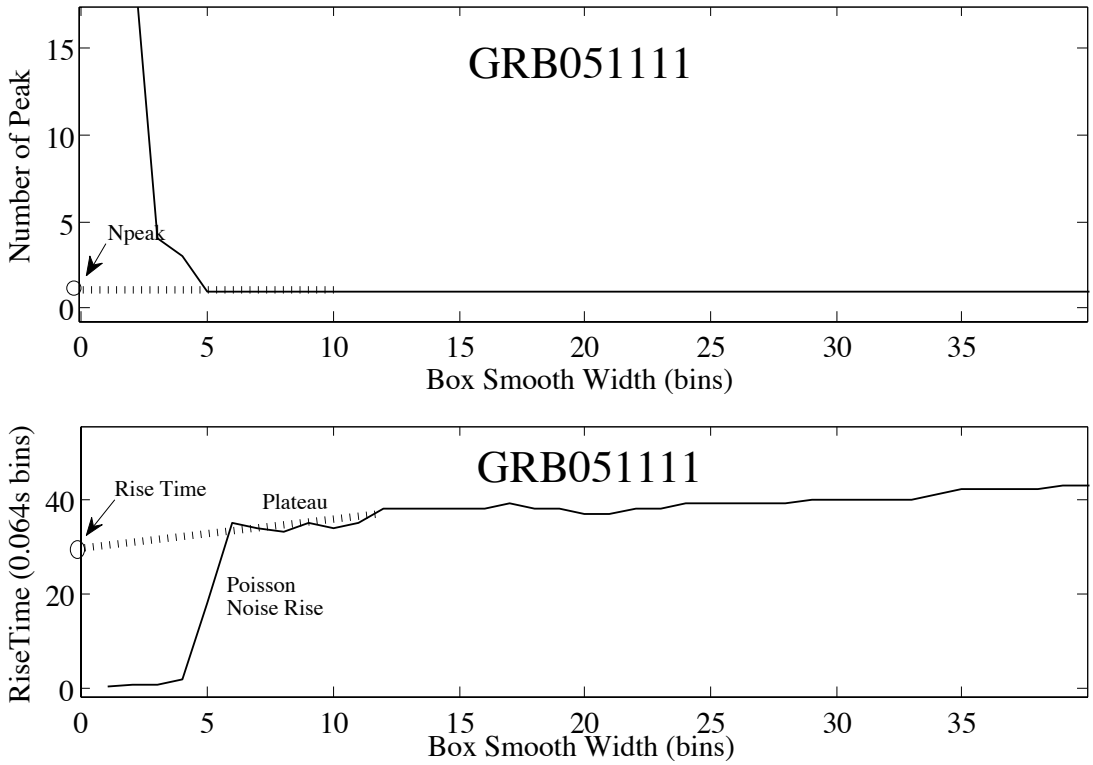

Figure 2.2 The calculation of τ_{RT} and N_{peak}. We can see an apparent 'plateau' in the lower plot, for box smoothing widths of more than 5. By simply extrapolating the plateau back to the y-axis (see dashed line), we get a minimum rise time (see circle at intercept on y-axis) which is appropriate for zero smoothing, and which is not affected by the Poisson noise.

2.2.3 Number of Peaks

N_{peak} is defined as the number of peaks in the light curve. With C_{max} as the overall maximum of the background-subtracted light curve, we define a peak to be a local maximum that rises higher than $C_{max}/4$ and is also separated from all other peaks by a local minimum that is at least $C_{max}/4$ below the lower peak. In principle, N_{peak} is easy to count, either automatically or manually. In practice, we have the same problem of the Poisson noise and the smoothing factor effect, as we had in the calculation of τ_{RT} . Faint bursts will have their unsmoothed light curves dominated by apparent peaks produced by Poisson noise, resulting in large numbers of false peaks. A random noise spike can satisfy our definition for a peak if we do not smooth the light curve, yet if we smooth it too much there will always be just one peak. Here we adopted the same procedure of calculation as that in the calculation of τ_{RT} . We vary the box smooth width from 0 bins to a relatively large number, and calculate the number of peaks for each of the smoothed light curves. As in the case for τ_{RT} , we see a fast falling curve (where Poisson noise is contributing spurious peaks), with a plateau, where neither the Poisson noise effect nor the smoothing effect dominates. By extrapolating the plateau back to the y-axis, we get an N_{peak} value for an unsmoothed case of the light curve, with the effects of Poisson noise removed.

2.3 GRB Luminosity Relations

Each of the luminosity indicators discussed above has one or more corresponding luminosity relations. In these luminosity relations, the indicators shows correlations either with the luminosity L, the total emitted energy assuming an isotropic explosion $E_{\gamma,iso}$, or the total energy with the jet beaming angle correction E_{γ}. These relations are $\tau_{lag}-L$, $V-L$, $E_{peak}-L$, $E_{peak}-E_{\gamma,iso}$ (so called Amati relation) and $E_{peak}-E_{\gamma}$ (so called Ghirlanda relation), $\tau_{RT}-L$, and $N_{peak}-L$ relation, which are described and explained in detail in (Schaefer, 2007). There

Table 2.1. Luminosity Relations

Indicator	Relation	σ_a [a]	σ_b [a]	σ_{sys} [a]
τ_{lag}	$\log L = 52.21 - 0.98 \log[\tau_{lag}(1+z)^{-1}/0.1s]$	0.04	0.03	0.48
V	$\log L = 51.06 + 1.35 \log[V(1+z)/0.02]$	0.09	0.09	0.87
E_{peak}	$\log L = 52.10 + 1.88 \log[E_{peak}(1+z)/300keV]$	0.03	0.01	0.57
E_{peak}	$\log E_\gamma = 50.57 + 1.63 \log[E_{peak}(1+z)/300keV]$	0.09	0.03	0.16
τ_{RT}	$\log L = 52.84 - 1.70 \log[\tau_{RT}(1+z)^{-1}/0.1s]$	0.04	0.05	0.53
N_{peak}	$\log L \geq 50.32 + 2 \log[N_{peak}]$ for $N_{peak} \geq 2$	...	...	...

[a]The σ_a, σ_b are the $1-\sigma$ uncertainties of the fitting parameters, while a is the intercept on the y-axis, and b is the slope of the fitting line. σ_{sys} is the systematic uncertainty added in quadrature to the measurement errors, with which the χ^2_{red} of the points about the best fit line is unity.

is another luminosity relation which relates E_{peak}, an effective duration (called T_{45}), and the luminosity by Firmani et al. (2006). However, with more GRBs and E_{peak} data added in, it is realized that this luminosity relation is not making any improvement on the $E_{peak} - L$ relation (Collazzi & Schaefer , 2008). The equation of those luminosity relations are shown in Table 2.1

(1) $\tau_{lag} - L$ relation. It is a simple consequence of the conservation of energy in the shock material (Schaefer, 2004).The delay time between the soft and hard light curves indicates the cooling off time of the material. For the shocked material being dominated by radiative cooling, the cooling of the shocked material is what generates the luminosity of the burst. That is, high-luminosity bursts will have fast radiative cooling and hence short lags, while low-luminosity bursts will have slow radiative cooling and hence long lags (Schaefer, 2003a). This general result predicts that the burst luminosity should be proportional to τ_{lag}^{-1} and that is exactly what is observed.

(2) $V - L$ relation. According to the relativistic shocked jets model, luminosity is a moderately-high power law function of the bulk Lorentz factor of the jet (Γ_{jet}). At the same

time, the rise times and durations of the light curve pulses will be proportional to a power of Γ_{jet} through the angular size of the visible region in the jet. The variability in the light curve is primarily a function of the rise times and the pulse duration. Both L and V depend on Γ_{jet}, so L and V should be correlated. Detailed predictions gave $L \propto V^2$, and this is close to the observed relation (Schaefer, 2007). As a result, the light curves of high luminosity bursts will be spiky with a high V value and those of low luminosity bursts will be smooth with a low V value.

(3) E_{peak} is correlated with the luminosity L, the total isotropic energy $E_{\gamma,iso}$, and the total collimation-corrected energy E_γ. The $E_{peak} - L$ relation was first predicted and shown by (Schaefer, 2003a), and is related to the instantaneous physics at the time of the peak luminosity. Since both the luminosity and E_{peak} vary as some power function of Γ_{jet}, with detailed analysis, the relation between E_{peak} and luminosity can be written as $L \propto [E_{peak}(1+z)]^{N/(M+1)}$, with $N/(M+1) \sim 2.5$. The observed slope is somewhat more shallow than this prediction, with an exponent more like 1.7 (Schaefer, 2007).

Amati et al. (2002) introduced the relationship between E_{peak} and $E_{\gamma,iso}$, while Ghirlanda et al. (2004) found a much tighter relation between E_{peak} and E_γ, which corrects for the effect of the jet opening angle. The physics of the $E_{peak} - E_\gamma$ relation is completely different from that of $E_{peak} - L$ relation. It can be easily explained as the relativistic effects within a standard model, the details of which is shown by Eichler & Levinson (2004); Yamazaki et al. (2004); Rees & Mészáros (2005); Levinson & Eichler (2005).

Of the three relations for E_{peak}, we adopt the $E_{peak} - L$ relation and Ghirlanda's $E_{peak} - E_\gamma$ relation. We are not including Amati's relation for the following two reasons: First, Amati's relations has been challenged as it returns ambiguous redshifts (Li , 2007), while the $E_{peak} - L$ relation (also the $\tau_{lag} - L$, $V - L$, $\tau_{RT} - L$, and $N_{peak} - L$ relations) passed the same test (Schaefer & Collazzi, 2007). Second, the physics of the Amati's relation is nearly the same

as that of Ghirlanda's $E_{peak} - E_\gamma$ relation, except that Ghirlanda's $E_{peak} - E_\gamma$ relation has a correction for the jet opening angle, while the latter is much tighter.

(4) $\tau_{RT} - L$ relation. The rise time is taken to be more fundamental than the variability, and its physics is much more apparent than that of variability. In the shocked jet model, for a sudden collision of a material within a jet, the minimum rise time represents the time delay between the arrival time of photons from the center and the edge of the visible region. As the delay time depends on the angular size of the visible region, which depends on Γ_{jet}, and through this is related to the luminosity. The relation between τ_{RT} and luminosity has been predicted by Schaefer (2002) as $L \sim \tau_{RT}^{-N/2}$, with $N \approx 3$. This is reasonably close to the observed luminosity relation (Schaefer, 2007).

(5) $N_{peak} - L$ relation provides us with a lower limit on the luminosity. The peaks of a GRB are caused by the collisions of isolated clouds of materials in the relativistic jet, and it depends on many different factors. However, a limit can be placed on the number of peaks that are distinguishable. This limit arises because the individual peak rise times (and hence durations) are determined by the size of the visible region (and hence an Γ_{jet}). For high-luminosity bursts (with high Γ_{jet} and small visible regions), the pulse rise times and durations will be short, so there will be no overlap between pulses. In this case, every internal collision will result in a distinct peak in the light curve. Whereas, for low-luminosity bursts (with low Γ_{jet} and a large visible region), the pulse rise times and durations will be long. In this case, the individual pulses will likely overlap with each other, resulting in few distinct peaks in the light curve. If we see a light curve with many peaks, it must be of high luminosity, because that is the only way that the pulses can be narrow enough to be distinguished. But if we see a light curve with few peaks, then we cannot conclude much about its luminosity, because the burst could either be a low-luminosity event with all its peaks smeared together or it could be a high-luminosity event with few collisions. It is this last point that forces the $N_{peak} - L$ relation to provide only a lower limit on the luminosity. A detailed analysis give

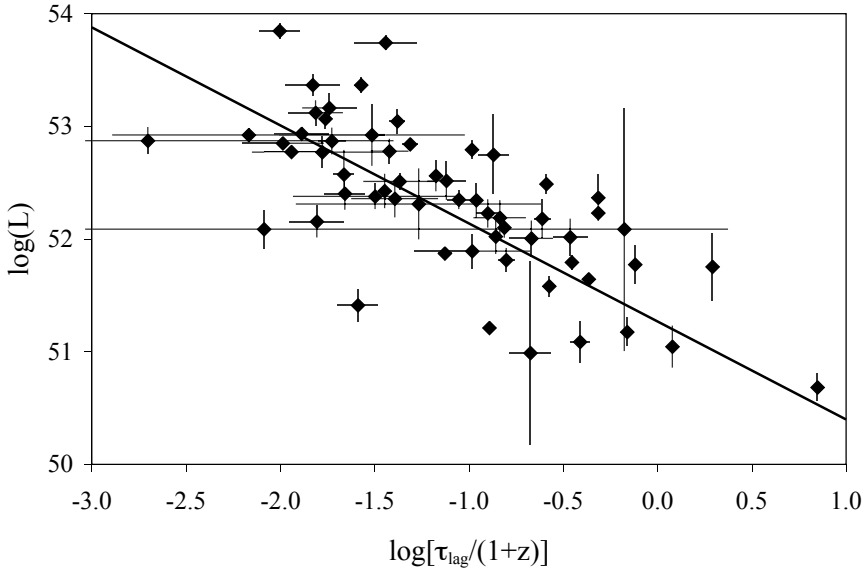

Figure 2.3 Luminosity relation between spectral lag τ_{lag} and the luminosity L. τ_{lag} shows a inverse power law relation with L after the redshift correction.

a limiting function, which is well approximated as $L > cN_{peak}^2$ for a constant 'c'. And this theoretical prediction was strongly confirmed with observation (Schaefer, 2007).

2.4 Instrument Detection Threshold Effect?

Butler et al. (2007) estimated the Amati's relation ($E_{peak} - E_{\gamma,iso}$) with *Swift* and pre-*Swift* data. They report an inconsistency in the relations from the two data sets, which they then attributed to differences in threshold between *Swift* and earlier detectors. Their claimed difference has not been reproduced by other groups (including Cabrera et al. 2007; Schaefer 2007b; Krimm et al. 2009), while their claimed threshold effects have been found to not significantly affect the observed Amati relation (Schaefer 2007b; Nava et al. 2008; Ghirlanda et al. 2008; but see Shahmoradi & Nemiroff 2009). Indeed, their analysis is based on Bayesian priors which systematically push high-E_{peak} values below $\sim$ 400 keV, as demonstrated by detailed comparisons with Konus, Suzaku, and RHESSI measures. Nevertheless, here we

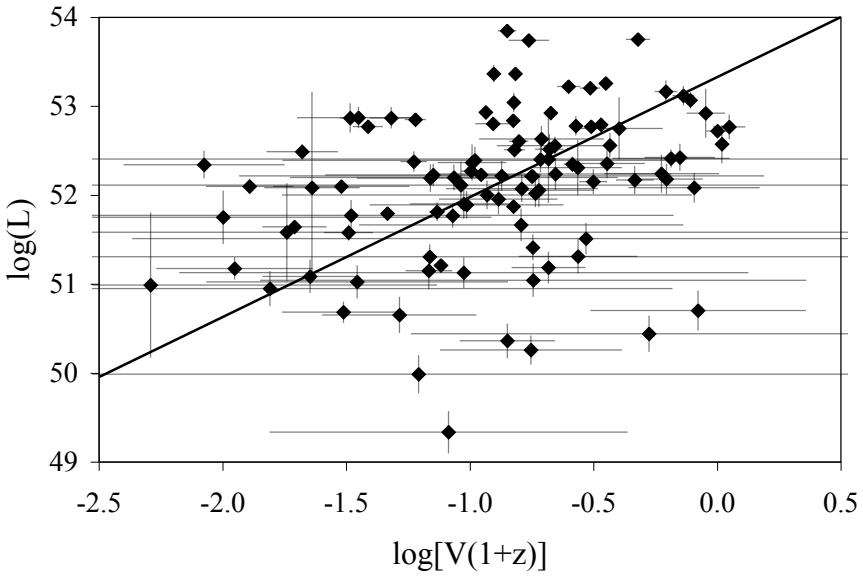

Figure 2.4 Luminosity relation between variability V and luminosity L. V showed a loose power law relation with L in the previous studies using BATSE and early *Swift* data. However, when we expanded the sample with more *Swift* GRBs, the relation gets even looser, and no significant relation was found with the expanded sample.

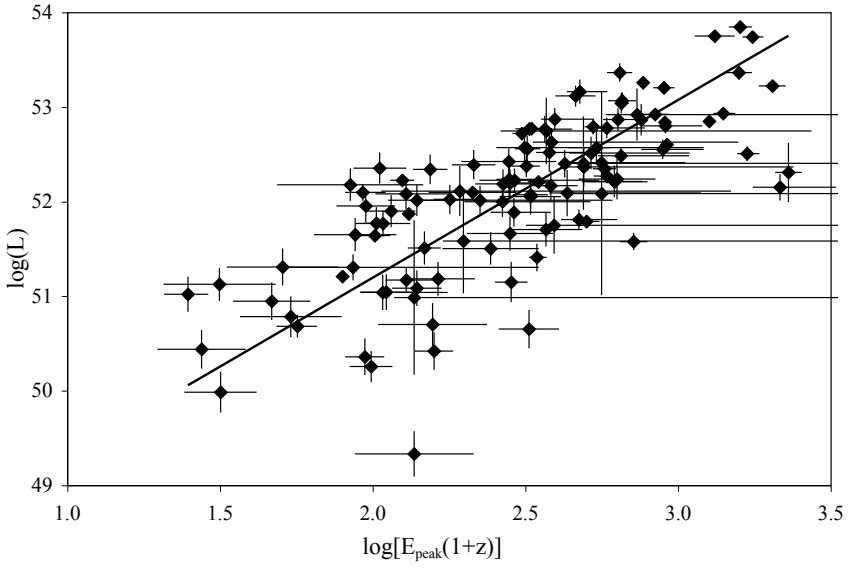

Figure 2.5 Luminosity relation between peak photon energy in the spectrum E_{peak} and luminosity L, with E_{peak} showing a power law relation with L after the redshift correction.

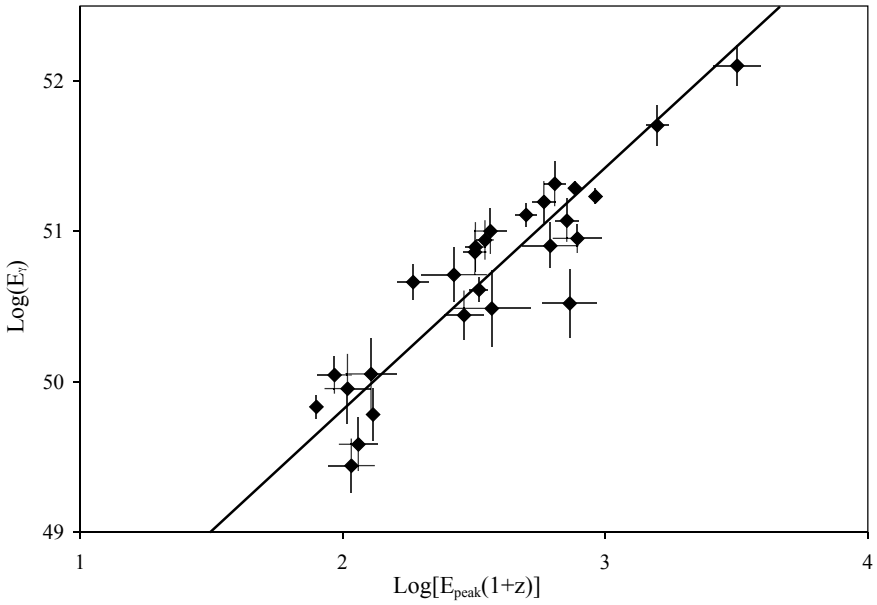

Figure 2.6 Ghirlanda's Relation, which is the relation between peak photon energy of the spectrum E_{peak}, jet break time in the optical afterglow t_{jet}, and total energy emitted from the GRB explosion after the beaming angle correction E_γ. This is the tightest among all of these luminosity relations. However, only a small fraction of GRBs have their jet break time measured, so this relation is not able to be used for a large fraction of GRBs.

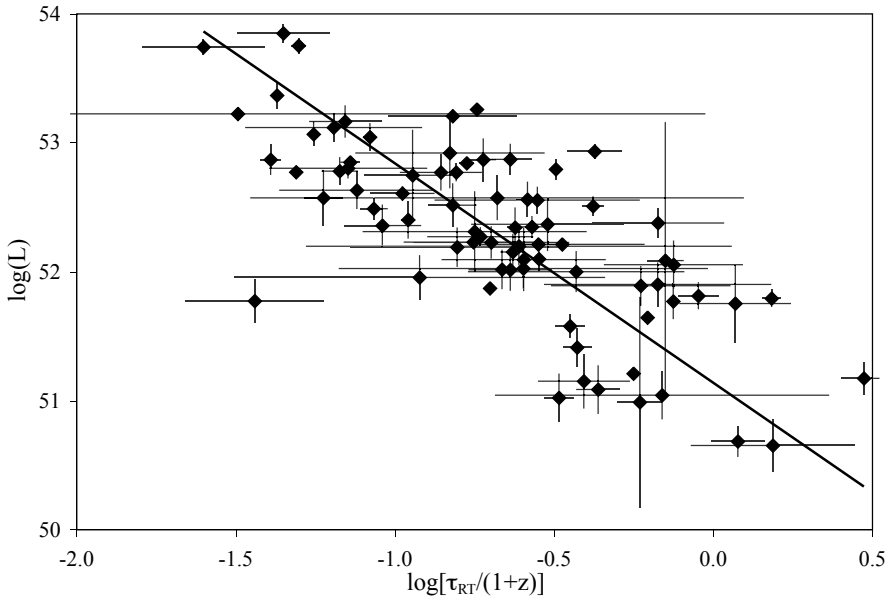

Figure 2.7 Luminosity relation between the minimum rise time τ_{RT} and luminosity L, with τ_{RT} showing an inverse power law relation with L after the redshift correction.

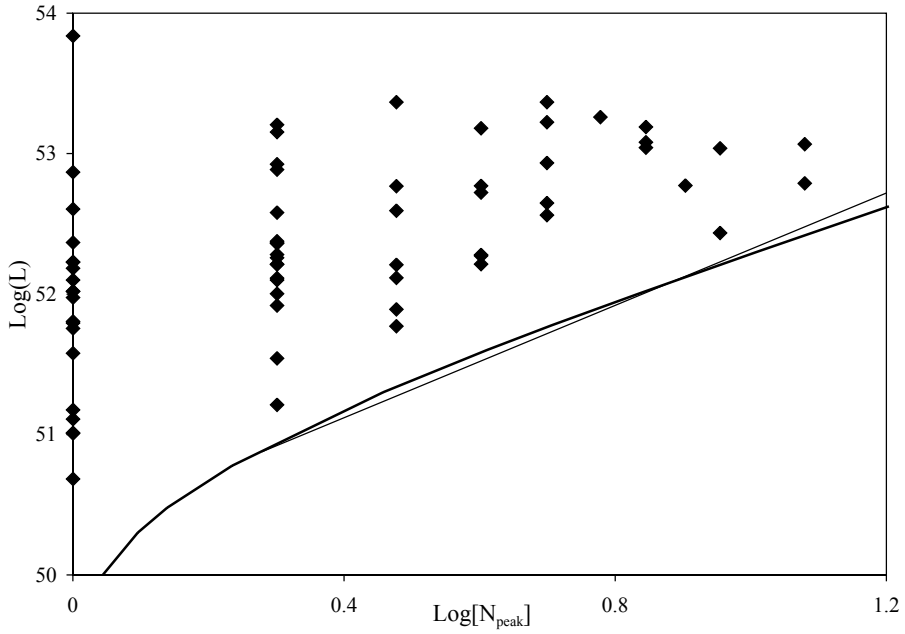

Figure 2.8 Luminosity relation between number of peaks in the light curve N_{peak} and luminosity L, with N_{peak} providing a strict lower limit of L.

can perform yet another test to see whether the claimed threshold differences between *Swift* and pre-*Swift* bursts cause any significant change in the luminosity relations. Butler et al. (2007) include *Swift* BAT bursts between GRBs 041220 and 070509, 77 of which have a spectroscopic redshift measured, while in our analysis on *Swift* GRBs, we are including all bursts with spectroscopic redshift between 050126 and 080721. With both samples being based on largely overlapping samples selected in a nearly identical manner, we conclude that the flux limits of the two samples are essentially identical.

To this end, we have separately fitted the pre-*Swift* and *Swift* data. This test was only done for four luminosity relations ($\tau_{lag} - L$, $V - L$, $E_{peak} - L$, and $\tau_{RT} - L$), with the $E_{peak} - E_{\gamma}$ relation having too few bursts, and the $N_{peak} - L$ relation not being usable for the comparison as a limit. The best fit luminosity relations are given in Table 2.2. The data and best fit models are displayed in Figure 2.9. At first glance, we see that the difference

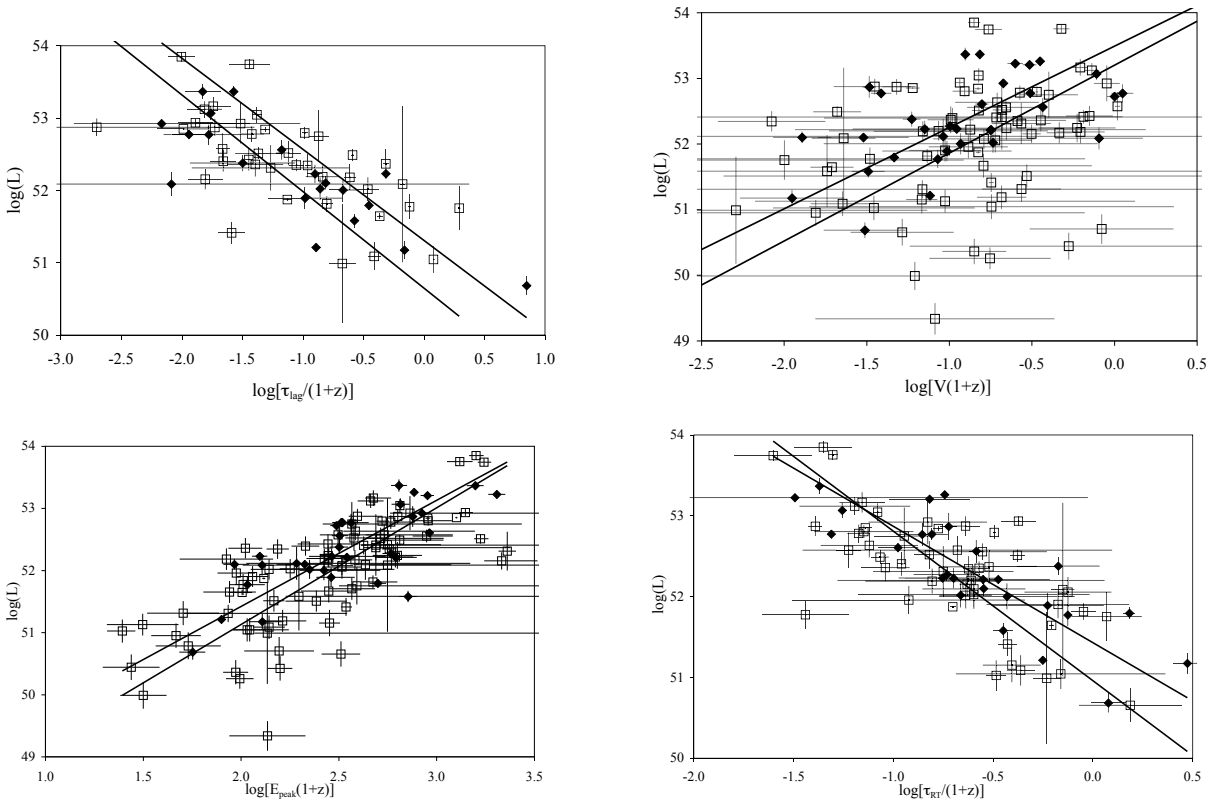

Figure 2.9 Comparison of the luminosity relations for pre-Swift and Swift bursts. The filled diamonds are for pre-Swift bursts, while the open squares are for Swift bursts. From the plot we can tell that the luminosity relations are identical between pre-Swift and Swift bursts to within the usual uncertainties. Ghirlanda's relation is not compared because the sample of bursts with both E_{peak} and jet break time is too small.

between the two best fit lines are small compared to the scatter in the data, and a detailed analysis is described below.

We made a F-test for the fitting results for these four relations. First we made a bisector linear fit on the combined data with both pre-*Swift* and *Swift* bursts, and recorded the χ^2 value of the fit as χ^2_{JOINT}. Then we separate the data to two sample sets, pre-*Swift* and *Swift*, and made the same bisector linear fit separately on each set of the data. The sum of the two χ^2 values for the separately fitted lines are recorded as $\chi^2_{SEPARATE}$. Then the F value can be calculated as

$$F = \frac{\chi^2_{JOINT}/(N_{pre} + N_{sw} - 2)}{\chi^2_{SEPARATE}/(N_{pre} + N_{sw} - 4)} \tag{2.4}$$

where N_{pre} is the number of pre-*Swift* bursts, and N_{sw} is the number of *Swift* bursts. $N_{pre} + N_{sw} - 2$ is the degree of freedom of the fitting on the combined data, and $N_{pre} + N_{sw} - 4$ is the degrees of freedom of the fitting on separated data.

These F values for each of the luminosity relations are listed in Table 2.2. If the pre-*Swift* and *Swift* relations differ much from each other, the separate fitting has been significantly improved over the fitting on the mixed data, the F value would be much larger than unity. Otherwise, if there is no significant difference between pre-*Swift* and *Swift* relations, the F value would be around unity. From Table 2.2 we see that F is rather close to unity. All of the results shows that the separately fitted result is not significantly improved over the fitted results on all data mixed together, which means that luminosity relations for pre-*Swift* luminosity relations and *Swift* luminosity relations do not significantly differ from each other. And by looking at the plots in Figure 2.9, we see that (1) the envelope of squares and diamonds are indistinguishable and (2) the pre-*Swift* and *Swift* best fit lines are close to each other compared to the scatter in the data. And hence, we have no significant evidence that these four luminosity relations differ for *Swift* bursts.

The $1 - \sigma$ range on the normalization difference between *Swift* and pre-*Swift* bursts for all these four luminosity relations are also listed in Table 2.2. We can make an analysis with the normalization difference on Amati's relation claimed by Butler et al. (2007), which corresponds to a 0.39 difference in log space. By making the comparison between Butler's factor (0.39) and our normalization difference, we can exclude Butler's factor at a 2.5 sigma level for the $\tau_{lag} - L$ relation, a 3.7 sigma level for the $\tau_{RT} - L$ relation, a 1.3 sigma level for the $E_{peak} - L$ relation (which is not significant), and we cannot exclude the Butler factor for $V - L$ relation.

Table 2.2. Comparison of Luminosity Relations

Luminosity Relation	pre-Swift burst	Swift burst	F	$\sigma_{norm,diff}$[a]
τ_{lag}-L	$\log L = 52.14 - 0.95 \log[\tau_{lag}(1+z)^{-1}/0.1s]$	$\log L = 52.26 - 1.00 \log[\tau_{lag}(1+z)^{-1}/0.1s]$	0.98	0.11
Variability-L	$\log L = 51.38 + 1.24 \log[V(1+z)/0.02]$	$\log L = 50.92 + 1.34 \log[V(1+z)/0.02]$	1.04	0.09
E_{peak}-L	$\log L = 51.42 + 1.71 \log[E_{peak}(1+z)/300keV]$	$\log L = 51.13 + 1.88 \log[E_{peak}(1+z)/300keV]$	1.02	0.08
τ_{RT}-L	$\log L = 52.87 - 1.44 \log[\tau_{RT}(1+z)^{-1}/0.1s]$	$\log L = 52.81 - 1.85 \log[\tau_{RT}(1+z)^{-1}/0.1s]$	1.00	0.18

[a]The $\sigma_{norm,diff}$ is the $1-\sigma$ range of the difference of normalization values between *Swift* and pre-*Swift* luminosity relations. It is calculated by $\sqrt{\sigma^2_{norm,preSwift} + \sigma^2_{norm,Swift}}$.

3. GRB Redshift Estimation

3.1 Method

Our aim is to test our method of redshift calculation. No matter whether we are dealing with the bursts with known z_{spec} or not, these known z_{spec} are only involved in the fitting of luminosity relations, and this effect is negligible in our calculation.

Below we will describe how our method applies on one Gamma-Ray Burst step by step:

(1) First, we measure each of the luminosity indicators of the burst. The definition and method of calculations have been discussed in Sections 2. The results of the indicators for all bursts in the sample are listed in Table 3.1 & Table 3.2.

(2) We next derive the luminosity values for each luminosity relation. A complexity is that the luminosity relations depend on the redshift of the burst (so as to correct the luminosity indicators back to the burst rest frame), so we have to perform this calculation for an array of trial redshifts (we take it to be from redshifts of 0 to 20 at intervals of 0.005), and then we will obtain a list of luminosities (or isotropic energies for Ghirlanda's relation) values depending on the list of trial redshifts for each of the indicators. We notate each of these calculated luminosities (as a function of redshift z_{trial}) for the ith relation as $L_i(z_{trial})$ (or $E_{\gamma,i}$ for the Ghirlanda's relation).

(3) With the values of the peak flux P, fluence S, E_{peak} and the power law indices in the broken power law model α and β (or α from the power law with exponential cutoff model), the bolometric peak flux P_{bolo} and fluence S_{bolo} can be calculated. The range for 'bolometric' is set to be 1 keV to 10000 keV in the GRB rest frame, and the equations for the detailed calculation are taken from Schaefer (2007). As a result, for each burst, we calculated $P_{bolo}(z_{trial})$ and $S_{bolo}(z_{trial})$ for each trial redshift value from 0 to 20.

Table 3.1. Temporal Luminosity Indicators.

GRB	Satellite	τ_{lag}(sec)	V	τ_{RT}(sec)	N_{peak}
970228	Konus	...	0.016 ± 0.010	...	2
970508	BATSE	0.49 ± 0.02	0.018 ± 0.004	0.65 ± 0.07	1
970828	Konus	...	0.052 ± 0.005	0.36 ± 0.14	4
971214	BATSE	0.03 ± 0.05	0.048 ± 0.002	...	2
980703	BATSE	0.69 ± 0.02	0.024 ± 0.001	3.00 ± 0.19	1
990123	BATSE	0.07 ± 0.01	0.059 ± 0.003	...	3
990506	BATSE	0.04 ± 0.01	0.337 ± 0.001	0.13 ± 0.01	12
990510	BATSE	0.03 ± 0.01	0.118 ± 0.001	0.13 ± 0.01	8
990705	Konus	...	0.097 ± 0.004	0.62 ± 0.37	4
991208	Konus	...	0.023 ± 0.003	0.27 ± 0.01	4
991216	BATSE	0.03 ± 0.01	0.062 ± 0.003	0.09 ± 0.01	5
000131	Konus	...	0.056 ± 0.005	0.84 ± 0.39	2
000210	Konus	...	0.018 ± 0.002	0.45 ± 0.03	1
000911	Konus	...	0.122 ± 0.013	0.07 ± 0.22	5
000926	Konus	...	0.326 ± 0.034	...	4
010222	Konus	...	0.143 ± 0.004	0.45 ± 0.01	6
010921	HETE	1.00 ± 0.04	0.008 ± 0.006	4.31 ± 0.71	1
020124	HETE	0.07 ± 0.06	0.266 ± 0.040	0.59 ± 0.17	3
020405	Konus	...	0.104 ± 0.007	0.48 ± 0.09	2
020813	HETE	0.15 ± 0.01	0.164 ± 0.004	0.59 ± 0.05	5
021004	HETE	0.71 ± 0.19	0.035 ± 0.067	1.23 ± 0.96	2
021211	HETE	0.31 ± 0.01	0.006 ± 0.003	0.57 ± 0.01	1
030115	HETE	0.44 ± 0.06	0.020 ± 0.020	0.70 ± 0.40	1
030226	HETE	0.31 ± 0.22	0.033 ± 0.029	1.76 ± 1.15	3
030323	HETE	...	0.021 ± 0.338	...	2
030328	HETE	0.08 ± 0.08	0.024 ± 0.003	1.69 ± 0.81	2
030329	HETE	0.15 ± 0.01	0.065 ± 0.002	0.66 ± 0.01	2
030429	HETE	0.03 ± 0.17	0.220 ± 0.135	...	2
030528	HETE	12.56 ± 0.14	0.017 ± 0.010	2.13 ± 0.42	1
040924	HETE	0.90 ± 0.01	0.060 ± 0.003	0.33 ± 0.17	1
041006	HETE	...	0.050 ± 0.002	1.28 ± 0.01	3
050408	HETE	0.31 ± 0.02	0.082 ± 0.005	0.49 ± 0.02	1
051022	Konus	...	0.088 ± 0.008	0.19 ± 0.04	1
050126	Swift	2.74 ± 0.02	-0.010 ± 0.065	1.58 ± 1.91	1
050223	Swift	...	0.111 ± 0.094	...	1
050315	Swift	...	0.032 ± 0.016	1.97 ± 1.62	2
050401	Swift	0.06 ± 0.02	0.187 ± 0.019	0.25 ± 0.16	3

Table 3.1 (cont'd)

GRB	Satellite	τ_{lag}(sec)	V	τ_{RT}(sec)	N_{peak}
050406	Swift	...	0.020 ± 0.274	...	2
050416A	Swift	...	0.021 ± 0.030	0.54 ± 0.06	1
050505	Swift	0.71 ± 0.13	0.076 ± 0.031	0.60 ± 0.21	3
050525A	Swift	0.12 ± 0.01	0.093 ± 0.003	0.32 ± 0.01	2
050603	Swift	-0.01 ± 0.01	0.125 ± 0.014	0.19 ± 0.01	1
050730	Swift	...	0.027 ± 0.066	...	2
050802	Swift	...	0.070 ± 0.036	2.03 ± 1.02	4
050814	Swift	...	-0.009 ± 0.180	...	2
050820A	Swift	...	0.061 ± 0.033	1.01 ± 0.75	3
050824	Swift	...	0.289 ± 0.640	...	1
050826	Swift	...	0.063 ± 0.105	1.11 ± 2.28	1
050908	Swift	...	-0.017 ± 0.046	1.10 ± 1.47	1
050922C	Swift	0.06 ± 0.01	0.015 ± 0.003	0.13 ± 0.01	2
051016B	Swift	...	0.008 ± 0.030	...	2
051109A	Swift	...	-0.006 ± 0.025	0.70 ± 1.25	1
051111	Swift	1.70 ± 0.07	0.009 ± 0.004	1.80 ± 0.24	1
060108	Swift	...	0.006 ± 0.040	...	2
060115	Swift	...	0.019 ± 0.029	1.11 ± 1.71	2
060206	Swift	0.01 ± 0.03	0.007 ± 0.004	1.16 ± 0.18	1
060210	Swift	0.15 ± 0.17	0.183 ± 0.033	0.73 ± 0.50	4
060223A	Swift	...	0.036 ± 0.021	0.41 ± 0.23	4
060418	Swift	0.22 ± 0.03	0.104 ± 0.008	0.67 ± 0.08	2
060502A	Swift	4.90 ± 0.11	0.004 ± 0.010	2.94 ± 1.19	1
060510B	Swift	...	0.110 ± 0.060	...	4
060512	Swift	...	0.043 ± 0.173	...	1
060522	Swift	...	0.034 ± 0.185	...	1
060526	Swift	0.17 ± 0.09	0.085 ± 0.030	0.38 ± 0.11	2
060604	Swift	...	0.080 ± 0.338	...	2
060605	Swift	...	-0.013 ± 0.068	1.22 ± 0.72	3
060607A	Swift	1.98 ± 0.11	0.025 ± 0.008	1.23 ± 0.68	1
060707	Swift	...	0.050 ± 0.054	...	2
060714	Swift	...	0.125 ± 0.022	...	≥ 3
060729	Swift	...	0.092 ± 0.041	...	2
060814	Swift	0.29 ± 0.03	0.040 ± 0.003	1.65 ± 0.24	2
060904B	Swift	0.36 ± 0.09	0.003 ± 0.008	1.00 ± 0.16	1
060908	Swift	0.26 ± 0.06	0.061 ± 0.008	0.52 ± 0.09	3
060926	Swift	1.03 ± 0.11	0.148 ± 0.050	...	2

Table 3.1 (cont'd)

GRB	Satellite	τ_{lag}(sec)	V	τ_{RT}(sec)	N_{peak}
060927	Swift	0.12 ± 0.04	0.094 ± 0.010	0.46 ± 0.12	2
061007	Swift	0.11 ± 0.01	0.066 ± 0.003	0.38 ± 0.02	4
061110A	Swift	...	-0.038 ± 0.050	...	1
061110B	Swift	0.24 ± 0.36	0.155 ± 0.064	0.79 ± 0.64	9
061121	Swift	0.03 ± 0.01	0.050 ± 0.003	0.98 ± 0.19	2
061222B	Swift	...	0.024 ± 0.043	...	2
070110	Swift	...	-0.010 ± 0.031	...	1
070208	Swift	...	0.083 ± 0.211	...	2
070318	Swift	...	0.037 ± 0.008	0.72 ± 0.24	1
070411	Swift	...	0.041 ± 0.029	...	2
070506	Swift	2.52 ± 0.04	0.010 ± 0.030	0.12 ± 0.06	1
070508	Swift	0.04 ± 0.01	0.106 ± 0.003	0.20 ± 0.01	4
070521	Swift	0.04 ± 0.01	0.116 ± 0.004	0.58 ± 0.06	5
070529	Swift	...	0.170 ± 0.091	...	1
070611	Swift	...	0.053 ± 0.080	...	1
070612A	Swift	...	0.032 ± 0.023	2.49 ± 1.48	2
070714B	Swift	0.03 ± 0.01	0.164 ± 0.021	0.45 ± 0.04	1
070802	Swift	...	-0.156 ± 0.150	...	1
070810A	Swift	1.09 ± 0.23	-0.006 ± 0.015	0.73 ± 0.22	1
071003	Swift	0.38 ± 0.05	0.072 ± 0.007	0.88 ± 0.07	4
071010A	Swift	...	-0.076 ± 0.153	...	1
071010B	Swift	0.84 ± 0.04	0.010 ± 0.003	1.21 ± 0.03	1
071031	Swift	...	-0.038 ± 0.108	...	2
071117	Swift	0.60 ± 0.01	0.009 ± 0.003	0.20 ± 0.02	1
071122	Swift	...	0.391 ± 0.392	...	1
080210	Swift	0.53 ± 0.17	0.019 ± 0.013	0.57 ± 0.44	3
080310	Swift	...	0.038 ± 0.021	0.41 ± 0.55	3
080319B	Swift	0.02 ± 0.01	0.031 ± 0.003	0.14 ± 0.01	10
080319C	Swift	...	0.042 ± 0.007	0.21 ± 0.12	4
080330	Swift	...	0.109 ± 0.060	...	3
080411	Swift	0.21 ± 0.01	0.167 ± 0.003	0.65 ± 0.01	2
080413A	Swift	0.13 ± 0.03	0.078 ± 0.004	0.23 ± 0.03	3
080413B	Swift	0.23 ± 0.01	0.004 ± 0.003	0.50 ± 0.03	1
080430	Swift	0.68 ± 0.08	0.009 ± 0.004	0.76 ± 0.12	1
080516	Swift	0.15 ± 0.01	0.168 ± 0.055	...	2
080520	Swift	...	0.037 ± 0.098	...	1
080603B	Swift	0.08 ± 0.01	0.283 ± 0.010	0.22 ± 0.03	6

Table 3.1 (cont'd)

GRB	Satellite	τ_{lag}(sec)	V	τ_{RT}(sec)	N_{peak}
080605	Swift	0.11 ± 0.01	0.057 ± 0.003	0.22 ± 0.01	4
080607	Swift	0.04 ± 0.01	0.035 ± 0.003	0.18 ± 0.06	6
080707	Swift	...	0.093 ± 0.032	...	2
080721	Swift	0.13 ± 0.05	0.048 ± 0.009	0.09 ± 0.04	4

Table 3.2. Spectral Luminosity Indicators.

GRB	Satellite	E_{peak} (keV)[a]	α[a]	β[a]	Ref.[b]	$t_{jet}(day)$	Ref.[b]
970228	Konus	115^{+38}_{-38}	-1.54 ± 0.08	-2.5 ± 0.4	...	...	...
970508	BATSE	$389^{+[40]}_{-[40]}$	$-1.19 \pm [0.1]$	$-1.83 \pm [0.4]$	2	25.00 ± 5.00	40
970828	Konus	$298^{+[30]}_{-[30]}$	$-0.704 \pm [0.1]$	$-2.07 \pm [0.4]$	2	2.20 ± 0.40	40
971214	BATSE	$190^{+[20]}_{-[20]}$	$-0.78 \pm [0.1]$	$-2.57 \pm [0.4]$	2	...	...
980703	BATSE	$254^{+[25]}_{-[25]}$	$-1.31 \pm [0.1]$	$-2.4 \pm [0.4]$	2	3.40 ± 0.50	40
990123	BATSE	$604^{+[60]}_{-[60]}$	$-0.9 \pm [0.1]$	$-2.48 \pm [0.4]$	2	2.04 ± 0.46	41
990506	BATSE	$283^{+[30]}_{-[30]}$	$-1.37 \pm [0.1]$	$-2.15 \pm [0.4]$	2	...	...
990510	BATSE	$126^{+[10]}_{-[10]}$	$-1.28 \pm [0.1]$	$-2.67 \pm [0.4]$	2	1.60 ± 0.20	42
990705	Konus	189^{+15}_{-15}	-1.05 ± 0.21	-2.2 ± 0.1	1	1.00 ± 0.20	40
991208	Konus	$190^{+[20]}_{-[20]}$	$[-1.1] \pm [0.4]$	$[-2.2] \pm [0.4]$	3	...	...
991216	BATSE	$318^{+[30]}_{-[30]}$	$-1.23 \pm [0.1]$	$-2.18 \pm [0.4]$	2	1.20 ± 0.40	40
000131	Konus	163^{+13}_{-13}	-1.2 ± 0.1	-2.4 ± 0.1	4	...	...
000210	Konus	408^{+14}_{-14}	$[-1.1] \pm [0.4]$	$[-2.2] \pm [0.4]$	5	...	...
000911	Konus	$986^{+[100]}_{-[100]}$	$-0.84 \pm [0.1]$	$[-2.2] \pm [0.4]$	6	...	...
000926	Konus	100^{+7}_{-7}	$[-1.1] \pm [0.4]$	$-2.43 \pm [0.4]$	5	...	...
010222	Konus	309^{+12}_{-12}	-1.35 ± 0.19	-1.64 ± 0.02	5	0.93 ± 0.10	40
010921	HETE	89^{+22}_{-14}	-1.6 ± 0.1	$[-2.2] \pm [0.4]$	7	...	...
020124	HETE	87^{+18}_{-12}	$-0.8^{+0.2}_{-0.1}$	$[-2.2] \pm [0.4]$	7	3.00 ± 0.40	43
020405	Konus	364^{+90}_{-90}	$[-1.1] \pm [0.4]$	-1.87 ± 0.2	8	1.67 ± 0.52	44
020813	HETE	140^{+14}_{-13}	-0.94 ± 0.03	$-1.57^{+0.03}_{-0.04}$	7	0.43 ± 0.06	40
021004	HETE	80^{+53}_{-23}	-1 ± 0.2	$[-2.2] \pm [0.4]$	7	4.74 ± 0.50	45
021211	HETE	46^{+8}_{-6}	-0.9 ± 0.1	$-2.2^{+0.1}_{-0.3}$	7	...	...
030115	HETE	83^{+53}_{-22}	-1.3 ± 0.1	$[-2.2] \pm [0.4]$	7	...	...
030226	HETE	97^{+27}_{-17}	-0.9 ± 0.2	$[-2.2] \pm [0.4]$	7	1.04 ± 0.12	46
030323	HETE	44^{+90}_{-26}	-0.8 ± 0.8	$[-2.2] \pm [0.4]$	9	...	...
030328	HETE	130^{+14}_{-13}	-1.14 ± 0.03	$-2.1^{+0.2}_{-0.4}$	7	0.80 ± 0.10	47
030329	HETE	68^{+2}_{-2}	-1.26 ± 0.02	-2.28 ± 0.06	7	0.50 ± 0.10	43
030429	HETE	35^{+12}_{-8}	$-1.1^{+0.3}_{-0.2}$	$[-2.2] \pm [0.4]$	7	1.77 ± 1.00	48
030528	HETE	32^{+5}_{-5}	$-1.3^{+0.2}_{-0.1}$	$-2.7^{+0.3}_{-1.0}$	7	...	...
040924	HETE	67^{+6}_{-6}	$-1.17 \pm [0.1]$	$[-2.2] \pm [0.4]$	10, 11	...	...
041006	HETE	63^{+13}_{-13}	$-1.37 \pm [0.1]$	$[-2.2] \pm [0.4]$	11	0.16 ± 0.04	49
050126	Swift	47^{+23}_{-8}	$[-1.1] \pm [0.4]$	$[-2.2] \pm [0.4]$	12	...	...
050223	Swift	$62^{+[10]}_{-[10]}$	$-1.46 \pm [0.1]$	$[-2.2] \pm [0.4]$	13	...	...
050315	Swift	39^{+7}_{-7}	$[-1.1] \pm [0.4]$	$[-2.2] \pm [0.4]$	14	...	...
050401	Swift	118^{+18}_{-18}	-0.9 ± 0.3	-2.55 ± 0.3	15	...	...
050406	Swift	25^{+35}_{-13}	$[-1.1] \pm [0.4]$	-2.56 ± 0.35	16	...	...
050408	HETE	$[100]^{+[100]}_{-[50]}$	$[-1.1] \pm [0.4]$	$[-2.2] \pm [0.4]$	...	...	...

Table 3.2 (cont'd)

GRB	Satellite	E_{peak} (keV)[a]	α[a]	β[a]	Ref.[b]	$t_{jet}(day)$	Ref.[b]
050416A	Swift	15^{+2}_{-3}	$[-1.1] \pm [0.4]$	-3.4 ± 0.4	17	...	...
050505	Swift	70^{+140}_{-24}	-0.31 ± 1	$[-2.2] \pm [0.4]$	12	...	...
050525A	Swift	81^{+1}_{-1}	-1.01 ± 0.06	-3.26 ± 0.2	15	0.40 ± 0.10	50, 51
050603	Swift	344^{+52}_{-52}	-1.03 ± 0.06	-2.03 ± 0.1	15	...	...
050730	Swift	124^{+26}_{-26}	$[-1.1] \pm [0.4]$	$[-2.2] \pm [0.4]$	14	...	...
050802	Swift	121^{+28}_{-28}	$[-1.1] \pm [0.4]$	$[-2.2] \pm [0.4]$	14	...	...
050814	Swift	60^{+24}_{-6}	0 ± 0.6	$[-2.2] \pm [0.4]$	18	...	...
050820A	Swift	246^{+76}_{-40}	-1.25 ± 0.1	$[-2.2] \pm [0.4]$	15	$18^{g} \pm 2.00$	52
050824	Swift	15^{+5}_{-5}	$[-1.1] \pm [0.4]$	$[-2.2] \pm [0.4]$	14	...	...
050826	Swift	105^{+47}_{-47}	$[-1.1] \pm [0.4]$	$[-2.2] \pm [0.4]$	14	...	...
050908	Swift	41^{+9}_{-5}	$[-1.1] \pm [0.4]$	$[-2.2] \pm [0.4]$	12	...	...
050922C	Swift	198^{+38}_{-22}	-0.95 ± 0.07	$[-2.2] \pm [0.4]$	15	0.11 ± 0.03	53
051016B	Swift	24^{+7}_{-7}	$[-1.1] \pm [0.4]$	$[-2.2] \pm [0.4]$	14	...	...
051022	Konus	510^{+22}_{-20}	-1.18 ± 0.02	$[-2.2] \pm [0.4]$	19	2.90 ± 0.20	54
051109A	Swift	161^{+130}_{-35}	$-1.25^{+0.27}_{-0.36}$	$[-2.2] \pm [0.4]$	20	0.60 ± 0.10	55
051111	Swift	220^{+1703}_{-48}	-1 ± 0.18	$[-2.2] \pm [0.4]$	18	0.0080 ± 0.0003	56
060108	Swift	65^{+600}_{-10}	$[-1.1] \pm 0.4$	$[-2.2] \pm [0.4]$	13	...	...
060115	Swift	62^{+19}_{-6}	-1 ± 0.3	$[-2.2] \pm [0.4]$	21	...	...
060206	Swift	78^{+23}_{-8}	-1.2 ± 0.18	$[-2.2] \pm [0.4]$	22	0.57 ± 0.06	57, 58
060210	Swift	149^{+400}_{-35}	-1.18 ± 0.03	$[-2.2] \pm [0.4]$	13	...	...
060223A	Swift	71^{+100}_{-10}	-1.18 ± 0.31	$[-2.2] \pm [0.4]$	13	...	...
060418	Swift	$230^{+[20]}_{-[20]}$	$-1.5 \pm [0.1]$	$[-2.2] \pm [0.4]$	23	...	...
060502A	Swift	156^{+400}_{-33}	-1.18 ± 0.15	$[-2.2] \pm [0.4]$	13	...	...
060510B	Swift	$95^{+[60]}_{-[30]}$	-1.47 ± 0.18	$[-2.2] \pm [0.4]$	13	...	...
060512	Swift	22^{+6}_{-6}	$[-1.1] \pm [0.4]$	$[-2.2] \pm [0.4]$	14	...	...
060522	Swift	80^{+382}_{-12}	-0.7 ± 0.48	$[-2.2] \pm [0.4]$	18	...	...
060526	Swift	$25^{+[5]}_{-[5]}$	$[-1.1] \pm [0.4]$	$[-2.2] \pm [0.4]$	13	2.41 ± 0.06	59
060604	Swift	$40^{+[5]}_{-[5]}$	$-1.34 \pm [0.3]$	$[-2.2] \pm [0.4]$	13	...	...
060605	Swift	90^{+91}_{-12}	-0.3 ± 0.42	$[-2.2] \pm [0.4]$	18	0.24 ± 0.02	60
060607A	Swift	120^{+190}_{-17}	-1.06 ± 0.18	$[-2.2] \pm [0.4]$	13	...	...
060707	Swift	63^{+13}_{-6}	-0.6 ± 0.42	$[-2.2] \pm [0.4]$	22	...	...
060714	Swift	103^{+21}_{-16}	$[-1.1] \pm [0.4]$	$[-2.2] \pm [0.4]$	24	$0.12 \pm [0.01]$	24
060729	Swift	61^{+9}_{-9}	$[-1.1] \pm [0.4]$	$[-2.2] \pm [0.4]$	25	0.50 ± 0.06	61
060814	Swift	257^{+74}_{-35}	-1.43 ± 0.09	$[-2.2] \pm [0.4]$	26	...	...
060904B	Swift	80^{+770}_{-12}	-1 ± 0.42	$[-2.2] \pm [0.4]$	18	...	...
060908	Swift	151^{+112}_{-25}	-1 ± 0.18	$[-2.2] \pm [0.4]$	22	...	...
060926	Swift	20^{+11}_{-11}	$[-1.1] \pm [0.4]$	$[-2.2] \pm [0.4]$	14	...	...

Table 3.2 (cont'd)

GRB	Satellite	E_{peak} (keV)[a]	α[a]	β[a]	Ref.[b]	$t_{jet}(day)$	Ref.[b]
060927	Swift	72^{+15}_{-7}	-0.9 ± 0.24	$[-2.2] \pm [0.4]$	22	...	...
061007	Swift	399^{+12}_{-11}	-0.7 ± 0.02	-2.61 ± 0.09	14	...	...
061110A	Swift	90^{+13}_{-13}	$[-1.1] \pm [0.4]$	$[-2.2] \pm [0.4]$	14	...	...
061110B	Swift	517^{+53}_{-53}	$[-1.1] \pm [0.4]$	$[-2.2] \pm [0.4]$	14	...	...
061121	Swift	606^{+55}_{-44}	$-1.32^{+0.02}_{-0.03}$	$[-2.2] \pm [0.4]$	27	$1.16 \pm [0.16]$	62
061222B	Swift	49^{+8}_{-8}	$[-1.1] \pm [0.4]$	$[-2.2] \pm [0.4]$	14	...	...
070110	Swift	110^{+30}_{-30}	$[-1.1] \pm [0.4]$	$[-2.2] \pm [0.4]$	28	...	...
070208	Swift	51^{+10}_{-10}	$[-1.1] \pm [0.4]$	$[-2.2] \pm [0.4]$	14	...	...
070318	Swift	154^{+19}_{-19}	$[-1.1] \pm [0.4]$	$[-2.2] \pm [0.4]$	14	...	...
070411	Swift	83^{+11}_{-11}	$[-1.1] \pm [0.4]$	$[-2.2] \pm [0.4]$	14	...	...
070506	Swift	31^{+2}_{-3}	-5.00 ± 1.82	2.01 ± 0.22	18	...	...
070508	Swift	233^{+7}_{-7}	-0.96 ± 0.13	$[-2.2] \pm [0.4]$	14	...	...
070521	Swift	222^{+16}_{-12}	-0.93 ± 0.07	$[-2.2] \pm [0.4]$	14	...	...
070529	Swift	180^{+52}_{-52}	$[-1.1] \pm [0.4]$	$[-2.2] \pm [0.4]$	14	...	...
070611	Swift	92^{+30}_{-30}	$[-1.1] \pm [0.4]$	$[-2.2] \pm [0.4]$	14	...	...
070612A	Swift	87^{+17}_{-17}	$[-1.1] \pm [0.4]$	$[-2.2] \pm [0.4]$	14	...	...
070714B	Swift	1120^{+473}_{-230}	-0.86 ± 0.06	$[-2.2] \pm [0.4]$	14	...	...
070802	Swift	70^{+25}_{-25}	$[-1.1] \pm [0.4]$	$[-2.2] \pm [0.4]$	14	...	...
070810A	Swift	44^{+9}_{-9}	$[-1.1] \pm [0.4]$	$[-2.2] \pm [0.4]$	14	...	...
071003	Swift	799^{+75}_{-61}	-0.97 ± 0.04	$[-2.2] \pm [0.4]$	14	...	...
071010A	Swift	27^{+10}_{-10}	$[-1.1] \pm [0.4]$	$[-2.2] \pm [0.4]$	14	...	...
071010B	Swift	52^{+6}_{-8}	$-1.25^{+0.45}_{-0.30}$	$-2.65^{+0.18}_{-0.30}$	29	3.44 ± 0.39	63
071031	Swift	24^{+7}_{-7}	$[-1.1] \pm [0.4]$	$[-2.2] \pm [0.4]$	14	...	...
071117	Swift	278^{+143}_{-48}	-1.53 ± 0.09	$[-2.2] \pm [0.4]$	30	...	...
071122	Swift	73^{+30}_{-30}	$[-1.1] \pm [0.4]$	$[-2.2] \pm [0.4]$	14	...	...
080210	Swift	73^{+15}_{-15}	$[-1.1] \pm [0.4]$	$[-2.2] \pm [0.4]$	14	...	...
080310	Swift	28^{+6}_{-6}	$[-1.1] \pm [0.4]$	$[-2.2] \pm [0.4]$	14	...	...
080319B	Swift	651^{+8}_{-8}	-0.82 ± 0.01	$-3.87^{+0.27}_{-0.66}$	31	...	...
080319C	Swift	307^{+85}_{-56}	-1.01 ± 0.08	$-1.87^{+0.09}_{-0.38}$	32	...	...
080330	Swift	20^{+9}_{-9}	$[-1.1] \pm [0.4]$	$[-2.2] \pm [0.4]$	14	...	...
080411	Swift	259^{+21}_{-16}	$-1.51^{+0.02}_{-0.03}$	$[-2.2] \pm [0.4]$	33	...	...
080413A	Swift	170^{+48}_{-24}	-1.20 ± 0.06	$[-2.2] \pm [0.4]$	34	...	...
080413B	Swift	73^{+10}_{-10}	-1.26 ± 0.16	$[-2.2] \pm [0.4]$	35	...	...
080430	Swift	80^{+15}_{-15}	$[-1.1] \pm [0.4]$	$[-2.2] \pm [0.4]$	14	...	...
080516	Swift	66^{+24}_{-24}	$[-1.1] \pm [0.4]$	$[-2.2] \pm [0.4]$	14	...	...
080520	Swift	12^{+5}_{-5}	$[-1.1] \pm [0.4]$	$[-2.2] \pm [0.4]$	14	...	...
080603B	Swift	85^{+55}_{-18}	$-0.94^{+0.73}_{-0.45}$	$-1.96 \pm [0.4]$	36	...	...

Table 3.2 (cont'd)

GRB	Satellite	E_{peak} (keV)[a]	α[a]	β[a]	Ref.[b]	$t_{jet}(day)$	Ref.[b]
080605	Swift	246^{+14}_{-11}	-1.02 ± 0.06	$[-2.2] \pm [0.4]$	37	...	...
080607	Swift	394^{+35}_{-33}	-1.06 ± 0.05	$[-2.2] \pm [0.4]$	38	...	...
080707	Swift	73^{+20}_{-20}	$[-1.1] \pm [0.4]$	$[-2.2] \pm [0.4]$	14	...	...
080721	Swift	485^{+41}_{-36}	$-0.93^{+0.06}_{-0.05}$	$-2.43^{+0.15}_{-0.25}$	39	...	...

[a]The values reported in square brackets are conservative estimations for uncertainties not reported in the original paper.

Reference of Table 3.2: (1) Amati et al. 2002; (2) Jimenez, Band, & Piran 2001; (3) Golenetskii 2005, private communication; (4) Andersen et al. 2000; (5) Ulanov et al. 2005; (6) Price et al. 2002a; (7) Sakamoto et al. 2005; (8) Price et al. 2003a; (9) Atteia et al. 2005; (10) Golenetskii et al. 2004; (11) HETE Bursts 2006, available at http://space.mit.edu/HETE/Bursts/; (12) Krimm 2005, private communication; (13) Krimm 2006, private communication; (14) calculated from the relation in Zhang et al. 2007; (15) Krimm et al. 2006a; (16) Schady et al. 2006; (17) Sakamoto et al. 2006; (18) Butler et al. 2007; (19) Golenetskii et al. 2005a; (20) Golenetskii et al. 2005b; (21) Barbier et al. 2006a; (22) Sakamoto et al. 2008; (23) Golenetskii et al. 2006a; (24) Krimm et al. 2007; (25) Rykoff et al. 2006; (26) Golenetskii et al. 2006b; (27) Golenetskii et al. 2006c; (28) Amati et al. 2007; (29) Golenetskii et al. 2007a; (30) Golenetskii et al. 2007b; (31) Golenetskii et al. 2008a; (32) Golenetskii et al. 2008b; (33) Golenetskii et al. 2008c; (34) Ohno et al. 2008; (35) Barthelmy et al. 2008; (36) Golenetskii et al. 2008d; (37) Golenetskii et al. 2008e; (38) Golenetskii et al. 2008f; (39) Golenetskii et al. 2008g; (40) Bloom et al. 2003b; (41) Kulkarni et al. 1999; (42) Israel et al. 1999; (43) Berger et al. 2003; (44) Price et al. 2003a; (45) Holland et al. 2003; (46) Klose et al. 2004; (47) Andersen et al. 2003; (48) Jakobsson et al. 2004; (49) Stanek et al. 2005; (50) Liang et al. 2008; (51) Mirebel et al. 2007; (52) Cenko et al. 2006a; (53) Li et al. 2005; (54) Racusin et al. 2005; (55) Yost et al. 2007; (56) Guidozi et al. 2007; (57) Curran et al. 2007; (58)

Stenik et al. 2005; (59) Thoene et al. 2008c; (60) Ferrero et al. 2009; (61) Grupe et al. 2007; (62) Page et al. 2007; (63) Kann et al. 2007;

For those bursts with t_{jet} values, the jet opening angle θ_{jet} (in units of degrees) can be calculated as

$$\theta_{jet} = 0.161 \times [\frac{t_{jet}}{1+z_{trial}}]^{3/8}[\frac{n\eta_\gamma}{E_{\gamma,iso,52}}]^{1/8}, \tag{3.1}$$

where t_{jet} is the jet break time in the unit of days, n is the density of the circumburst medium in particles per cubic centimeter, η_γ is the radiative efficiency, and $E_{\gamma,iso,52}$ is the isotropic energy in units of 10^{52} erg (Rhoads 1997 & Sari et al. 1999). We simply adopt $\eta_\gamma = 0.2$ and $n = 3cm^{-3}$ in Equation 3.1. The beaming factor F_{beam}, is then calculated as

$$F_{beam} = 1 - \cos\theta_{jet}. \tag{3.2}$$

From above we see that, since both θ_{jet} and $E_{\gamma,iso}$ are redshift sensitive, our calculated F_{beam} value also varies between different z_{trial} values.

(4) From all the parameters above, for each of the indicators, a list of the luminosity distances can be calculated as

$$d_{L,i}(z_{trial}) = \sqrt{\frac{L_i(z_{trial})}{4\pi \times P_{bolo}(z_{trial})}}. \tag{3.3}$$

For Ghirlanda's relation, the list of luminosity distances is calculated as

$$d_{L,i}(z_{trial}) = \sqrt{\frac{E_{\gamma,i}(z_{trial})[1+z_{trial}]}{4\pi F_{beam} S_{bolo}(z_{trial})}}. \tag{3.4}$$

Then from each list of luminosity distance above, the distance modulus can be obtained:

$$\mu_i(z_{trial}) = 5\log[d_{L,i}(z_{trial})] - 5, \tag{3.5}$$

with $d_{L,i}(z_{trial})$ expressed in units of parsecs. The uncertainties are propagated strictly following the calculation.

From all above, we are able to get up to four lists of measured distance moduli $\mu_i(z_{trial})$ with their $1-\sigma$ uncertainties: $\mu_{\tau_{lag}} \pm \sigma_{\mu_{\tau_{lag}}}$, $\mu_{E_{peak}} \pm \sigma_{\mu_{E_{peak}}}$, $\mu_{E_{peak}-E_\gamma} \pm \sigma_{\mu_{E_{peak}-E_\gamma}}$, and $\mu_{\tau_{RT}} \pm \sigma_{\mu_{\tau_{RT}}}$. As we have asymmetric uncertainties for E_{peak}, we carry the uncertainties on both directions in the calculation, and generated both plus and minus uncertainties for $\mu_{E_{peak}}$ and $\mu_{E_{peak}-E_\gamma}$. $\mu_{N_{peak}}$ is also calculated, as a lower limit on the distance modulus. All of these distance moduli are a function of the assumed z_{trial} for $0 < z_{trial} < 20$.

(5) Given each trial redshift, we can calculate its distance modulus directly from the cosmological model, $\mu_{cos}(z_{trial})$. Here we adopt the concordance model, with equation of state for dark energy $p = w\rho c^2$, $w = -1$, $\Omega_M = 0.27$, $\Omega_\Lambda = 1 - \Omega_M = 0.73$, and $H_0 = 70(km/s)/Mpc$. In this case, the luminosity distance can be expressed as

$$d_L(z_{trial}) = cH_0^{-1}(1 + z_{trial}) \int_0^{z_{trial}} dz'[(1+z')^3\Omega_M + \Omega_\Lambda]^{-1/2}. \tag{3.6}$$

From the equation above and our list of trial redshifts, a list of luminosity distances $d_L(z_{trial})$ will be calculated, and also a list of distance modulus $\mu_{cos}(z_{trial})$ which equals $5\ log[d_L(z_{trial})] - 5$. The $\mu_{cos}(z_{trial})$ values are only depending on the trial redshift (running from 0 to 20) and the cosmological model we choose.

(6) For each of the trial redshifts from 0 to 20, we have distance moduli lists of $\mu_{\tau_{lag}}$, $\mu_{E_{peak}}$, $\mu_{E_{peak}-E_\gamma}$, $\mu_{\tau_{RT}}$ along with their $1-\sigma$ uncertainties as well as μ_{cos}. We can then compare these $\mu_i(z_{trial})$ with $\mu_{cos}(z_{trial})$ in a χ^2 sense. Thus, $\chi^2_{\tau_{lag}} = [(\mu_{\tau_{lag}} - \mu_{cos})/\sigma_{\mu_{\tau_{lag}}}]^2$ and so on for the other relations. We get a χ^2_i versus z_{trial} plot, as shown in the left panel of Figure 3.1. Then sum over all the χ^2_i, we get a χ^2_{total} ($\chi^2_{total} = \chi^2_{\tau_{lag}} + \chi^2_{E_{peak}} + \chi^2_{E_{peak}-E_\gamma} + \chi^2_{\tau_{RT}} + \chi^2_{N_{peak}}$) versus z_{trial} plot , as in the right panel of Figure 3.1. Our best redshift (z_{best}) corresponds with the minimum χ^2_{total}, where the luminosity relations and the cosmological model agree with each other best. We are also able to find the uncertainties of our z_{best}. By searching through the $\chi^2_{total} - z_{trial}$ plot, we can find the redshifts with which the $\chi^2_{total} = \chi^2_{total,min} + 1$, which corresponds with the edges of the $1-\sigma$ range of our redshift. Similarly, the redshifts

with $\chi^2_{total} = \chi^2_{total,min} + 4$ gives us the $2-\sigma$ range and that with $\chi^2_{total} = \chi^2_{total,min} + 9$ gives the $3-\sigma$ range of our redshift.

3.2 GRBs with Spectroscopic Redshift

We have 107 long GRBs with their spectroscopic/photometric redshifts measured, ranging from Feb. 28, 1997 (GRB970228) to July 21, 2008 (GRB080721), observed by BATSE, Konus, HETE, and *Swift*. The average redshift for pre-*Swift* bursts is about 1.50 and that of the *Swift* bursts is 2.15.

The light curves of *Swift* GRBs are generated from the original data published on the legacy ftp site[1], and the *Swift* Software ver 2.9 (HEAsoft 6.5). To generate a background-subtracted light curve of a GRB, we downloaded an event file sw00xxxxxx000.bevshsp_uf.evt.gz and a mask file sw00xxxxxx000bcbdq.hk.gz, with xxxxxx being the six digit *Swift* trigger number. By running a task 'batbinevt', we can specify the time interval, energy bins, time bin method, output file name and format on generating the light curve. In our work, we adopted a time interval of 0.064 s with uniform time bins, and four continuous energy bands (15-25 keV, 25-50 keV, 50-100 keV and 100-350 keV). For the calculation of V, τ_{RT} and N_{peak}, we have been using the light curve over the whole energy range (15-350 keV), and for the calculation of τ_{lag} value, we use 25-50 keV and 100-350 keV. The light curves of pre-*Swift* bursts are obtained from previous work (Schaefer, 2007).

We calculated the τ_{lag}, V, τ_{RT}, and N_{peak} values for each of these bursts, as listed in Table 3.1. The first column lists the ID number of the GRBs. The second column lists the satellite with the detection of the burst. Columns three to six show all the calculated indicator values, with the name of the indicators shown on the header row. Indicators not measured due to low signal-to-noise ratio of the burst are represented as '...'.

The values of E_{peak} as well as the power law indexes α, β in Band's smoothly broken

[1] ftp://legacy.gsfc.nasa.gov/swift/data/obs

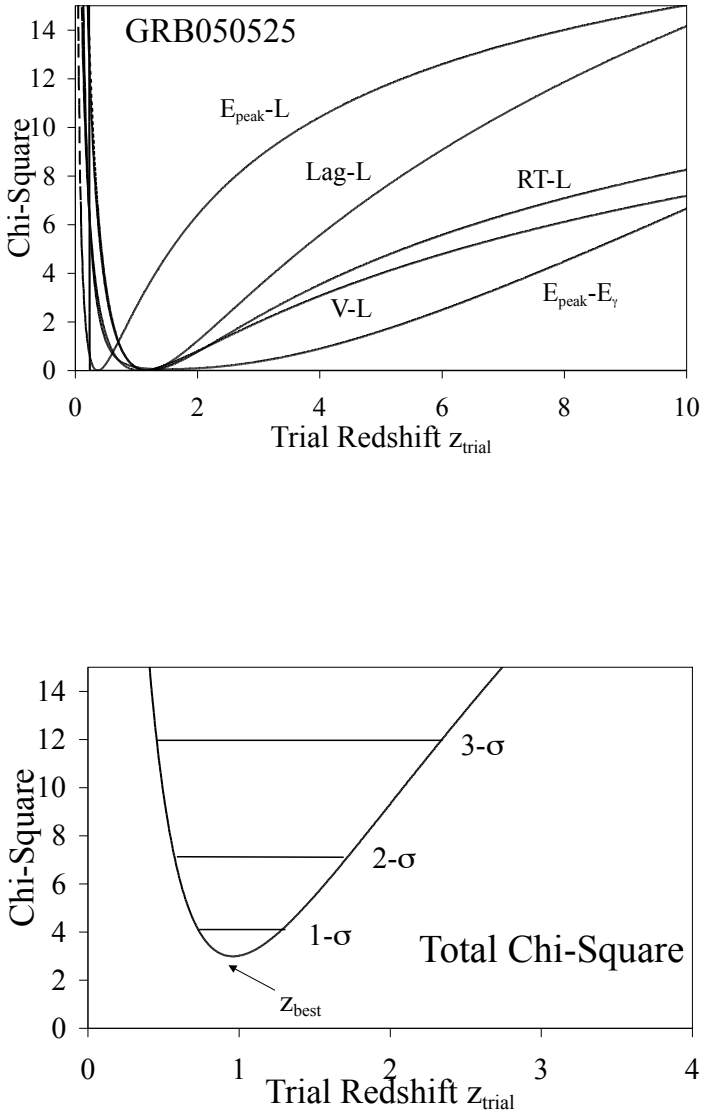

Figure 3.1 One example of the χ^2 plot in our calculation. Taking the μ_{cos} as model value and each of the μ_i as observed value, we can have the χ^2 for each of the indicators, as shown in the top panel. Each of the luminosity relations corresponding with these curves are labeled just beside the lines, and the vertical line on the left is the luminosity lower limit given by the $N_{peak} - L$ relation. We sum up all the included χ^2s to get a total χ^2 plot, as shown in the bottom panel. Then the minimum χ^2 corresponds with our z_{best}, and $\chi^2 = \chi^2_{min} + 1$, 4, 9 gives us the 1,2,3-σ range of our estimated redshifts.

power law model (Band et al. 1993) or E_{peak} and α values in a power law with exponential cutoff model are obtained from various sources, as shown in Table 3.2. The first column in Table 3.2 lists the ID number of the GRBs. The second column lists the satellite with the detection of the burst. Column three to six are the values of E_{peak} and the power law index α and β values, as well as the reference sources of these values. Our jet break time (t_{jet}) values from optical observations and their sources are also listed in Table 3.2, column seven and eight. Bursts without measured jet break time are filled by '...' also. From the table we see that only 33 of the bursts have their optical t_{jet} reported. Various jet break time in the X-ray afterglows have been reported, however, as there are usually multiple breaks for the X-ray afterglows, which are not well understood and distinguished for their causes, we are not including any of these reported t_{jet} values from X-ray detections. Values in square brackets for α and β are assumed values for those bursts without exact α and β values measured, which is taken to be the average value of known α and β (Schaefer et al. 1994; Krimm, et al. 2009; Kaneko et al. 2006; Band, et al. 1993). Some uncertainties of E_{peak} and t_{jet} are also quoted in square brackets. These uncertainties are conservative assumed values, which are normally 10% of the measured E_{peak} or t_{jet} values. All of the peak flux (P) and fluence (S) values of pre-*Swift* bursts we use here are the same as were used in Schaefer (2007), and those of *Swift* bursts are from the data table on the Swift webpage[2]. All the quoted error bars in Table 3.1 and Table 3.2 are converted to $1-\sigma$ level.

The resulting values of z_{best} and $1-\sigma$ range of z for each burst are shown in Table 3.3. We have also collected the spectroscopic redshifts for these bursts (see values and references in Table 3.3). The last column of Table 3.3 lists the effective luminosity relations we used for each burst in our calculation. The number of luminosity indicators used in the redshift calculation for each of the burst is listed in Table 3.3. A comparison can be made between

[2]http://swift.gsfc.nasa.gov/docs/swift/archive/grb_table/

our calculated redshifts and their spectroscopic (or photometric) redshifts. The comparison plot is shown is Figure 3.2, and below are some of the conclusions after we made the analysis:

(1) Of the total 115 bursts, 8 have only a lower z limit that can be calculated. For the remaining 107 bursts, we took the spectroscopic redshifts z_{spec} as the model value, and our calculated redshift z_{best} as a measured value, with the $1-\sigma$ uncertainty of $\sigma_{z_{Plus}}$ and $\sigma_{z_{Minus}}$. Then the χ^2 can be calculated as

$$\chi^2 = \sum_{j=1}^{N_{burst}} (z_{j,best} - z_{j,spec})^2/\sigma_j^2, \tag{3.7}$$

with σ_j equals to $\sigma_{j,z_{Plus}}$ or $\sigma_{j,z_{Minus}}$, depending on whether our $z_{i,best}$ is smaller or larger than the $z_{i,spec}$. Each j represents an index number identifying the burst. The number of degrees of freedom in this comparison equals the number of bursts (N_{burst}), so the reduced χ^2 is χ^2/N_{burst}. The reduced χ^2 value is 1.28, which is somewhat larger than unity. While after excluding one $3-\sigma$ outliers GRB010222, whose contribution to χ^2 is as high as 44, our reduced χ^2 is equal to 0.86. This is certainly not a significant deviation from unity. So we conclude that the scatter in Figure 3.2 is consistent with our quoted error bars being correct.

(2) Of the 107 bursts with their z_{best} calculated, 73 have their z_{spec} falling into the $1-\sigma$ range of our z. The ratio of the numbers is about 70%, which is slightly larger than the ideal case 68.5%. And for the 8 bursts with only lower z limit calculated, 6 of them have their z_{spec} larger than our $1-\sigma$ lower limit of z. This is another way of testing our quoted error bars, and as in the previous item, we find no significant deviation from the expected results. As such, to a close degree, we see that our derived error bars are accurate.

(3) We can test to see whether our z_{best} is biased high or low. For this, we calculated the average value of $log_{10}(z_{best}/z_{spec})$. If our result is unbiased, the average should be zero to within the error bars. We find the average is 0.01. This demonstrates that our z_{best} is not biased to within the 1% level.

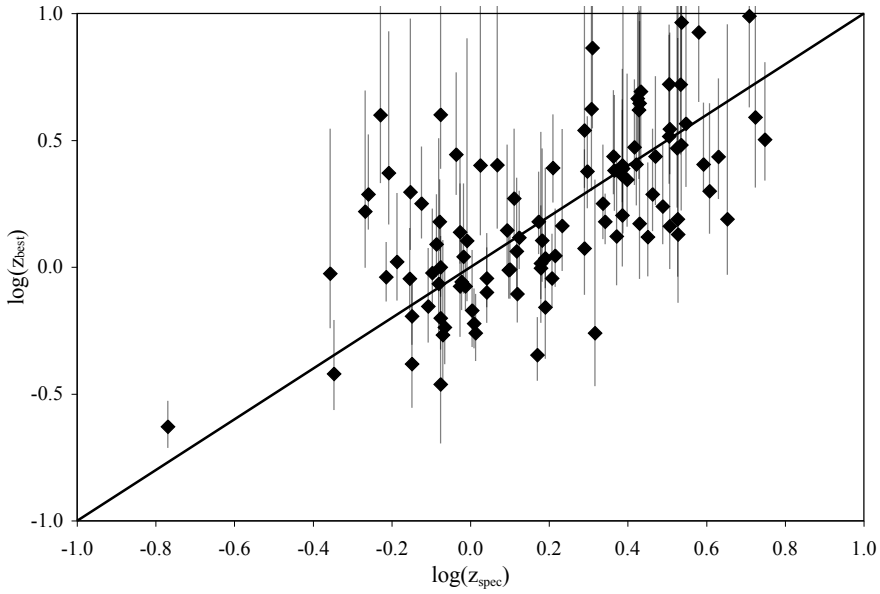

Figure 3.2 Comparison of our redshifts with spectroscopic redshifts. The diamonds are our z_{best} and the error bars gives the 1-σ redshift range. We can see that 70% of the spectroscopic redshifts fall in our 1-σ range, and our z_{best} scatter uniformly around the spectroscopic redshift (with $\langle log(z_{best}/z_{spec})\rangle = 0.01$). This demonstrates that our method has accurate error bars and negligible biases.

Table 3.3. Our Redshifts and Spectroscopic Redshifts.

GRB	Experiment	z_{spec}	Ref.[a]	z_{best}	z_{min}	z_{max}	N_{rel}
970228	Konus	0.84	1	0.38	0.18	0.86	2
970508	BATSE	0.84	2	1.51	1.11	2.09	4
970828	Konus	0.96	3	1.10	0.73	1.83	4
971214	BATSE	3.42	4	5.21	2.00	20	3
980703	BATSE	0.97	5	0.84	0.66	1.11	4
990123	BATSE	1.61	6	0.91	0.67	1.27	4
990506	BATSE	1.31	7	1.16	0.77	1.84	4
990510	BATSE	1.62	8	2.47	1.69	3.66	5
990705	Konus	0.84	9	0.63	0.45	0.94	4
991208	Konus	0.71	10	0.46	0.29	0.78	3
991216	BATSE	1.02	11	0.60	0.47	0.79	5
000131	Konus	4.50	12	1.75	0.90	4.41	3
000210	Konus	0.85	13	0.59	0.35	1.04	2
000911	Konus	1.06	14	2.88	1.06	18.31	3
000926	Konus	2.07	15	0.60	0.31	1.41	2
010222	Konus	1.48	16	0.45	0.35	0.61	4
010921	HETE	0.45	17	0.40	0.28	0.59	3
020124	HETE	3.20	18	5.27	3.24	8.12	5
020405	Konus	0.70	19	0.90	0.64	1.32	4
020813	HETE	1.25	20	0.98	0.72	1.36	5
021004	HETE	2.32	21	2.41	1.53	4.06	5
021211	HETE	1.01	22	0.71	0.49	1.07	3
030115	HETE	2.50	23	2.24	1.34	4.12	3
030226	HETE	1.98	24	2.39	1.59	3.58	5
030323	HETE	3.37	25	1.52	0.55	20	2
030328	HETE	1.52	26	1.28	0.80	2.34	5
030329	HETE	0.17	27	0.24	0.19	0.29	5
030429	HETE	2.66	28	4.62	2.41	8.25	4
030528	HETE	0.78	29	0.77	0.53	1.14	3
040924	HETE	0.86	30	0.61	0.42	0.91	3
041006	HETE	0.71	31	0.64	0.48	0.89	4
050126	Swift	1.29	32	1.64	1.00	2.91	3
050223	Swift	0.59	33	2.80	0.94	20	1
050315	Swift	1.95	34	0.82	0.45	1.78	3
050401	Swift	2.90	35	2.02	1.23	3.63	4
050406	Swift	2.44	36	1.68	0.71	20	2
050408	HETE	1.24	37	1.43	0.90	2.40	3

Table 3.3 (cont'd)

GRB	Experiment	z_{spec}	Ref.[a]	z_{best}	z_{min}	z_{max}	N_{rel}
050416A	Swift	0.65	38	0.73	0.43	1.33	2
050505	Swift	4.27	39	2.73	1.68	4.67	4
050525A	Swift	0.61	40	0.92	0.71	1.21	5
050603	Swift	2.82	41	1.24	0.69	2.69	2
050730	Swift	3.97	42	> 2.53			2
050802	Swift	1.71	43	1.09	0.61	2.41	3
050814	Swift	5.30	44	2.70	0.89	20.00	2
050820A	Swift	2.61	45	2.97	1.96	4.80	4
050824	Swift	0.83	46	0.61	0.30	1.50	1
050826	Swift	0.30	47	> 2.42			2
050908	Swift	3.35	48	2.02	0.84	9.23	2
050922C	Swift	2.20	49	1.51	1.20	1.90	5
051016B	Swift	0.94	50	0.65	0.32	1.52	2
051022	Konus	0.80	51	0.95	0.66	1.51	3
051109A	Swift	2.35	52	1.33	0.74	2.34	3
051111	Swift	1.55	53	1.09	0.79	1.48	4
060108	Swift	2.03	54	2.96	0.74	20	2
060115	Swift	3.53	55	2.63	0.99	20	3
060206	Swift	4.05	56	1.73	0.93	4.02	4
060210	Swift	3.91	57	2.54	1.95	3.97	4
060223A	Swift	4.41	58	> 2.06			3
060418	Swift	1.49	59	1.41	0.92	2.25	4
060502A	Swift	1.51	60	0.86	0.55	1.37	3
060510B	Swift	4.90	61	> 1.72			2
060512	Swift	0.44	62	0.64	0.31	1.69	1
060522	Swift	5.11	63	7.24	1.08	20	1
060526	Swift	3.21	64	3.50	2.07	6.57	5
060604	Swift	2.68	65	2.72	0.97	20	2
060605	Swift	3.80	66	6.79	1.96	20	4
060607A	Swift	3.08	67	1.47	0.92	2.48	3
060707	Swift	3.43	68	2.15	0.78	20	2
060714	Swift	2.71	69	3.77	1.09	20	3
060729	Swift	0.54	70	1.66	0.81	3.48	3
060814	Swift	0.84	71	0.93	0.63	1.43	4
060904B	Swift	0.70	72	1.89	0.81	5.46	3
060908	Swift	2.43	73	2.13	1.30	3.84	4
060926	Swift	3.21	74	1.44	0.83	2.71	3

Table 3.3 (cont'd)

GRB	Experiment	z_{spec}	Ref.[a]	z_{best}	z_{min}	z_{max}	N_{rel}
060927	Swift	5.60	75	3.24	1.81	6.44	4
061007	Swift	1.26	76	0.94	0.65	1.42	4
061110A	Swift	0.76	77	> 1.82			1
061110B	Swift	3.44	78	8.28	3.35	20	4
061121	Swift	1.31	79	0.79	0.58	1.11	5
061222B	Swift	3.36	80	1.10	0.50	3.68	2
070110	Swift	2.35	81	> 1.995			1
070208	Swift	1.17	82	1.76	0.70	10.15	2
070318	Swift	0.84	83	3.42	1.43	18.32	2
070411	Swift	2.95	84	2.73	1.53	4.72	2
070506	Swift	2.31	85	2.73	1.80	4.38	3
070508	Swift	0.82	86	1.25	0.81	2.02	4
070521	Swift	0.55	87	2.08	1.27	3.73	4
070529	Swift	2.50	88	> 1.67			1
070611	Swift	2.04	89	5.55	1.24	20	1
070612A	Swift	0.62	90	1.82	0.85	5.61	3
070714B	Swift	0.92	91	3.12	1.74	6.97	3
070802	Swift	2.45	92	9.37	1.51	20	1
070810A	Swift	2.17	93	1.53	0.97	2.56	3
071003	Swift	1.10	94	0.83	0.56	1.25	4
071010A	Swift	0.98	95	0.86	0.38	2.88	1
071010B	Swift	0.95	96	0.76	0.53	1.12	4
071031	Swift	2.69	97	1.10	0.52	3.40	2
071117	Swift	1.33	98	1.13	0.76	1.74	3
071122	Swift	1.14	99	> 1.05			1
080210	Swift	2.64	100	2.35	1.37	4.42	4
080310	Swift	2.43	101	1.19	0.60	3.22	3
080319B	Swift	0.94	102	1.45	0.95	2.34	4
080319C	Swift	1.95	103	3.62	1.31	20	3
080330	Swift	1.51	104	0.79	0.37	1.94	2
080411	Swift	1.03	105	0.51	0.36	0.74	4
080413A	Swift	2.43	106	2.42	1.47	4.36	4
080413B	Swift	1.10	107	0.73	0.50	1.11	3
080430	Swift	0.77	108	1.56	1.00	2.60	3
080516	Swift	3.20	109	3.62	1.86	7.96	3
080520	Swift	1.55	110	0.52	0.25	1.21	1
080603B	Swift	2.69	111	4.55	2.40	9.88	4

Table 3.3 (cont'd)

GRB	Experiment	z_{spec}	Ref.[a]	z_{best}	z_{min}	z_{max}	N_{rel}
080605	Swift	1.64	112	1.06	0.71	1.65	4
080607	Swift	3.04	113	1.32	0.82	2.29	4
080707	Swift	1.23	114	2.35	0.77	20	2
080721	Swift	2.60	115	1.13	0.72	1.86	4

References of Table 3.3. — (1) Djorgovski et al. 1997; (2) Metzger et al. 1997; (3) Djorgovski et al. 2001a; (4) Kulkarni et al. 1998; (5) Djorgovski et al. 1998a; (6) Kelson et al. 1999; (7) Bloom et al. 2003a; (8) Vreeswijk et al. 1999a; (9) Le Floc'h et al. 2002; (10) Dodonov et al. 1999; (11) Vreeswijk et al. 1999b; (12) Andersen et al. 2000; (13) Piro et al. 2002; (14) Price et al. 2002b; (15) Fynbo et al. 2000; (16) Calkins 2000; (17) Djorgovski et al. 2001b; (18) Hjorth et al. 2003; (19) Masetti et al. 2002; (20) Price et al. 2002a; (21) Chornock & Filippenko 2002; (22) Vreeswijk et al. 2002; (23) Levan et al. 2006; (24) Price et al. 2003b; (25) Vreeswijk et al. 2003; (26) Martini et al. 2003; (27) Greiner et al. 2003; (28) Weidinger et al. 2003; (29) Rau, Salvato, & Greiner 2005; (30) Wiersema et al. 2004; (31) Fugazza et al. 2004; (32) Berger et al. 2005a; (33) Berger & Min-Su Shin 2006; (34) Kelson & Berger 2005; (35) Fynbo et al. 2005a; (36) Schady et al. 2006; (37) Berger et al. 2005c; (38) Cenko et al. 2005; (39) Berger et al. 2005b; (40) Foley et al. 2005; (41) Berger & Becker 2005; (42) Chen et al. 2005; (43) Fynbo et al. 2005b; (44) Jakobsson et al. 2005b; (45) Prochaska et al. 2005b; (46) Fynbo, et al. 2005c; (47) Halpern & Mirabal et al. 2005; (48) Fugazza et al. 2005; (49) Jakobsson et al. 2005a; (50) Soderberg et al. 2005; (51) Gal-Yam et al. 2005; (52) Quimby et al. 2005; (53) Hill et al. 2005; (54) Melandri et al. 2006; (55) Piranomonte et al. 2006; (56) Fynbo et al. 2006a; (57) Cucchiara et al. 2006a; (58) Berger et al. 2006a; (59) Dupre et al. 2006; (60) Cucchiara et al. 2006b; (61) Price et al. 2006; (62) Bloom et al. 2006a; (63) Cenko et al. 2006b; (64) Berger & Gladders 2006; (65) Castro-Tirado et al. 2006; (66) Peterson et al. 2006; (67) Ledoux et al. 2006; (68) Jakobsson et al. 2006a; (69)

Jakobsson et al. 2006b; (70) Thoene et al. 2006a; (72) Fugazza et al. 2006; (73) Rol et al. 2006; (74) D'Elia, et al. 2006; (75) Fynbo et al. 2006b; (76) Osip et al. 2006; (77) Thoene et al. 2006b; (78) Fynbo et al. 2006c; (79) Bloom et al. 2006; (80) Berger 2006; (81) Jaunsen et al. 2007a; (82) Cucchiara et al. 2007; (83) Jaunsen et al. 2007b; (84) Jakobsson et al. 2007a; (85) Thoene et al. 2007a; (86) Jakobsson et al. 2007b; (87) Hattori et al. 2007; (88) Berger et al. 2007; (89) Thoene et al. 2007b; (90) Cenko et al. 2007a; (91) Graham et al. 2007; (92) Prochaska et al. 2007a; (93) Thoene et al. 2007c; (94) Perley et al. 2007; (95) Prochaska, J. X. et al. 2007b; (96) Cenko et al. 2007b; (97) Ledoux et al. 2007; (98) Jakobsson et al. 2007c; (99) Cucchiara et al. 2007b; (100) Jakobsson et al. 2008a; (101) Prochaska, et al. 2008a; (102) Vreeswijk et al. 2008a; (103) Wiersema et al. 2008; (104) Malesani et al. 2008; (105) Thoene et al. 2008a; (106) Thoene et al. 2008b; (107) Vreeswijk et al. 2008b; (108) Cucchiara & Fox 2008; (109) Filgas et al. 2008; (110) Jakobsson et al. 2008b; (111) Fynbo et al. 2008a; (112) Jakobsson et al. 2008c; (113) Prochaska, et al. 2008b; (114) Fynbo et al. 2008b; (115) D'Avanzo et al. 2008;

(4) To test the accuracy of our z_{best} comparing with the z_{spec}, we calculated the RMS scatter of $log_{10}(z_{best}/z_{spec})$. The result comes out to be 0.26, while the RMS scatter of $log_{10}(z_{spec})$ is 0.30. In Schaefer (2007) it was pointed out that the accuracy of the redshift estimation is 26% (corresponding to a $log_{10}(z_{best}/z_{spec})$ RMS of 0.11), which is better than what we are claiming here. The reason for the larger RMS scatter is, although we are dealing with the GRBs with known z_{spec}, we are not making any use of the z_{spec} in our whole calculation, and our luminosity L, luminosity distance d_L, distance modulus μ_{ind}, as well as the bolometric flux and fluence P_{bolo} and S_{bolo} are all varying with our trial redshift. This brought us one extra degree of freedom in the calculation, which caused larger uncertainties in our result. When the known z_{spec} value is used (as for the Hubble diagram work in Schaefer 2007), the scatter becomes substantially small as compared to our work

in this paper. Another reason for the large RMS is because it is mostly dominated by the very noisy bursts (those bursts with low signal to noise ratio, inaccurate measurement of luminosity indicators, and large error bars for z_{best} results), which are not able to be used for the notification of the redshifts. If we make a selection on bursts with relatively accurate redshift estimation, say bursts with $\sigma_{z_{minus}/z_{best}} < 0.5$ and $\sigma_{z_{plus}/z_{best}} < 1$, we get the RMS of $log(z_{best}/z_{spec})$ of 0.19, which is much smaller, and the RMS scatter of $log_{10}(z_{spec})$ for this subsample is 0.28.

(5)We made the same calculation with pre-*Swift* luminosity relations for calculating *Swift* redshifts and *Swift* luminosity relations for calculating pre-*Swift* redshifts, which we call $z_{best,II}$. Our calculation of $z_{best,II}$ is totally independent of the spectroscopic redshifts, as for each burst, the luminosity relations used in the calculation are calibrated independent of the z_{spec} for any individual burst. The comparison between z_{best} and $z_{best,II}$ will also show the difference between *Swift* and pre-*Swift* luminosity relations. The comparison plot between z_{spec} and $z_{best,II}$ is shown on Figure 3.3. From the comparison between Figure 3.3 and Figure 3.2 we see that, the scatter and distribution of z_{best} and $z_{best,II}$ do not differ significantly from each other. Actually, from our calculation, the average value of $log_{10}(z_{best,II}/z_{spec})$ is -0.02, and the RMS scatter of $log_{10}(z_{best,II}/z_{spec})$ is 0.27, both of which are equal to those of our z_{best} value within error bars. This result demonstrate that those two sets of z_{best} values do not differ from each other, which means that these two sets of luminosity relations do not have significant difference. It also tells us that the effect of redshift involved in our calculation (in fitting luminosity relations) is negligible.

(6)We need to verify whether our result is effective in selecting high redshift bursts. If our predicted redshift is z, the possibility of a real redshift to be higher than z and lower than z are both 50%, which cannot be used as a test. However, by considering our uncertainties of z_{best}, if our predicted redshift is 2z, we can make a test by counting how many of the GRBs are with real redshifts larger than z. As there are not many bursts with high redshifts, a

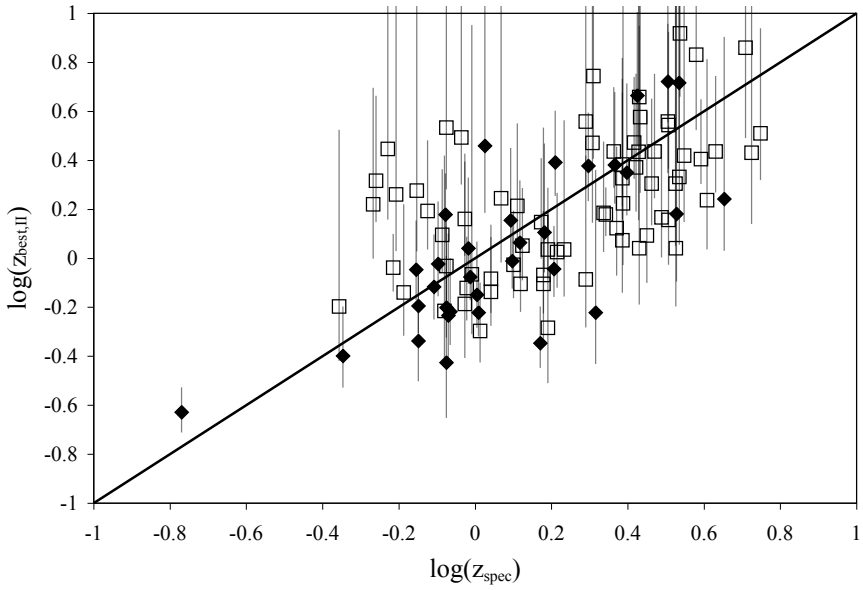

Figure 3.3 We made a comparison between our z_{best} and $z_{best,II}$. $z_{best,II}$ are the calculated redshift values when we apply *Swift* luminosity relations on pre-*Swift* data and pre-*Swift* relations on *Swift* data. The analysis on $z_{spec,II}$ and z_{spec} data shows that the average value of $log_{10}(z_{best,II}/z_{spec})$ is -0.02, and the RMS scatter of $log_{10}(z_{best,II}/z_{spec})$ is 0.27, both of which are equal to those of our z_{best} value within error bars. From this we see that these two sets of redshifts do not differ much from each other, which also means that the pre-*Swift* luminosity relations and *Swift* luminosity relations do not have significant difference. It also tells us that the effect of redshift involved in our calculation is negligible.

test is done on a relatively lower redshift region, where most of the GRBs are involved. We picked up all our GRBs with predicted $z > 4$, the total number is 12, and 0 out of 12 have their spectroscopic redshift $z < 2$. This result tells us that our method is actually effective in demographic studies and in picking up high z bursts, if we take into account the error bars before we make the prediction.

From all the analysis above, we can conclude that our z_{best} is not biased on average, and our $1-\sigma$ error bars are accurate. We can claim that our method works well on the bursts with known spectroscopic redshifts, and can be applied to all long GRBs (even without their z_{spec} measured).

3.3 Swift GRB Redshift Catalog

3.3.1 Our Data

We collected all the *Swift* GRBs from 2004, December 20 (GRB041220) to 2008, July 23 (GRB080723A). Most of the data are downloaded from the legacy ftp site[3], and the *Swift* software ver 2.9 (HEAsoft 6.5) is used.

The total number of GRBs within the time range is 339. Several types of GRBs are not included in our catalog, which are listed as below. Some of these GRBs are those with short time duration and hard spectrum, which are classified in the short-duration class. These short-duration GRBs do not follow the luminosity relations that we are using in our analysis, and we are not able to generate their redshifts from the light curve and spectrum. Some of the GRBs are reported by the detection from the ground analysis or from the *Swift* BAT slew survey, for which the BAT light curve can not be obtained from either of these sources listed above. Some of the bursts are marked as 'possible burst' in their original discovery. These bursts either have abnormal light curves, or the signal to noise ratio is too low to be identified as a burst. Some of the bursts are originally included in our sample, and

[3]ftp://legacy.gsfc.nasa.gov/swift/data/obs

were later found out to be too noisy or too faint that no useful information can be obtained from the light curve and the spectrum. By excluding all the these GRBs listed above, the number of remaining GRBs in our catalog is 277. Bursts not included in our catalog are listed in Table 3.4. Of those 277 bursts, 83 have their spectroscopic/photometric redshift reported, which accounts for about 30% of the sample. Redshifts of bursts with multiple or conflicted reported values are not counted.

E_{peak} values as well as the power law indexes α and β are drawn from various sources, and the remaining luminosity indicators (τ_{lag}, V, τ_{RT} and N_{peak}) are directly calculated from the light curves. Peak flux P and fluence S values between energy band 15 keV to 150 keV with 90% measurement errors are all downloaded from the *Swift* data table[4]. To be consistent in our whole calculation, we converted the 90% measurement error to $1-\sigma$ errors. All of the indicator values and their sources are listed in Table 3.6.

3.3.2 Our Redshift Measurements

Besides our method of measuring GRB redshift through the luminosity indicators and relations, we also collected some other information which will be useful to make an estimation or a constraint on the GRB redshift. These information are mostly from the UVOT detection and from the community with photometric or spectroscopic observations of the GRB afterglow.

As described in the first section, *Swift* is a multi-wavelength GRB detection satellite which has fast localizing with a wide field Gamma ray alert instrument BAT, and two narrow field fast responding instrument in X-ray and UV/optical bands (XRT and UVOT). The accurate position is then distributed to the community through GCN, and large ground telescopes will be able to make their own observations. With the analysis of the spectroscopic features (e.g. absorption lines) of the afterglows, redshifts of the GRBs are measured, with relatively

[4]http://swift.gsfc.nasa.gov/docs/swift/archive/grb_table/

high accuracy. We collected all the reported spectroscopic redshifts from the GCN Circulars archive and the literature. Some of the GRBs have multiple or conflicted redshifts reported and we did not include them. All the spectroscopic redshifts and their sources are listed in Table 3.7.

Detections from optical telescopes are also used to put the upper limit on redshifts of given GRBs. As we know, in the rest frame of a GRB, a complete break exists in the spectrum at a wavelength of around 912Å due to the ionization edge of hydrogen, known as the Lyman break. In the observers' rest frame, this 912Å Lyman break line will be redshifted. The wavelength of the break line λ would be

$$\lambda = 912\mathring{A} \times (1 + z), \tag{3.8}$$

where z is the redshift of the GRB. For GRBs with $z > 1$, the Lyman break line will be redshifted to the optical and observable ultraviolet region. If we search through the optical and observable UV detections and find the break at wavelength λ, the photometric redshift will be

$$z_{phot} = \lambda/912\mathring{A} - 1. \tag{3.9}$$

Table 3.4. Bursts not included in our catalog.

GRBs	Cause	GRBs	Cause
050202	short burst	050318	incomplete light curve
050507	incomplete light curve	050509B	short burst
050724	short burst	050813	short burst
050906	short burst	050911	short burst
050922B	too noisy	050925	short burst[a]
051012	ground analysis discovery	051105A	short burst
051114	ground analysis discovery	051210	short burst
051221A	short burst	051227	possibly short burst
060123	BAT no trigger	060124	incomplete light curve
060218	incomplete light curve	060219	too noisy
060313	short burst	060323	incomplete light curve
060502B	short burst	060505	possible short burst
060516	too noisy	060614	possible short burst
060728	questionable burst	060801	short burst
060906	too noisy[e]	061006	short burst
061027	questionable burst	061201	short burst
061210	short burst	061217	short burst
061218	too noisy	070126	too noisy
070129	too noisy	070209	short burst
070224	too noisy	070227	ground analysis discovery
070326	BATSS[c]	070406	short burst
070419A	too noisy	070429B	short burst
070610	questionable burst	070714B	short burst[b]
070724A	short burst	070729	short burst
070809	possible short burst	070810B	short burst
070923	short burst	071006	ground analysis discovery
071010C	ground analysis discovery	071013	too noisy
071018	questionable burst	071028A	too noisy
071028B	ground analysis discovery	071112B	short burst
071112C	no event files	071118	too noisy
071227	possible short burst	080121	short burst[d]
080123	short burst	080129	too noisy
080130	BATSS[d]	080207	too noisy
080218A	too noisy	080315	questionable burst
080325	too noisy	080405	ground analysis discovery
080503	short burst[b]	080524	ground analysis discovery
080604	too noisy	080702A	short burst

Table 3.4 (cont'd)

GRBs	Cause	GRBs	Cause
080702B	BATSS[c]	080710	too noisy

[a]suggested a probable Soft Gamma-Ray Reperter

[b]short hard burst with long extended emissions

[c]*Swift* BAT slew survey discovery

[d]below *Swift* threshold

[e]possible incomplete light curve

In most cases, optical fluxes are detected in some energy band (e.g. R), and not in the adjacent energy band (e.g. V). It might be because the Lyman break is somewhere between V and R band, in which case the photometric redshift of the GRB can be determined. There are some other factors that might affect the results, e.g. detection time after the discovery of the burst (the afterglow fades fast after the burst), magnitude limit of the detection (no detection in some certain energy band might be just because the detector cannot go deep enough), etc. As a result, we cannot simply claim that the Lyman break is between energy bands R and V. What we can claim is that at least the Lyman break is redshifted to a wavelength which is shorter than the typical wavelength of R band, because at least the Lyman break did not show up in R band. In this case, an upper limit on λ and hence the redshift of the GRB can be calculated. It is complex to choose the wavelength of each energy band that can produce a detection. To be conservative, we take the maximum wavelength of the bluest band with afterglow detection as the limit wavelength of the Lyman break, and a loose limit on the redshift of the GRB is then calculated from equation (2), the maximum wavelength for each energy band and the corresponding redshift limits are listed in Table

Table 3.5. Optical Detection Redshift Limit

Energy Band	Typical Wavelength	Redshift Limit
R	6900	6.57
V	5500	5.03
B	4300	3.71
U	3500	2.84
W1	2500	1.74
M2	2200	1.41
W2	1900	1.08
g'	4900	4.37
r'	6300	5.91
I'	7700	7.44
z'	8800	8.65

3.5. The first column of the table is the energy band. The second is the typical wavelength we choose, and the third column is the corresponding redshift upper limit for the GRB.

In our work, we collected all the reported optical detections of each GRB, most of which are UVOT detections of *Swift*, and the others are typically from various ground telescopes. The energy bands that UVOT is using are V, B, U, UVW1, UVM2, and UVW2, from long to short wavelength. Other energy band that have been using by ground telescopes are the sloan filters i', r', g', u'. All the redshift limits from the photometric observations are shown in Table 5, labeled as $z_{phot,lim}$.

3.3.3 Our Results

For those bursts with spectroscopic redshifts, we made a cumulative redshift distribution comparison plot for z_{spec} and our z_{best}, as shown in Figure 3.4. The figure shows slight difference between these two cumulative distributions. By running a Kolmogorov-Smirnov test, we find that the maximum difference between these two cumulative distribution functions is 0.15, and the p value for the test is 0.30. The difference between these two cumulative

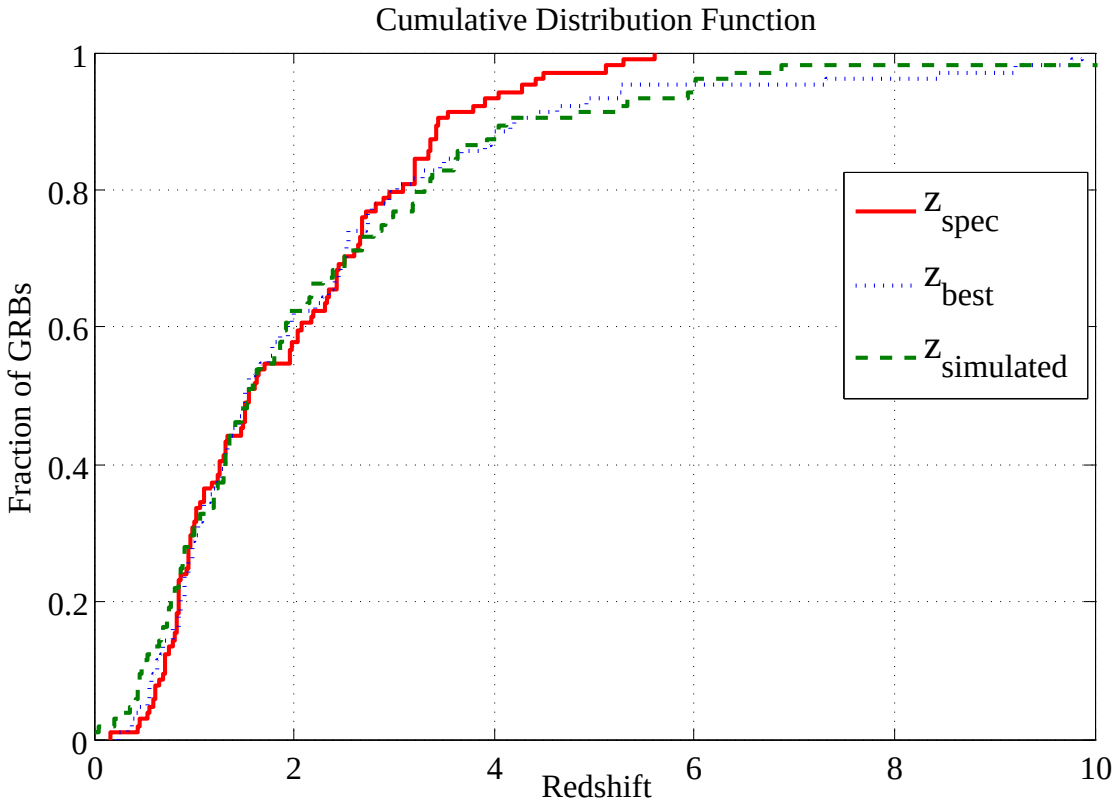

Figure 3.4 Redshift distribution plot for GRBs with spectroscopic redshift. The comparison is made between z_{spec} and our z_{best}. The figures show no big difference between these two cumulative distributions. By running a Kolmogorov-Smirnov test between these two distribution, we find that the maximum difference between these two cumulative distribution function is 0.15, and the p value for the test is 0.30, which means that these two cumulative distributions agree well with each other, hence it is evidence to show that our redshift distribution is not biased.

distribution plot is mostly contributed by the high redshift tail, where the typical offset is about 5%. This high redshift tail is simply caused by the random offset of our z_{best} on z_{spec}, which is mainly caused by the noise effect. This effect is simulated by running a Monte Carlo process.

Table 3.6. Luminosity Indicators.

GRB	$\tau_{lag}(sec)$	Variability	τ_{RT}(sec)	N_{peak}	E_{peak}(keV)[a]	α[a]	β[a]	Ref.	t_{jet}(day)	Ref.
041220	0.35 ± 0.03	0.035 ± 0.011	0.21 ± 0.09	1	92^{+20}_{-20}	[-1.1] ± [0.4]	[-2.2] ± [0.4]	1	...	...
041223	0.09 ± 0.01	0.123 ± 0.003	0.29 ± 0.04	8	400^{+242}_{-61}	0.9 ± 0.06	[-2.2] ± [0.4]	2	...	...
041224	0.54 ± 0.42	0.057 ± 0.012	0.65 ± 0.80	3	74^{+10}_{-5}	-1.1 ± 0.18	[-2.2] ± [0.4]	3	...	...
041226	...	-0.074 ± 0.091	1.35 ± 1.08	1	171^{+117}_{-117}	[-1.1] ± [0.4]	[-2.2] ± [0.4]	1	...	...
041228	...	0.001 ± 0.020	1.28 ± 1.26	2	105^{+19}_{-19}	[-1.1] ± [0.4]	[-2.2] ± [0.4]	1	...	...
050117	0.14 ± 0.02	0.321 ± 0.015	0.77 ± 0.25	14	143^{+65}_{-20}	-1.2 ± 0.12	[-2.2] ± [0.4]	3	...	...
050124	0.03 ± 0.02	0.039 ± 0.008	0.15 ± 0.04	2	95^{+24}_{-10}	0.7 ± 0.24	[-2.2] ± [0.4]	3	...	...
050126	2.74 ± 0.02	-0.010 ± 0.065	1.58 ± 1.91	1	47^{+23}_{-8}	[-1.1] ± [0.4]	[-2.2] ± [0.4]	4	...	...
050128	-0.06 ± 0.03	0.152 ± 0.016	0.58 ± 0.36	4	113^{+28}_{-12}	-0.7 ± 0.24	[-2.2] ± [0.4]	3	...	...
050215A	...	0.146 ± 0.100	...	2	147^{+61}_{-61}	[-1.1] ± [0.4]	[-2.2] ± [0.4]	1	...	...
050215B	...	0.900 ± 1.030	...	1	18^{+6}_{-13}	[-1.1] ± [0.4]	[-2.2] ± [0.4]	5	...	...
050219A	1.99 ± 0.21	0.013 ± 0.007	4.09 ± 1.01	1	92^{+7}_{-5}	-0.1 ± 0.18	[-2.2] ± [0.4]	3	...	...
050219B	0.97 ± 0.03	0.036 ± 0.005	0.59 ± 0.17	3	108^{+21}_{-10}	-1 ± 0.18	[-2.2] ± [0.4]	3	...	...
050223	...	0.111 ± 0.094	...	1	$62^{+[10]}_{-[10]}$	-1.46 ± [0.1]	[-2.2] ± [0.4]	6	...	...
050306	...	0.134 ± 0.025	...	6	140^{+73}_{-18}	-0.9 ± 0.18	[-2.2] ± [0.4]	2	...	...
050315	...	0.032 ± 0.016	1.97 ± 1.62	2	39^{+7}_{-7}	[-1.1] ± [0.4]	[-2.2] ± [0.4]	1	[b]	78, 79, 80
050326	0.12 ± 0.01	0.151 ± 0.005	0.40 ± 0.04	3	201^{+15}_{-15}	-0.74 ± 0.05	-2.49 ± 0.1	7	...	...
050401	0.06 ± 0.02	0.187 ± 0.019	0.25 ± 0.16	3	118^{+18}_{-18}	-0.9 ± 0.3	-2.55 ± 0.3	8	[c]	78, 81, 82
050406	...	0.020 ± 0.274	...	2	25^{+35}_{-13}	[-1.1] ± [0.4]	-2.56 ± 0.35	9	...	...
050410	...	-0.013 ± 0.029	...	3	74^{+12}_{-5}	-0.8 ± 0.24	[-2.2] ± [0.4]	3	...	...
050412	...	0.093 ± 0.054	2.86 ± 5.59	1	1706^{+890}_{-890}	[-1.1] ± [0.4]	[-2.2] ± [0.4]	1	...	...
050416A	...	0.021 ± 0.030	0.54 ± 0.06	1	15^{+2}_{-3}	[-1.1] ± [0.4]	-3.4 ± 0.4	10	[c]	78, 81, 82
050416B	0.56 ± 0.01	0.024 ± 0.014	0.10 ± 0.01	1	94^{+40}_{-11}	[-1.1] ± [0.4]	[-2.2] ± [0.4]	3	...	...
050418	0.84 ± 0.10	0.012 ± 0.005	2.98 ± 0.27	4	130^{+624}_{-24}	-1.3 ± 0.18	[-2.2] ± [0.4]	2	...	...
050421	...	0.087 ± 0.361	...	2	116^{+72}_{-72}	[-1.1] ± [0.4]	[-2.2] ± [0.4]	1	...	...
050422	...	0.064 ± 0.091	...	2	166^{+54}_{-54}	[-1.1] ± [0.4]	[-2.2] ± [0.4]	1	...	...
050502B	0.47 ± 0.04	0.029 ± 0.014	1.04 ± 0.31	1	108^{+26}_{-26}	[-1.1] ± [0.4]	[-2.2] ± [0.4]	1	...	...
050505	0.71 ± 0.13	0.076 ± 0.031	0.60 ± 0.21	3	70^{+140}_{-24}	-0.31 ± 1	[-2.2] ± [0.4]	4	[bc]	79, 62

Table 3.6 (cont'd)

GRB	$\tau_{lag}(sec)$	Variability	τ_{RT}(sec)	N_{peak}	E_{peak}(keV)[a]	α[a]	β[a]	Ref.	t_{jet}(day)	Ref.
050509A	0.39 ± 0.12	0.048 ± 0.043	...	2	39^{+9}_{-9}	[-1.1] ± [0.4]	[-2.2] ± [0.4]	1	...	...
050525A	0.12 ± 0.01	0.093 ± 0.003	0.32 ± 0.01	2	81^{+1}_{-1}	-1.01 ± 0.06	-3.26 ± 0.2	8	0.40 ± 0.10	78, 83
050528	...	0.017 ± 0.117	...	3	30^{+9}_{-9}	[-1.1] ± [0.4]	[-2.2] ± [0.4]	1	...	...
050603	-0.01 ± 0.01	0.125 ± 0.014	0.19 ± 0.01	1	344^{+52}_{-52}	-1.03 ± 0.06	-2.03 ± 0.1	8	[d]	84, 81, 82
050607	0.85 ± 0.13	0.041 ± 0.034	0.54 ± 0.37	4	55^{+13}_{-13}	[-1.1] ± [0.4]	[-2.2] ± [0.4]	1	...	...
050701	...	0.024 ± 0.006	0.47 ± 0.15	1	85^{+16}_{-16}	[-1.1] ± [0.4]	[-2.2] ± [0.4]	1	...	...
050712	...	-0.015 ± 0.169	...	2	133^{+40}_{-40}	[-1.1] ± [0.4]	[-2.2] ± [0.4]	1	...	...
050713A	0.01 ± 0.07	0.027 ± 0.006	0.64 ± 0.17	3	312^{+30}_{-30}	-1.12 ± 0.05	[-2.2] ± [0.4]	11	...	...
050713B	...	0.053 ± 0.101	...	1	175^{+53}_{-53}	[-1.1] ± [0.4]	[-2.2] ± [0.4]	1	...	...
050714B	...	-0.648 ± 0.672	...	1	23^{+7}_{-7}	[-1.1] ± [0.4]	[-2.2] ± [0.4]	1	...	...
050715	...	0.081 ± 0.050	0.93 ± 0.57	3	105^{+26}_{-26}	[-1.1] ± [0.4]	[-2.2] ± [0.4]	1	...	...
050716	...	0.034 ± 0.017	3.23 ± 2.55	4	123^{+37}_{-15}	-0.8 ± 0.18	[-2.2] ± [0.4]	3	...	...
050717	0.01 ± 0.04	0.104 ± 0.007	0.20 ± 0.02	1	1890^{+970}_{-461}	$-1.12^{+0.08}_{-0.10}$	$-1.71^{+0.13}_{-0.58}$	12	...	...
050721	...	0.011 ± 0.049	...	1	57^{+13}_{-13}	[-1.1] ± [0.4]	[-2.2] ± [0.4]	1	...	...
050726	...	0.018 ± 0.091	...	1	842^{+445}_{-445}	[-1.1] ± [0.4]	[-2.2] ± [0.4]	1	...	...
050730	...	0.027 ± 0.066	...	2	124^{+26}_{-26}	[-1.1] ± [0.4]	[-2.2] ± [0.4]	1	0.12[ef]	78
050801	...	-0.038 ± 0.073	...	1	48^{+15}_{-15}	[-1.1] ± [0.4]	[-2.2] ± [0.4]	1	0.0022 ± 0.0002[f]	22
050802	...	0.070 ± 0.036	2.03 ± 1.02	4	121^{+28}_{-28}	[-1.1] ± [0.4]	[-2.2] ± [0.4]	1	...	...
050803	...	...	0.06 ± 0.03	5	180^{+40}_{-40}	[-1.1] ± [0.4]	[-2.2] ± [0.4]	1	[b]	79
050814	...	-0.009 ± 0.180	...	2	60^{+24}_{-6}	0 ± 0.6	[-2.2] ± [0.4]	2	[b]	79
050815	...	0.047 ± 0.095	...	1	44^{+5}_{-4}	-0.9 ± 1.15	[-2.2] ± [0.4]	3	...	...
050819	...	0.151 ± 0.341	...	1	16^{+5}_{-5}	[-1.1] ± [0.4]	[-2.2] ± [0.4]	1	...	...
050820A	...	0.061 ± 0.033	1.01 ± 0.75	3	246^{+76}_{-40}	-1.25 ± 0.1	[-2.2] ± [0.4]	8	18[g]± 2.00	76
050820B	0.15 ± 0.03	0.022 ± 0.003	1.41 ± 0.05	1	111^{+13}_{-8}	-0.6 ± 0.12	[-2.2] ± [0.4]	3	...	...
050822	...	0.124 ± 0.090	...	3	26^{+5}_{-5}	[-1.1] ± [0.4]	[-2.2] ± [0.4]	1	...	...
050824	...	0.289 ± 0.640	...	1	15^{+5}_{-5}	[-1.1] ± [0.4]	[-2.2] ± [0.4]	1	...	...
050826	...	0.063 ± 0.105	1.11 ± 2.28	1	105^{+47}_{-47}	[-1.1] ± [0.4]	[-2.2] ± [0.4]	1	...	...
050827	...	0.060 ± 0.013	4.46 ± 1.26	1	180^{+38}_{-38}	[-1.1] ± [0.4]	[-2.2] ± [0.4]	1	...	...

Table 3.6 (cont'd)

GRB	$\tau_{lag}(sec)$	Variability	τ_{RT}(sec)	N_{peak}	E_{peak}(keV)[a]	α[a]	β[a]	Ref.	t_{jet}(day)	Ref.
050904	...	0.044 ± 0.079	...	1	436^{+200}_{-90}	-1.11 ± 0.06	[-2.2] ± [0.4]	8	2.60 ± 1.00	65
050908	...	-0.017 ± 0.046	1.10 ± 1.47	1	41^{+9}_{-5}	[-1.1] ± [0.4]	[-2.2] ± [0.4]	4	...	...
050915A	...	0.185 ± 0.069	0.48 ± 0.65	6	175^{+53}_{-53}	[-1.1] ± [0.4]	[-2.2] ± [0.4]	1	...	...
050915B	0.29 ± 0.24	0.028 ± 0.013	1.06 ± 0.64	3	61^{+10}_{-5}	-1.4 ± 0.18	[-2.2] ± [0.4]	3	...	...
050916	...	...	...	1	75^{+22}_{-22}	[-1.1] ± [0.4]	[-2.2] ± [0.4]	1	...	...
050922C	0.06 ± 0.01	0.015 ± 0.003	0.13 ± 0.01	2	198^{+38}_{-22}	-0.95 ± 0.07	[-2.2] ± [0.4]	8	0.11 ± 0.03	66
051001	...	0.008 ± 0.068	...	1	48^{+12}_{-6}	-1.2 ± 0.42	[-2.2] ± [0.4]	2	...	...
051006	0.19 ± 0.03	0.281 ± 0.057	...	3	130^{+37}_{-37}	[-1.1] ± [0.4]	[-2.2] ± [0.4]	1	...	...
051008	0.03 ± 0.05	0.029 ± 0.004	1.16 ± 0.19	1	865^{+108}_{-82}	-0.975 ± 0.05	[-2.2] ± [0.4]	13	[b]	79
051016A	...	0.002 ± 0.065	1.33 ± 1.56	1	58^{+20}_{-20}	[-1.1] ± [0.4]	[-2.2] ± [0.4]	1	...	...
051016B	...	0.008 ± 0.030	...	2	24^{+7}_{-7}	[-1.1] ± [0.4]	[-2.2] ± [0.4]	1	[b]	78
051021B	1.46 ± 0.01	0.020 ± 0.040	2.27 ± 1.32	2	72^{+27}_{-8}	-0.6 ± 0.48	[-2.2] ± [0.4]	3	...	...
051109A	...	-0.006 ± 0.025	0.70 ± 1.25	1	161^{+130}_{-35}	$-1.25^{+0.27}_{-0.36}$	[-2.2] ± [0.4]	14	0.60 ± 0.10	67
051109B	...	0.062 ± 0.095	2.11 ± 3.96	1	50^{+24}_{-6}	0 ± 0.61	[-2.2] ± [0.4]	2	...	...
051111	1.70 ± 0.07	0.009 ± 0.004	1.80 ± 0.24	1	220^{+1703}_{-48}	-1 ± 0.18	[-2.2] ± [0.4]	2	0.0080 ± 0.0003	68
051113	1.24 ± 0.70	0.044 ± 0.036	1.15 ± 0.40	1	81^{+19}_{-19}	[-1.1] ± [0.4]	[-2.2] ± [0.4]	1	...	...
051117A	...	0.020 ± 0.024	5.52 ± 8.71	2	66^{+11}_{-11}	[-1.1] ± [0.4]	[-2.2] ± [0.4]	1	...	...
051117B	...	-0.001 ± 0.232	0.91 ± 0.72	1	124^{+58}_{-58}	[-1.1] ± [0.4]	[-2.2] ± [0.4]	1	...	...
051213	...	0.165 ± 0.167	...	2	70^{+218}_{-12}	-0.6 ± 0.55	[-2.2] ± [0.4]	2	...	...
051221B	...	0.049 ± 0.137	...	1	200^{+68}_{-68}	[-1.1] ± [0.4]	[-2.2] ± [0.4]	1	...	...
060102	1.12 ± 0.15	0.094 ± 0.093	0.90 ± 0.88	1	273^{+193}_{-193}	[-1.1] ± [0.4]	[-2.2] ± [0.4]	1	...	...
060105	0.01 ± 0.01	0.098 ± 0.004	0.12 ± 0.01	15	396^{+29}_{-29}	$-0.79^{+0.04}_{-0.03}$	$-2.7^{+0.21}_{-0.44}$	15	[b]	79
060108	...	0.006 ± 0.040	...	2	65^{+600}_{-10}	[-1.1] ± 0.4	[-2.2] ± [0.4]	6	...	...
060109	...	-0.042 ± 0.173	...	2	31^{+4}_{-3}	[-1.1] ± [0.4]	[-2.2] ± [0.4]	2	[b]	79
060110	0.95 ± 0.13	0.017 ± 0.008	0.64 ± 0.14	1	96^{+17}_{-17}	[-1.1] ± [0.4]	[-2.2] ± [0.4]	1	...	...
060111A	0.58 ± 0.18	0.002 ± 0.007	1.09 ± 0.66	1	74^{+12}_{-6}	-0.9 ± 0.18	[-2.2] ± [0.4]	3	...	...
060111B	...	0.121 ± 0.042	0.32 ± 0.31	4	555^{+113}_{-113}	[-1.1] ± [0.4]	[-2.2] ± [0.4]	1	...	...
060115	...	0.019 ± 0.029	1.11 ± 1.71	2	62^{+19}_{-6}	-1 ± 0.3	[-2.2] ± [0.4]	16	...	...

Table 3.6 (cont'd)

GRB	$\tau_{lag}(sec)$	Variability	τ_{RT}(sec)	N_{peak}	E_{peak}(keV)[a]	α[a]	β[a]	Ref.	t_{jet}(day)	Ref.
060116	...	0.047 ± 0.117	...	4	139^{+400}_{-36}	-1.02 ± 0.38	[-2.2] ± [0.4]	6	...	...
060117	0.04 ± 0.01	0.084 ± 0.003	0.22 ± 0.01	3	89^{+3}_{-3}	$-1.52^{+0.05}_{-0.04}$	$-2.91^{+0.15}_{-0.30}$	17	...	...
060202	...	0.250 ± 0.166	...	3	83^{+18}_{-18}	[-1.1] ± [0.4]	[-2.2] ± [0.4]	1	...	...
060203	...	0.001 ± 0.275	...	2	103^{+36}_{-36}	[-1.1] ± [0.4]	[-2.2] ± [0.4]	1	...	...
060204B	0.50 ± 0.28	0.031 ± 0.014	8.62 ± 4.09	1	100^{+45}_{-13}	-0.8 ± 0.24	[-2.2] ± [0.4]	3	[b]	79
060206	0.01 ± 0.03	0.007 ± 0.004	1.16 ± 0.18	1	78^{+23}_{-8}	-1.2 ± 0.18	[-2.2] ± [0.4]	3	0.57 ± 0.06	69, 85
060210	0.15 ± 0.17	0.183 ± 0.033	0.73 ± 0.50	4	149^{+400}_{-35}	-1.18 ± 0.03	[-2.2] ± [0.4]	6	[bh]	70, 85
060211A	...	-0.097 ± 0.101	...	3	58^{+11}_{-5}	-0.9 ± 0.36	[-2.2] ± [0.4]	3	...	...
060211B	...	0.032 ± 0.079	0.50 ± 1.07	2	113^{+37}_{-37}	[-1.1] ± [0.4]	[-2.2] ± [0.4]	1	...	...
060223A	...	0.036 ± 0.021	0.41 ± 0.23	4	71^{+100}_{-10}	-1.18 ± 0.31	[-2.2] ± [0.4]	6	...	...
060223B	0.03 ± 0.03	0.068 ± 0.010	0.12 ± 0.03	3	136^{+24}_{-24}	[-1.1] ± [0.4]	[-2.2] ± [0.4]	1	...	...
060306	0.09 ± 0.01	0.050 ± 0.008	0.19 ± 0.01	3	70^{+55}_{-6}	-1.2 ± 0.3	[-2.2] ± [0.4]	2	...	...
060312	...	0.021 ± 0.011	0.22 ± 0.94	2	63^{+13}_{-13}	-1.35 ± 0.21	[-2.2] ± [0.4]	18	...	...
060319	1.78 ± 0.17	0.040 ± 0.052	0.52 ± 0.41	1	27^{+8}_{-8}	[-1.1] ± [0.4]	[-2.2] ± [0.4]	1	...	...
060322	0.29 ± 0.19	0.165 ± 0.014	0.71 ± 1.29	3	96^{+55}_{-11}	-1.1 ± 0.18	[-2.2] ± [0.4]	3	...	...
060403	2.38 ± 0.25	0.001 ± 0.014	2.33 ± 1.04	1	170^{+121}_{-30}	-0.4 ± 0.24	[-2.2] ± [0.4]	2	...	...
060413	...	0.004 ± 0.010	11.10 ± 3.91	1	88^{+16}_{-16}	[-1.1] ± [0.4]	[-2.2] ± [0.4]	1	[b]	79
060418	0.22 ± 0.03	0.104 ± 0.008	0.67 ± 0.08	2	$230^{+[20]}_{-[20]}$	-1.5 ± [0.1]	[-2.2] ± [0.4]	19	[h]	86
060421	0.13 ± 0.01	0.065 ± 0.007	0.25 ± 0.07	5	120^{+127}_{-18}	-1.1 ± 0.18	[-2.2] ± [0.4]	2	...	...
060424	...	0.166 ± 0.051	0.23 ± 0.08	4	70^{+273}_{-12}	-0.8 ± 0.48	[-2.2] ± [0.4]	2	...	...
060427	...	0.001 ± 0.282	...	1	60^{+22}_{-22}	[-1.1] ± [0.4]	[-2.2] ± [0.4]	1	...	...
060428A	0.56 ± 0.11	0.006 ± 0.010	0.89 ± 0.23	2	50^{+18}_{-12}	-1.5 ± 0.3	[-2.2] ± [0.4]	2	[b]	79
060428B	...	0.083 ± 0.181	...	1	23^{+3}_{-8}	-0.8 ± 0.97	[-2.2] ± [0.4]	3	...	...
060501	1.00 ± 0.12	0.042 ± 0.025	0.98 ± 0.87	1	150^{+38}_{-38}	[-1.1] ± [0.4]	[-2.2] ± [0.4]	1	...	...
060502A	4.90 ± 0.11	0.004 ± 0.010	2.94 ± 1.19	1	156^{+400}_{-33}	-1.18 ± 0.15	[-2.2] ± [0.4]	6	[b]	78
060507	...	0.004 ± 0.038	3.80 ± 3.87	1	65^{+12}_{-12}	[-1.1] ± [0.4]	[-2.2] ± [0.4]	1	...	...
060510A	0.24 ± 0.06	0.049 ± 0.007	0.21 ± 0.10	4	184^{+22}_{-15}	-1.66 ± 0.04	[-2.2] ± [0.4]	20	...	...
060510B	...	0.110 ± 0.060	...	4	$95^{+[60]}_{-[30]}$	-1.47 ± 0.18	[-2.2] ± [0.4]	6	...	...

Table 3.6 (cont'd)

GRB	$\tau_{lag}(sec)$	Variability	τ_{RT}(sec)	N_{peak}	E_{peak}(keV)[a]	α[a]	β[a]	Ref.	t_{jet}(day)	Ref.
060512	...	0.043 ± 0.173	...	1	22^{+6}_{-6}	[-1.1] ± [0.4]	[-2.2] ± [0.4]	1	...	...
060515	0.99 ± 0.10	0.113 ± 0.104	...	1	110^{+97}_{-18}	0 ± 0.48	[-2.2] ± [0.4]	2	...	...
060522	...	0.034 ± 0.185	...	1	80^{+382}_{-12}	-0.7 ± 0.48	[-2.2] ± [0.4]	2	...	...
060526	0.17 ± 0.09	0.085 ± 0.030	0.38 ± 0.11	2	$25^{+[5]}_{-[5]}$	[-1.1] ± [0.4]	[-2.2] ± [0.4]	6	2.41 ± 0.06	87
060602A	...	-0.046 ± 0.112	...	1	257^{+80}_{-80}	[-1.1] ± [0.4]	[-2.2] ± [0.4]	1	...	...
060604	...	0.080 ± 0.338	...	2	$40^{+[5]}_{-[5]}$	-1.34 ± [0.3]	[-2.2] ± [0.4]	6	...	...
060605	...	-0.013 ± 0.068	1.22 ± 0.72	3	90^{+91}_{-12}	-0.3 ± 0.42	[-2.2] ± [0.4]	2	0.24 ± 0.02	88
060607A	1.98 ± 0.11	0.025 ± 0.008	1.23 ± 0.68	1	120^{+190}_{-17}	-1.06 ± 0.18	[-2.2] ± [0.4]	6	[b]	79
060607B	2.70 ± 0.23	0.013 ± 0.035	1.47 ± 0.76	2	94^{+20}_{-20}	[-1.1] ± [0.4]	[-2.2] ± [0.4]	1	...	...
060707	...	0.050 ± 0.054	...	2	63^{+13}_{-6}	-0.6 ± 0.42	[-2.2] ± [0.4]	3	...	...
060708	0.12 ± 0.09	0.021 ± 0.010	0.40 ± 0.35	1	100^{+109}_{-12}	-1 ± 0.3	[-2.2] ± [0.4]	2	...	...
060712	...	0.117 ± 0.268	...	1	101^{+47}_{-47}	[-1.1] ± [0.4]	[-2.2] ± [0.4]	1	...	...
060714	...	0.125 ± 0.022	...	> 3	103^{+21}_{-16}	[-1.1] ± [0.4]	[-2.2] ± [0.4]	21	0.12 ± [0.01][I]	21
060717	0.70 ± 0.19	0.029 ± 0.098	0.55 ± 0.97	1	50^{+36}_{-6}	0 ± 1.21	[-2.2] ± [0.4]	2	...	...
060719	0.80 ± 0.09	0.105 ± 0.014	0.47 ± 0.10	2	56^{+11}_{-11}	[-1.1] ± [0.4]	[-2.2] ± [0.4]	1	...	...
060729	...	0.092 ± 0.041	...	2	61^{+9}_{-9}	[-1.1] ± [0.4]	[-2.2] ± [0.4]	22	0.50 ± 0.06[f]	72
060804	...	0.085 ± 0.096	...	2	80^{+29}_{-29}	[-1.1] ± [0.4]	[-2.2] ± [0.4]	1	...	...
060805	...	0.023 ± 0.271	...	1	30^{+3}_{-3}	[-1.1] ± [0.4]	[-2.2] ± [0.4]	2	...	...
060807	...	0.042 ± 0.079	0.13 ± 1.49	2	110^{+36}_{-36}	[-1.1] ± [0.4]	[-2.2] ± [0.4]	1	[b]	79
060813	0.01 ± 0.02	0.019 ± 0.003	0.57 ± 0.08	1	192^{+12}_{-11}	$-0.53^{+0.10}_{-0.08}$	$-2.65^{+0.16}_{-0.30}$	23	[b]	79
060814	0.29 ± 0.03	0.040 ± 0.003	1.65 ± 0.24	2	257^{+74}_{-35}	-1.43 ± 0.09	[-2.2] ± [0.4]	24	[b]	78
060825	0.29 ± 0.07	0.032 ± 0.009	0.62 ± 0.21	2	73^{+17}_{-7}	-1.2 ± 0.18	[-2.2] ± [0.4]	3	...	...
060904A	0.11 ± 0.02	0.031 ± 0.003	0.29 ± 0.05	6	163^{+19}_{-19}	$-1^{+0.14}_{-0.10}$	$-2.57^{+0.22}_{-0.61}$	25	...	...
060904B	0.36 ± 0.09	0.003 ± 0.008	1.00 ± 0.16	1	80^{+770}_{-12}	-1 ± 0.42	[-2.2] ± [0.4]	2	...	...
060908	0.26 ± 0.06	0.061 ± 0.008	0.52 ± 0.09	3	151^{+112}_{-25}	-1 ± 0.18	[-2.2] ± [0.4]	3	[b]	78
060912	0.07 ± 0.01	0.010 ± 0.003	0.45 ± 0.01	1	78^{+14}_{-14}	-1.74 ± 0.09	[-2.2] ± [0.4]	1	...	...
060919	0.27 ± 0.11	-0.004 ± 0.020	0.36 ± 0.20	1	62^{+17}_{-17}	[-1.1] ± [0.4]	[-2.2] ± [0.4]	1	...	...
060923A	...	0.155 ± 0.108	0.51 ± 0.65	3	50^{+24}_{-6}	0 ± 0.61	[-2.2] ± [0.4]	2	...	...

Table 3.6 (cont'd)

GRB	$\tau_{lag}(sec)$	Variability	τ_{RT}(sec)	N_{peak}	E_{peak}(keV)[a]	α[a]	β[a]	Ref.	t_{jet}(day)	Ref.
060923B	...	0.231 ± 0.178	1.09 ± 1.72	1	21^{+6}_{-6}	[-1.1] ± [0.4]	[-2.2] ± [0.4]	1	...	...
060923C	...	0.244 ± 0.454	...	1	34^{+5}_{-10}	0 ± 0.61	[-2.2] ± [0.4]	2	...	...
060926	1.03 ± 0.11	0.148 ± 0.050	...	2	20^{+11}_{-11}	[-1.1] ± [0.4]	[-2.2] ± [0.4]	1	...	...
060927	0.12 ± 0.04	0.094 ± 0.010	0.46 ± 0.12	2	72^{+15}_{-7}	-0.9 ± 0.24	[-2.2] ± [0.4]	3	[j]	89
061002	...	-0.157 ± 0.169	...	1	75^{+22}_{-22}	[-1.1] ± [0.4]	[-2.2] ± [0.4]	1	...	...
061004	...	0.018 ± 0.007	0.49 ± 0.07	1	68^{+13}_{-13}	[-1.1] ± [0.4]	[-2.2] ± [0.4]	1	...	...
061007	0.11 ± 0.01	0.066 ± 0.003	0.38 ± 0.02	4	399^{+12}_{-11}	-0.7 ± 0.02	$-2.61^{+0.09}_{-0.13}$	26	$> 1.7d$	90, 82
061019	...	0.025 ± 0.154	...	2	55^{+18}_{-18}	[-1.1] ± [0.4]	[-2.2] ± [0.4]	1	...	...
061021	0.23 ± 0.02	0.031 ± 0.004	0.53 ± 0.03	1	777^{+333}_{-144}	$-1.22^{+0.07}_{-0.08}$	[-2.2] ± [0.4]	27	...	...
061028	...	0.518 ± 0.489	...	1	80^{+32}_{-32}	[-1.1] ± [0.4]	[-2.2] ± [0.4]	1	...	...
061102	...	0.111 ± 0.362	...	1	116^{+62}_{-62}	[-1.1] ± [0.4]	[-2.2] ± [0.4]	1	...	...
061110A	...	-0.038 ± 0.050	...	1	90^{+13}_{-13}	[-1.1] ± [0.4]	[-2.2] ± [0.4]	1	...	...
061110B	0.24 ± 0.36	0.155 ± 0.064	0.79 ± 0.64	9	517^{+53}_{-53}	[-1.1] ± [0.4]	[-2.2] ± [0.4]	1	...	...
061121	0.03 ± 0.01	0.050 ± 0.003	0.98 ± 0.19	2	606^{+55}_{-44}	$-1.32^{+0.02}_{-0.03}$	[-2.2] ± [0.4]	28	1.16^{k}± [0.16]	77
061126	0.10 ± 0.01	0.092 ± 0.005	0.81 ± 0.09	2	935^{+218}_{-218}	$-0.95^{+0.18}_{-0.14}$	[-2.2] ± [0.4]	29	...	...
061202	...	0.028 ± 0.004	0.90 ± 0.41	2	130^{+339}_{-24}	-1.2 ± 0.18	[-2.2] ± [0.4]	2	[b]	79
061222A	0.08 ± 0.01	0.052 ± 0.003	0.22 ± 0.03	2	283^{+36}_{-25}	-0.94 ± 0.08	$-2.41^{+0.17}_{-0.73}$	30	[b]	79
061222B	...	0.024 ± 0.043	...	2	49^{+8}_{-8}	[-1.1] ± [0.4]	[-2.2] ± [0.4]	1	...	...
070103	0.52 ± 0.13	0.310 ± 0.098	0.31 ± 0.28	2	52^{+15}_{-15}	[-1.1] ± [0.4]	[-2.2] ± [0.4]	1	...	...
070107	1.10 ± 0.02	0.041 ± 0.015	2.01 ± 3.04	1	206^{+44}_{-44}	[-1.1] ± [0.4]	[-2.2] ± [0.4]	1	[b]	79
070110	...	-0.010 ± 0.031	...	1	110^{+30}_{-30}	[-1.1] ± [0.4]	[-2.2] ± [0.4]	31	[b]	78
070208	...	0.083 ± 0.211	...	2	51^{+10}_{-10}	[-1.1] ± [0.4]	[-2.2] ± [0.4]	1	...	...
070219	...	0.087 ± 0.101	...	1	72^{+22}_{-22}	[-1.1] ± [0.4]	[-2.2] ± [0.4]	1	...	...
070220	...	0.066 ± 0.004	0.90 ± 0.18	8	299^{+124}_{-79}	$-1.21^{+0.18}_{-0.12}$	$-2.02^{+0.16}_{-0.27}$	32	[b]	79
070223	...	0.058 ± 0.084	0.92 ± 1.44	3	60^{+115}_{-6}	-1.2 ± 0.36	[-2.2] ± [0.4]	2	...	...
070306	1.27 ± 0.07	0.011 ± 0.003	2.77 ± 0.81	1	92^{+18}_{-18}	[-1.1] ± [0.4]	[-2.2] ± [0.4]	1	[b]	79
070318	...	0.037 ± 0.008	0.72 ± 0.24	1	154^{+19}_{-19}	[-1.1] ± [0.4]	[-2.2] ± [0.4]	1	...	...
070328	0.28 ± 0.02	0.034 ± 0.003	2.06 ± 0.32	2	496^{+104}_{-71}	$-0.99^{+0.08}_{-0.07}$	$-1.99^{+0.11}_{-0.24}$	33	...	...

Table 3.6 (cont'd)

GRB	$\tau_{lag}(sec)$	Variability	τ_{RT}(sec)	N_{peak}	E_{peak}(keV)[a]	α[a]	β[a]	Ref.	t_{jet}(day)	Ref.
070330	2.15 ± 0.24	0.083 ± 0.059	...	1	36^{+4}_{-4}	-0.33 ± 1.07	[-2.2] ± [0.4]	34	...	...
070411	...	0.041 ± 0.029	...	2	83^{+11}_{-11}	[-1.1] ± [0.4]	[-2.2] ± [0.4]	1	[l]	73
070412	...	0.119 ± 0.086	0.43 ± 0.29	3	150^{+50}_{-50}	[-1.1] ± [0.4]	[-2.2] ± [0.4]	1	...	...
070419B	1.51 ± 0.15	0.062 ± 0.007	1.66 ± 0.86	4	85^{+14}_{-14}	[-1.1] ± [0.4]	[-2.2] ± [0.4]	1	...	...
070420	0.86 ± 0.36	0.018 ± 0.006	3.96 ± 2.60	1	147^{+18}_{-12}	-1.23 ± 0.11	[-2.2] ± [0.4]	35	...	...
070427	0.23 ± 0.09	0.034 ± 0.011	0.22 ± 0.40	1	41^{+8}_{-8}	[-1.1] ± [0.4]	[-2.2] ± [0.4]	1	...	...
070429A	...	0.024 ± 0.090	...	1	39^{+12}_{-12}	[-1.1] ± [0.4]	[-2.2] ± [0.4]	1	...	...
070506	2.52 ± 0.04	0.010 ± 0.030	0.12 ± 0.06	1	31^{+2}_{-3}	-5.00 ± 1.82	2.01 ± 0.22	2	...	...
070508	0.04 ± 0.01	0.106 ± 0.003	0.20 ± 0.01	4	233^{+7}_{-7}	-0.96 ± 0.13	[-2.2] ± [0.4]	36	...	...
070509	0.57 ± 0.46	0.020 ± 0.060	0.83 ± 0.40	1	27^{+8}_{-8}	[-1.1] ± [0.4]	[-2.2] ± [0.4]	1	...	...
070517	...	-0.021 ± 0.046	...	2	68^{+22}_{-22}	[-1.1] ± [0.4]	[-2.2] ± [0.4]	1	...	...
070518	...	0.035 ± 0.054	0.34 ± 0.37	1	39^{+12}_{-12}	[-1.1] ± [0.4]	[-2.2] ± [0.4]	1	...	...
070520A	...	-0.047 ± 0.180	...	1	105^{+50}_{-50}	[-1.1] ± [0.4]	[-2.2] ± [0.4]	1	...	...
070520B	...	-0.105 ± 0.103	...	1	347^{+147}_{-147}	[-1.1] ± [0.4]	[-2.2] ± [0.4]	1	...	...
070521	0.04 ± 0.01	0.116 ± 0.004	0.58 ± 0.06	5	222^{+16}_{-13}	-0.93 ± 0.07	[-2.2] ± [0.4]	37	...	...
070529	...	0.170 ± 0.091	...	1	180^{+52}_{-52}	[-1.1] ± [0.4]	[-2.2] ± [0.4]	1	...	...
070531	...	0.009 ± 0.057	1.68 ± 0.63	1	166^{+57}_{-57}	[-1.1] ± [0.4]	[-2.2] ± [0.4]	1	...	...
070611	...	0.053 ± 0.080	...	1	92^{+30}_{-30}	[-1.1] ± [0.4]	[-2.2] ± [0.4]	1	...	...
070612A	0.77 ± 0.43	-0.010 ± 0.030	2.10 ± 1.79	1	87^{+17}_{-17}	[-1.1] ± [0.4]	[-2.2] ± [0.4]	1	...	...
070612B	...	-0.001 ± 0.015	2.24 ± 0.93	1	118^{+25}_{-25}	[-1.1] ± [0.4]	[-2.2] ± [0.4]	1	...	...
070616	...	0.156 ± 0.006	0.03 ± 0.00	7	103^{+16}_{-16}	[-1.1] ± [0.4]	[-2.2] ± [0.4]	1	...	...
070621	0.51 ± 0.03	0.024 ± 0.010	2.52 ± 1.82	4	113^{+19}_{-19}	[-1.1] ± [0.4]	[-2.2] ± [0.4]	1	...	...
070628	1.11 ± 0.20	0.003 ± 0.004	2.03 ± 0.56	1	56^{+10}_{-10}	[-1.1] ± [0.4]	[-2.2] ± [0.4]	1	...	...
070704	0.12 ± 0.09	0.001 ± 0.005	1.52 ± 0.21	3	70^{+13}_{-13}	[-1.1] ± [0.4]	[-2.2] ± [0.4]	1	...	...
070714A	...	0.012 ± 0.009	0.27 ± 0.07	1	18^{+4}_{-4}	[-1.1] ± [0.4]	[-2.2] ± [0.4]	1	...	...
070721A	...	0.087 ± 0.077	0.80 ± 1.54	1	22^{+9}_{-9}	[-1.1] ± [0.4]	[-2.2] ± [0.4]	1	...	...
070721B	...	0.032 ± 0.023	2.49 ± 1.48	2	200^{+45}_{-45}	[-1.1] ± [0.4]	[-2.2] ± [0.4]	1	...	...
070731	...	0.067 ± 0.032	...	1	94^{+32}_{-32}	[-1.1] ± [0.4]	[-2.2] ± [0.4]	1	...	...

Table 3.6 (cont'd)

GRB	$\tau_{lag}(sec)$	Variability	τ_{RT}(sec)	N_{peak}	E_{peak}(keV)[a]	α[a]	β[a]	Ref.	t_{jet}(day)	Ref.
070802	...	-0.156 ± 0.150	...	1	70^{+25}_{-25}	[-1.1] ± [0.4]	[-2.2] ± [0.4]	1	...	...
070805	...	0.081 ± 0.068	...	1	64^{+18}_{-18}	[-1.1] ± [0.4]	[-2.2] ± [0.4]	1	...	...
070808	0.54 ± 0.14	0.033 ± 0.016	0.88 ± 0.12	1	143^{+36}_{-36}	[-1.1] ± [0.4]	[-2.2] ± [0.4]	1	...	...
070810A	1.09 ± 0.23	-0.006 ± 0.015	0.73 ± 0.22	1	44^{+9}_{-9}	[-1.1] ± [0.4]	[-2.2] ± [0.4]	1	...	...
070911	0.15 ± 0.04	0.101 ± 0.003	0.55 ± 0.15	7	170^{+170}_{-30}	-1.60 ± 0.06	[-2.2] ± [0.4]	39	...	...
070913	...	0.147 ± 0.065	...	1	103^{+31}_{-31}	[-1.1] ± [0.4]	[-2.2] ± [0.4]	1	...	...
070917	0.06 ± 0.01	0.017 ± 0.003	0.21 ± 0.01	1	211^{+58}_{-29}	$-1.36^{+0.13}_{-0.15}$	[-2.2] ± [0.4]	40	...	...
070920A	...	0.098 ± 0.129	...	1	87^{+27}_{-27}	[-1.1] ± [0.4]	[-2.2] ± [0.4]	1	...	...
070920B	...	0.019 ± 0.016	5.77 ± 2.36	1	41^{+3}_{-3}	-0.67 ± 0.35	[-2.2] ± [0.4]	41	...	...
071001	...	0.041 ± 0.027	0.51 ± 1.00	3	101^{+27}_{-27}	[-1.1] ± [0.4]	[-2.2] ± [0.4]	1	...	...
071003	0.09 ± 0.04	0.072 ± 0.007	0.88 ± 0.07	4	799^{+75}_{-61}	-0.97 ± 0.04	[-2.2] ± [0.4]	42	...	...
071008	...	-0.003 ± 0.079	...	1	32^{+10}_{-10}	[-1.1] ± [0.4]	[-2.2] ± [0.4]	1	...	...
071010A	...	-0.076 ± 0.153	...	1	27^{+10}_{-10}	[-1.1] ± [0.4]	[-2.2] ± [0.4]	1	...	...
071010B	0.84 ± 0.04	0.010 ± 0.003	1.21 ± 0.03	1	52^{+6}_{-8}	$-1.25^{+0.45}_{-0.30}$	$-2.65^{+0.18}_{-0.30}$	43	3.44 ± 0.39	74
071011	...	0.231 ± 0.058	0.92 ± 0.44	4	166^{+39}_{-39}	[-1.1] ± [0.4]	[-2.2] ± [0.4]	1	...	...
071020	0.09 ± 0.01	0.050 ± 0.003	0.13 ± 0.01	2	322^{+48}_{-32}	$-0.65^{+0.16}_{-0.19}$	[-2.2] ± [0.4]	44	...	...
071021	...	0.039 ± 0.053	...	1	85^{+26}_{-26}	[-1.1] ± [0.4]	[-2.2] ± [0.4]	1	...	...
071025	...	0.038 ± 0.010	...	3	70^{+11}_{-11}	[-1.1] ± [0.4]	[-2.2] ± [0.4]	1	...	...
071031	...	-0.038 ± 0.108	...	2	24^{+7}_{-7}	[-1.1] ± [0.4]	[-2.2] ± [0.4]	1	...	...
071101	2.36 ± 0.47	0.078 ± 0.099	0.39 ± 0.52	1	31^{+18}_{-18}	[-1.1] ± [0.4]	[-2.2] ± [0.4]	1	...	...
071117	0.60 ± 0.01	0.009 ± 0.003	0.20 ± 0.02	1	278^{+143}_{-48}	-1.53 ± 0.09	[-2.2] ± [0.4]	45	...	...
071122	...	0.391 ± 0.392	...	1	73^{+30}_{-30}	[-1.1] ± [0.4]	[-2.2] ± [0.4]	1	...	...
071129	...	0.007 ± 0.034	...	1	53^{+12}_{-12}	[-1.1] ± [0.4]	[-2.2] ± [0.4]	1	...	...
080205	...	0.207 ± 0.052	0.71 ± 0.71	6	41^{+8}_{-8}	[-1.1] ± [0.4]	[-2.2] ± [0.4]	1	...	...
080210	0.53 ± 0.17	0.019 ± 0.013	0.57 ± 0.44	3	73^{+15}_{-15}	[-1.1] ± [0.4]	[-2.2] ± [0.4]	1	...	...
080212	...	0.034 ± 0.054	...	2	68^{+8}_{-8}	-0.31 ± 0.39	[-2.2] ± [0.4]	46	...	...
080218B	...	0.110 ± 0.079	...	1	24^{+9}_{-9}	-0.11 ± 1.48	[-2.2] ± [0.4]	47	...	...
080229A	0.24 ± 0.03	0.048 ± 0.003	0.46 ± 0.09	3	56^{+9}_{-9}	[-1.1] ± [0.4]	[-2.2] ± [0.4]	1	...	...

Table 3.6 (cont'd)

GRB	$\tau_{lag}(sec)$	Variability	τ_{RT}(sec)	N_{peak}	E_{peak}(keV)[a]	α[a]	β[a]	Ref.	t_{jet}(day)	Ref.
080303	0.89 ± 0.15	0.069 ± 0.032	0.33 ± 0.16	1	121^{+46}_{-46}	[-1.1] ± [0.4]	[-2.2] ± [0.4]	1	...	...
080307	...	-0.035 ± 0.095	...	1	72^{+21}_{-21}	[-1.1] ± [0.4]	[-2.2] ± [0.4]	1	...	...
080310	...	0.038 ± 0.021	0.41 ± 0.55	3	28^{+6}_{-6}	[-1.1] ± [0.4]	[-2.2] ± [0.4]	1	...	...
080319A	...	-0.004 ± 0.045	0.82 ± 1.23	5	105^{+24}_{-24}	[-1.1] ± [0.4]	[-2.2] ± [0.4]	1	...	...
080319B	0.02 ± 0.01	0.031 ± 0.003	0.14 ± 0.01	10	651^{+8}_{-8}	-0.82 ± 0.01	$-3.87^{+0.27}_{-0.66}$	48	...	...
080319C	...	0.042 ± 0.007	0.21 ± 0.12	4	307^{+85}_{-56}	-1.01 ± 0.08	$-1.87^{+0.09}_{-0.38}$	49	...	...
080319D	...	-0.122 ± 0.303	...	1	55^{+23}_{-23}	[-1.1] ± [0.4]	[-2.2] ± [0.4]	1	...	...
080320	...	0.011 ± 0.060	0.81 ± 0.99	1	85^{+27}_{-27}	[-1.1] ± [0.4]	[-2.2] ± [0.4]	1	...	...
080328	0.17 ± 0.02	0.173 ± 0.007	...	5	289^{+56}_{-35}	$-1.13^{+0.10}_{-0.12}$	[-2.2] ± [0.4]	50	...	...
080330	...	0.109 ± 0.060	...	3	20^{+9}_{-9}	[-1.1] ± [0.4]	[-2.2] ± [0.4]	1	...	...
080409	0.17 ± 0.05	0.049 ± 0.010	0.47 ± 0.06	2	40^{+10}_{-10}	[-1.1] ± [0.4]	[-2.2] ± [0.4]	1	...	...
080411	0.21 ± 0.01	0.167 ± 0.003	0.65 ± 0.01	2	259^{+21}_{-16}	$-1.51^{+0.02}_{-0.03}$	[-2.2] ± [0.4]	51	...	...
080413A	0.13 ± 0.03	0.078 ± 0.004	0.23 ± 0.03	3	170^{+48}_{-24}	-1.20 ± 0.06	[-2.2] ± [0.4]	52	...	...
080413B	0.23 ± 0.01	0.004 ± 0.003	0.50 ± 0.03	1	73^{+10}_{-10}	-1.26 ± 0.16	[-2.2] ± [0.4]	53	...	...
080426	...	0.012 ± 0.004	0.15 ± 0.01	1	49^{+10}_{-10}	[-1.1] ± [0.4]	[-2.2] ± [0.4]	1	...	...
080430	0.68 ± 0.08	0.009 ± 0.004	0.76 ± 0.12	1	80^{+15}_{-15}	[-1.1] ± [0.4]	[-2.2] ± [0.4]	1	...	...
080506	...	-0.002 ± 0.143	...	1	60^{+16}_{-16}	[-1.1] ± [0.4]	[-2.2] ± [0.4]	1	...	...
080515	...	-0.011 ± 0.042	...	1	25^{+9}_{-9}	-0.94 ± 0.73	[-2.2] ± [0.4]	54	...	...
080516	0.15 ± 0.01	0.168 ± 0.055	...	2	66^{+24}_{-24}	[-1.1] ± [0.4]	[-2.2] ± [0.4]	1	...	...
080517	...	-0.011 ± 0.110	...	1	121^{+59}_{-59}	[-1.1] ± [0.4]	[-2.2] ± [0.4]	1	...	...
080520	...	0.037 ± 0.098	...	1	12^{+5}_{-5}	[-1.1] ± [0.4]	[-2.2] ± [0.4]	1	...	...
080523	...	-0.009 ± 0.049	0.45 ± 0.31	10	94^{+26}_{-26}	[-1.1] ± [0.4]	[-2.2] ± [0.4]	1	...	...
080602	...	0.180 ± 0.032	0.53 ± 0.27	5	667^{+977}_{-977}	$-0.96^{+0.32}_{-0.46}$	[-2.2] ± [0.4]	1, 55	...	...
080603B	0.08 ± 0.01	0.283 ± 0.010	0.22 ± 0.03	6	85^{+55}_{-18}	$-0.94^{+0.73}_{-0.45}$	-1.96 ± [0.4]	56	[h]	75, 92
080605	0.11 ± 0.01	0.057 ± 0.003	0.22 ± 0.01	4	246^{+14}_{-11}	-1.02 ± 0.06	[-2.2] ± [0.4]	57	...	...
080607	0.04 ± 0.01	0.035 ± 0.003	0.18 ± 0.06	6	394^{+35}_{-33}	-1.06 ± 0.05	[-2.2] ± [0.4]	58	...	...
080613B	0.01 ± 0.01	0.141 ± 0.008	...	2	733^{+173}_{-121}	-1.05 ± 0.11	-2.05 ± [0.4]	59	...	...
080623	0.38 ± 0.01	0.153 ± 0.045	...	3	195^{+55}_{-55}	[-1.1] ± [0.4]	[-2.2] ± [0.4]	1	...	...

Table 3.6 (cont'd)

GRB	$\tau_{lag}(sec)$	Variability	τ_{RT}(sec)	N_{peak}	E_{peak}(keV)[a]	α[a]	β[a]	Ref.	t_{jet}(day)	Ref.
080701	0.65 ± 0.18	0.004 ± 0.012	1.24 ± 0.17	1	31^{+7}_{-7}	[-1.1] ± [0.4]	[-2.2] ± [0.4]	1	...	...
080703	...	0.099 ± 0.075	...	2	124^{+43}_{-43}	[-1.1] ± [0.4]	[-2.2] ± [0.4]	1	...	...
080707	...	0.093 ± 0.032	...	2	73^{+20}_{-20}	[-1.1] ± [0.4]	[-2.2] ± [0.4]	1	...	...
080714	0.19 ± 0.05	0.005 ± 0.005	0.99 ± 0.13	1	137^{+61}_{-21}	$-1.24^{+0.28}_{-0.24}$	[-2.2] ± [0.4]	60	...	...
080721	0.13 ± 0.05	0.048 ± 0.009	0.09 ± 0.04	4	485^{+41}_{-36}	$-0.93^{+0.06}_{-0.05}$	$-2.43^{+0.15}_{-0.25}$	61	...	...
080723A	...	0.028 ± 0.031	0.60 ± 0.54	1	73^{+22}_{-22}	[-1.1] ± [0.4]	[-2.2] ± [0.4]	1	...	...

[a]The values reported in square brackets are conservative estimations for uncertainties not reported in the original paper.

[b]Jet break time reported from X-ray data only, not being used in this work.

[c]Multi-values for jet break reported, due to the confusing condition of the afterglow light curve, not using any of these values in this work.

[d]Grupe et al. (2006) shows no break between 0.4-2.5 day, with the slope of the light curve suggesting a break before 0.4 day, while both Ghirlanda et al. (2007) and Campana et al. (2007) suggest a break after 2.5 day, based on Ghirlanda's relation

[e]Value obtained from Liang et al. (2007) figure and text.

[f]With a pre-break slope too shallow for the forward shock model, not being used as a jet break time.

[g]Only one post-break data reported.

[h]Optical break not restrictive.

[i]Break not detected in X-ray data.

[j]Optical data confusing, not able to make decision where the jet break lies.

[k]Only taking R band jet break, as later data is lacked in V band.

Reference of Table 3.6: (1) calculated from the relation in Zhang et al. 2007; (2) Butler et al. 2007; (3) Sakamoto et al. 2007; (4) Krimm 2005, private communication; (5) Nakagawa et al. 2005; (6) Krimm 2006, private communication; (7) Golenetskii et al. 2005a; (8) Krimm et al. 2006a; (9) Schady et al. 2006; (10) Sakamoto et al. 2006; (11) Golenetskii et al. 2005b; (12) Golenetskii et al. 2005c; (13) Golenetskii et al. 2005d; (14) Golenetskii et al. 2005e; (15) Golenetskii et al. 2006a; (16) Barbier et al. 2006a; (17) Golenetskii et al. 2006b; (18) Krimm et al. 2006b; (19) Golenetskii et al. 2006c; (20) Golenetskii et al. 2006d; (21) Krimm et al. 2007; (22) Rykoff et al. 2006; (23) Golenetskii et al. 2006e; (24) Golenetskii et al. 2006f; (25) Golenetskii et al. 2006g; (26) Golenetskii et al. 2006h; (27) Golenetskii et al. 2006i; (28) Golenetskii et al. 2006j; (29) Bellm et al. 2006; (30) Golenetskii et al. 2006k; (31) Amati et al. 2007; (32) Golenetskii et al. 2007a; (33) Golenetskii et al. 2007b; (34) Fenimore et al. 2007; (35) Golenetskii et al. 2007c; (36) Uehara et al. 2007; (37) Golenetskii et al. 2007d; (38) Ohno et al. 2007; (39) Barbier et al. 2008; (40) Golenetskii et al. 2007e; (41) Barthelmy et al. 2007; (42) Golenetskii et al. 2007f; (43) Golenetskii et al. 2007g; (44) Golenetskii et al. 2007h; (45) Golenetskii et al. 2007i; (46) McLean et al. 2008; (47) Krimm et al. 2008; (48) Golenetskii et al. 2008a; (49) Golenetskii et al. 2008b; (50) Golenetskii et al. 2008c; (51) Golenetskii et al. 2008d; (52) Ohno et al. 2008; (53) Barthelmy et al. 2008; (54) Fenimore et al. 2008; (55) Golenetskii et al. 2008e; (56) Golenetskii et al. 2008f; (57) Golenetskii et al. 2008g; (58) Golenetskii et al. 2008h; (59) Golenetskii et al. 2008i; (60) Golenetskii et al. 2008j; (61) Golenetskii et al. 2008k; (62) Hurkett et al. 2006; (65) Tagliaferri et al. 2005; (66) Li et al. 2005; (67) Yost et al. 2007; (68) Guidozi et al. 2007; (69) Curran et al. 2007; (70) Dai & Stanek 2006; (72) Grupe et al. 2007; (73) Dai et al. 2008; (74) Kann et al. 2007; (75) Zhuchkov et al. 2008; (76) Cenko et al. 2006a; (77) Page et al. 2007; (78) Liang et al. 2008; (79) Panaitescu 2007; (80) Vaughan et al. 2005; (81) Ghirlanda et al. 2007; (82) Campana et al. 2007; (84) Grupe et al. 2006; (86) Molinari et al. 2007; (87) Thoene et al. 2008c; (88) Ferrero et al. 2008; (89) Ruiz-Velasco et al. 2007; (90) Schady et al. 2007; (92) Kann et al. 2008;

Table 3.7. Our Redshifts and Spectroscopic Redshifts.

GRB	z_{spec}	Ref.	z_{best}	z_{min}	z_{max}	$z_{phot,limit}$	Ref.	z_{final}
41220	...	...	3.79	2.47	6.16	...	...	3.79
41223	...	...	1.74	1.23	2.53	...	...	1.74
41224	...	...	2	1.29	3.24	...	...	2
41226	...	...	> 4.38	...	...	...	...	> 4.38
41228	...	...	2.38	1.15	6.65	...	...	2.38
50117	...	...	4.71	2.98	8	...	...	4.71
50124	...	...	3.72	2.34	6.44	< 6.68	85	3.72
50126	1.29	1	1.64	1	2.91	...	...	1.29
50128	...	...	1.67	1.03	2.94	...	...	1.67
050215A	...	...	> 8.66	...	...	...	...	> 8.66
050215B	...	...	5.58	1.9	20	< 5.47	86	5.47
050219A	...	...	0.65	0.48	0.89	...	...	0.65
050219B	...	...	0.51	0.38	0.68	...	...	0.51
50223	...	...	2.8	1.03	20	...	...	2.8
50306	...	...	4.01	1.82	12.21	...	...	4.01
50315	1.95	3	1.4	0.86	2.46	< 6.68	87	1.95
50326	...	...	1.4	1.05	1.94	...	...	1.4
50401	2.9	4	2.48	1.69	3.85	< 6.68	88	2.9
50406	2.44	5	1.92	0.89	20	< 5.47	89	2.44
50410	...	...	1.04	0.72	6.19	...	...	1.04
50412	...	...	5.05	2.3	13.77	...	...	5.05
050416A	0.65	6	1	0.67	1.58	< 3.28	90	0.65
050416B	...	...	1.715	1.22	2.485	...	...	1.72
50418	...	...	0.88	0.6	1.3	...	...	0.88
50421	...	...	> 4.03	...	...	...	...	> 4.03
50422	...	...	> 4.59	...	...	...	...	> 4.59
050502B	...	...	2.67	1.8	4.15	...	...	2.67
50505	4.27	7	2.73	1.68	4.67	...	...	4.27
050509A	...	...	4.15	2.41	7.69	...	...	4.15
050525A	0.61	8	0.97	0.75	1.27	< 2.29	91	0.61
50528	...	...	0.92	0.49	2.3	...	...	0.92
50603	2.82	9	2.44	0.71	2.84	< 5.47	92	2.82
50607	...	...	3.45	2.21	5.73	< 6.68	93	3.45
50701	...	...	2.14	1.34	3.72	...	...	2.14
50712	...	...	> 3.3	...	...	< 3.28	94	3.28
050713A	...	...	1.41	0.95	2.21	< 6.68	95	1.41
050713B	...	...	5.88	1.84	20	...	...	5.88

Table 3.7 (cont'd)

GRB	z_{spec}	Ref.	z_{best}	z_{min}	z_{max}	$z_{phot,limit}$	Ref.	z_{final}
050714B	...	...	> 5.17	...	...	...	...	> 5.17
50715	...	...	5.74	2.72	16.25	...	...	5.74
50716	...	...	1.5	0.92	2.66	...	...	1.5
50717	...	...	2.23	1.36	4.32	...	...	2.23
50721	...	...	1.17	0.56	3.02	< 6.68	96	1.17
50726	...	...	9.61	2.53	20	< 5.47	97	5.47
50730	3.97	10	4.89	0.59	20	< 5.47	98	3.97
50801	1.56	11	3.34	0.68	6.51	< 2.29	99	1.56
50802	...	...	1.63	1.01	2.85	< 2.29	100	1.63
50803	...	...	7.15	3	20	< 6.68	101, 102	6.68
50814	5.3	12	2.86	1.19	20	< 6.68	103	5.3
50815	...	...	3.62	1.43	17.58	...	...	3.62
50819	...	...	1.55	0.78	4.51	...	...	1.55
050820A	2.61	13	2.84	1.6	5.94	< 2.84	104	2.61
050820B	...	...	1.38	1	1.97	...	...	1.38
50822	...	...	1.63	0.87	3.52	...	...	1.63
50824	0.83	14	1.36	0.71	3.65	< 1.96	105	0.83
50826	0.3	15	> 2.42	...	...	...	...	0.3
50827	...	...	1.38	0.9	2.22	...	...	1.38
50904	6.29	16	8.92	4	17.9	...	...	6.29
50908	3.35	17	3.69	1.08	8.1	< 5.47	106	3.35
050915A	...	...	> 8.53	...	...	...	...	> 8.53
050915B	...	...	1.95	1.29	3.09	...	...	1.95
50916	...	...	5.19	1.5	20	...	...	5.19
050922C	2.2	18	1.51	1.2	1.9	< 2.84	107	2.2
51001	...	...	3.15	1.15	20	...	...	3.15
51006	...	...	6.96	3.92	13.63	...	...	6.96
51008	...	...	0.94	0.67	1.34	< 6.68	108	0.94
051016A	...	...	1.76	0.85	4.82	...	...	1.76
051016B	0.94	19	0.7	0.45	1.55	< 2.29	109	0.94
051021B	...	...	2.19	1.44	3.5	...	...	2.19
051109A	2.35	20	1.45	0.94	2.25	< 5.47	110	2.35
051109B	...	...	5.44	1.9	20	...	...	5.44
51111	1.55	22	0.96	0.52	1.81	< 2.84	111	1.55
51113	...	...	1.6	1.1	2.4	...	...	1.6
051117A	...	...	2.12	1.09	5.02	< 5.47	112	2.12
051117B	...	...	> 3.08	...	...	...	...	> 3.08

Table 3.7 (cont'd)

GRB	z_{spec}	Ref.	z_{best}	z_{min}	z_{max}	$z_{phot,limit}$	Ref.	z_{final}
51213	...	...	> 6.4	...	...	...	...	> 6.4
051221B	...	...	> 4.36	...	...	...	...	> 4.36
60102	...	...	5.09	2.84	9.94	...	...	5.09
60105	...	...	3.43	2.26	5.65	...	...	3.43
60108	2.03	23	1.66	0.56	10.96	...	...	2.03
60109	...	...	2.68	0.85	6.99	...	...	2.68
60110	...	...	1.95	1.37	2.88	< 6.68	113	1.95
060111A	< 5.0	2	2.01	1.32	3.24	< 5.47	114	< 5.0
060111B	...	...	9.36	3.66	20	< 5.47	115	5.47
60115	3.53	24	2.92	1.37	9	...	...	3.53
60116	6.6	25	7.05	1.75	20	< 6.68	116	6.6
60117	...	...	0.98	0.74	1.3	...	...	0.98
60202	...	...	> 10.06	...	...	...	...	> 10.06
60203	...	...	> 2.22	...	...	...	...	> 2.22
060204B	...	...	1.55	1.07	2.35	< 5.47	117	1.55
60206	4.05	26	1.39	1.01	1.97	< 4.37	118	4.05
60210	3.91	27	2.63	1.76	4.03	< 6.68	119	3.91
060211A	...	...	> 4.91	...	...	...	...	> 4.91
060211B	...	...	9.16	2.48	20	...	...	9.16
060223A	4.41	28	5.38	2.49	14.86	< 5.47	120	4.41
060223B	...	...	8.04	4.41	16.96	...	...	8.04
60306	...	...	3.16	2.09	4.94	...	...	3.16
60312	...	...	1.97	1.08	4.13	...	...	1.97
60319	...	...	2.01	1.33	3.15	...	...	2.01
60322	...	...	4.44	2.57	8.46	...	...	4.44
60403	...	...	1.35	0.91	2.09	...	...	1.35
60413	...	...	0.82	0.53	1.32	...	...	0.82
60418	1.49	29	1.63	1.19	2.3	< 1.96	121	1.49
60421	...	...	4.24	2.68	7.15	...	...	4.24
60424	...	...	> 6.99	...	...	...	...	> 6.99
60427	...	...	> 2.18	...	...	...	...	> 2.18
060428A	...	...	1.65	1.14	2.49	...	...	1.65
060428B	...	...	1.55	0.73	4.1	< 5.47	122	1.55
60501	...	...	1.83	1.24	2.84	...	...	1.83
060502A	1.51	30	0.9	0.62	1.34	< 2.84	123	1.51
60507	...	...	1.38	0.74	3.01	...	...	1.38
060510A	...	...	1.12	0.83	1.55	< 3.28	124	1.12

Table 3.7 (cont'd)

GRB	z_{spec}	Ref.	z_{best}	z_{min}	z_{max}	$z_{phot,limit}$	Ref.	z_{final}
060510B	4.9	31	> 6.81	...	...	< 6.68	125	4.9
60512	...	...	0.89	0.53	2.11	< 3.28	126	0.89
60515	...	...	3.35	1.96	6.25	...	...	3.35
60522	5.11	32	7.45	1.41	20	...	...	5.11
60526	3.21	33	3.5	2.07	6.57	< 4.37	127	3.21
060602A	...	...	> 4.54	...	...	...	...	> 4.54
60604	2.68	34	3.81	1.39	20	...	...	2.68
60605	3.8	35	5.6	2.35	20	< 4.37	128	3.8
060607A	3.08	36	1.74	1.2	2.59	< 3.28	129	3.08
060607B	...	...	1.37	0.94	2.04	...	...	1.37
60707	3.43	37	3.68	1.56	13.91	< 4.37	130	3.43
60708	...	...	3.69	2.13	7.08	< 2.84	131	2.84
60712	...	...	4.22	1.35	20	...	...	4.22
60714	2.71	38	4.66	2.24	12.43	< 5.47	132	2.71
60717	...	...	5.02	2.75	10.06	...	...	5.02
60719	...	...	2.71	1.86	4.1	...	...	2.71
60729	0.54	39	1.66	0.81	3.48	< 2.29	133	0.54
60804	...	...	5.86	2.05	20	< 5.47	134	5.47
60805	...	...	2.19	0.92	8.29	...	...	2.19
60807	...	...	7.41	2.17	20	< 6.68	135	6.68
60813	...	...	1.03	0.74	1.49	...	...	1.03
60814	0.84	40	0.98	0.74	1.33	...	...	0.84
60825	...	...	2.32	1.59	3.51	...	...	2.32
060904A	...	...	2.55	1.8	3.76	...	...	2.55
060904B	0.7	41	1.88	1.28	2.88	< 2.29	136	0.7
60906	3.69	42	...	...	...	< 6.68	137	3.69
60908	2.43	43	2.41	1.65	3.69	< 2.84	138	2.43
60912	0.937	2	1.38	1	1.975	< 1.96	139	0.94
60919	...	...	3.19	1.96	5.67	...	...	3.19
060923A	...	...	8.17	2.88	20	...	...	8.17
060923B	...	...	2.48	1.26	6.32	...	...	2.48
060923C	...	...	2.67	1.13	10.19	...	...	2.67
60926	3.21	44	3.05	1.9	5.2	< 6.68	140	3.21
60927	5.47	45	4.04	2.57	6.71	...	...	5.47
61002	...	...	> 3.85	...	...	...	...	> 3.85
61004	...	...	2.08	1.32	3.53	...	...	2.08
61007	...	...	0.92	0.71	1.23	< 2.29	141	0.92

Table 3.7 (cont'd)

GRB	z_{spec}	Ref.	z_{best}	z_{min}	z_{max}	$z_{phot,limit}$	Ref.	z_{final}
61019	...	...	1.2	0.55	3.41	...	...	1.2
61021	...	...	1.2	0.89	1.66	< 2.29	142	1.2
61028	...	...	> 9.7	...	...	...	...	> 9.7
61102	...	...	> 5.32	...	...	...	...	> 5.32
061110A	0.76	46	> 1.82	...	...	< 6.68	143	0.76
061110B	3.44	47	8.28	3.35	20	< 6.68	144	3.44
61121	1.31	48	1	0.78	1.3	< 2.29	145	1.31
61126	...	...	0.86	0.63	1.18	< 1.96	146	0.86
61202	...	...	1.9	1.15	3.46	...	...	1.9
061222A	...	...	1.83	1.32	2.63	...	...	1.83
061222B	3.36	49	1.48	0.74	3.61	...	...	3.36
70103	...	...	6.9	4.04	12.68	...	...	6.9
70107	...	...	1.71	1.15	2.67	...	...	1.71
70110	2.35	50	4.34	2.03	20	< 3.28	147	2.35
70208	1.17	51	2.81	1.11	13.46	< 6.68	148	1.17
70219	...	...	> 3	...	...	...	...	> 3
70220	...	...	1.21	0.82	1.88	...	...	1.21
70223	...	...	8.29	2.24	20	...	...	8.29
70306	1.5	21	0.78	0.58	1.06	...	...	1.5
70318	0.84	52	2.96	1.75	5.66	< 2.29	149	0.84
70328	...	...	0.87	0.66	1.18	...	...	0.87
70330	...	...	2.4	1.53	3.95	< 5.47	150	2.4
70411	2.95	53	2.86	1.69	4.55	< 4.37	151	2.95
70412	...	...	> 7.48	...	...	...	...	> 7.48
070419A	0.97	54	...	...	...	< 5.47	152	0.97
070419B	...	...	2.08	1.45	3.12	< 6.68	153	2.08
70420	...	...	0.66	0.48	0.93	< 3.28	154	0.66
70427	...	...	3.89	2.36	6.87	...	...	3.89
070429A	...	...	3.03	1.12	18.12	...	...	3.03
70506	2.31	55	2.73	1.8	4.38	< 4.37	155	2.31
70508	...	...	1.22	0.9	1.7	< 5.47	156	1.22
70509	...	...	3.63	2.11	7.02	...	...	3.63
70517	...	...	5.48	1.06	16.88	...	...	5.48
70518	...	...	5.15	2.09	20	< 5.47	157	5.15
070520A	...	...	8.56	2.64	20	...	...	8.56
070520B	...	...	> 6.82	...	...	...	...	> 6.82
70521	...	...	2.1	1.47	3.1	...	...	2.1

Table 3.7 (cont'd)

GRB	z_{spec}	Ref.	z_{best}	z_{min}	z_{max}	$z_{phot,limit}$	Ref.	z_{final}
70529	2.5	56	> 1.67	...	...	< 5.47	158	2.5
70531	...	...	2.5	1.33	5.74	...	...	2.5
70611	2.04	57	5.55	1.24	20	< 2.84	159	2.04
070612A	...	...	1.72	1.17	3.13	< 5.47	160	1.72
070612B	...	...	1.13	0.69	2.02	...	...	1.13
70616	...	...	1.88	1.22	3.1	< 3.28	161	1.88
70621	...	...	1.54	1.07	2.3	...	...	1.54
70628	...	...	0.69	0.5	0.95	< 4.37	162	0.69
70704	...	...	2.14	1.38	3.52	...	...	2.14
070714A	...	...	2.11	1.28	3.79	...	...	2.11
070721A	...	...	3.77	1.63	12.85	< 5.47	163	3.77
070721B	3.63	84	1.98	1.16	3.8	< 5.47	164	3.63
70731	...	...	6.01	2.46	20	...	...	6.01
70802	2.45	59	9.37	1.51	20	< 5.47	165	2.45
70805	...	...	9.48	3.06	20	...	...	9.48
70808	...	...	2.12	1.46	3.2	...	...	2.12
070810A	2.17	60	1.76	1.19	2.69	...	...	2.17
70911	...	...	2.64	1.83	4.06	...	...	2.64
70913	...	...	> 3.69	...	...	...	...	> 3.69
70917	...	...	1.91	1.36	2.76	< 6.68	166	1.91
070920A	...	...	> 6.95	...	...	...	...	> 6.95
070920B	...	...	1.36	0.86	2.27	...	...	1.36
71001	...	...	6	2.51	20	...	...	6
71003	...	...	1.11	0.82	1.53	< 3.28	167	1.11
71008	...	...	1.62	0.74	6.25	...	...	1.62
071010A	0.98	61	3.06	0.71	6.97	< 5.47	168	0.98
071010B	0.95	62	0.81	0.62	1.06	...	...	0.95
71011	...	...	6.07	2.94	17.18	< 6.68	169,170	6.07
71020	2.15	63	1.6	1.15	2.3	< 6.68	171	2.15
71021	...	...	6.44	2.17	20	< 5.5	172	5.5
71025	...	...	2.71	1.42	6.16	< 6.68	173	2.71
071028A	...	...	> 2.56	...	...	...	...	> 2.56
71031	2.69	64	2.27	0.71	5.05	< 3.28	174	2.69
71101	...	...	3.79	2.28	6.73	...	...	3.79
71117	1.33	65	0.99	0.74	1.33	< 2.1	65	1.33
71122	1.14	66	> 1.05	...	...	...	...	1.14
71129	...	...	2.04	0.87	7.43	...	...	2.04

Table 3.7 (cont'd)

GRB	z_{spec}	Ref.	z_{best}	z_{min}	z_{max}	$z_{phot,limit}$	Ref.	z_{final}
80205	...	...	6.74	2.96	20	< 5.47	175	5.47
80210	2.64	67	2.51	1.64	4.03	...	...	2.64
80212	...	...	2.61	1.16	8.72	...	...	2.61
080218B	...	...	1.46	0.76	3.27	...	...	1.46
080229A	...	...	1.1	0.83	1.48	...	...	1.1
80303	...	...	3.35	2.18	5.43	< 2.29	176	2.29
80307	...	...	4.87	2.21	20	< 6.68	177	4.87
80310	2.43	68	2.21	1.21	4.67	< 2.84	178	2.43
080319A	...	...	3.8	1.52	20	...	...	3.8
080319B	0.94	69	1.04	0.78	1.4	< 1.96	179	0.94
080319C	1.95	70	1.75	1.08	3.17	< 3.28	180	1.95
080319D	...	...	> 6.66	...	...	...	...	> 6.66
80320	...	...	6.93	2.22	20	...	...	6.93
80328	...	...	2.34	1.55	3.72	< 4.37	181	2.34
80330	1.51	71	0.79	0.37	1.94	< 3.28	182	1.51
80409	...	...	2.37	1.62	3.6	...	...	2.37
80411	1.03	72	0.61	0.47	0.79	< 2.29	183	1.03
080413A	2.43	73	2.59	1.79	3.94	< 3.28	184	2.43
080413B	1.1	74	0.67	0.5	0.9	< 2.29	185	1.1
80426	...	...	1.09	0.76	1.63	...	...	1.09
80430	0.77	75	1.53	1.1	2.19	< 1.96	186	0.77
80506	...	...	6.26	1.72	20	< 4.37	187	4.37
80515	...	...	0.56	0.28	0.93	...	...	0.56
80516	3.2 ± 0.3	58	3.62	1.86	7.96	...	...	3.2 ± 0.3
80517	...	...	> 2.29	...	...	...	...	> 2.29
80520	1.55	76	0.75	0.62	1.73	< 2.4	76	1.55
80523	...	...	> 5.11	...	...	< 4.37	188	4.37
80602	...	...	2.84	1.28	7.99	...	...	2.84
080603B	2.69	77	2.68	1.93	3.68	< 2.84	189	2.69
80604	1.42	78	...	...	...	...	...	1.42
80605	1.64	79	1.05	0.78	1.43	< 3.28	190	1.64
80607	3.04	80	1.04	0.78	1.44	< 5.47	191	3.04
080613B	...	...	9.36	4.36	20	...	...	9.36
80623	...	...	3.45	2.12	6.02	...	...	3.45
80701	...	...	1.42	0.99	2.12	...	...	1.42
80703	...	...	11.6	3.7	20	< 5.47	192	5.47
80707	1.23	81	2.35	0.77	8.87	...	...	1.23

Table 3.7 (cont'd)

GRB	z_{spec}	Ref.	z_{best}	z_{min}	z_{max}	$z_{phot,limit}$	Ref.	z_{final}
80710	0.85	82	...	...	...	< 1.96	193	0.85
80714	...	...	1.36	0.96	1.98	...	...	1.36
80721	2.6	83	1	0.75	1.39	< 3.28	194	2.6
080723A	...	...	4.61	2.11	14.23	...	...	4.61

References of table 3.7 : (1) Berger et al. 2005a; (2) Berger et al. 2006; (3) Kelson & Berger 2005; (4) Fynbo et al. 2005a; (5) UVOT, photometric; (6) Cenko et al. 2005; (7) Berger et al. 2005b; (8) Foley et al. 2005; (9) Berger & Becker 2005; (10) Chen et al. 2005; (11) de Pasquale et al. 2007; (12) Jakobsson et al. 2006a; (13) Prochaska et al. 2005; (14) Fynbo et al. 2005b; (15) Halpern & Mirabal et al. 2006; (16) Kawai et al. 2005; (17) Fugazza et al. 2005; (18) Jakobsson et al. 2005; (19) Soderberg et al. 2005; (20) Quimby et al. 2005; (21) Jaunsen et al. 2008; (22) Hill et al. 2005; (23) Melandri et al. 2006; (24) Piranomonte et al. 2006a; (25) Grazian et al. 2006; (26) Fynbo et al. 2006a; (27) Cucchiara et al. 2006a; (28) Berger et al. 2006; (29) Dupre et al. 2006; (30) Cucchiara et al. 2006b; (31) Price et al. 2006; (32) Cenko et al. 2006b; (33) Berger & Gladders 2006; (34) Castro-Tirado et al. 2005; (35) Peterson et al. 2006; (36) Ledoux et al. 2006; (37) Jakobsson et al. 2006b; (38) Jakobsson et al. 2006c; (39) Thoene et al. 2006a; (40) Thoene et al. 2006b; (41) Fugazza et al. 2006; (42) Vreeswijk et al. 2006; (43) Rol et al. 2006; (44) Piranomonte et al. 2006b; (45) Ruiz-Velasco et al. 2007; (46) Thoene et al. 2006c; (47) Fynbo et al. 2006c; (48) Bloom et al. 2006; (49) Berger 2006; (50) Jaunsen et al. 2007a; (51) Cucchiara et al. 2007a; (52) Jaunsen et al. 2007b; (53) Jakobsson et al. 2007a; (54) Cenko et al. 2007a; (55) Thoene et al. 2007a; (56) Berger et al. 2007; (57) Thoene et al. 2007b; (58) Filgas et al. 2008; (59) Prochaska et al. 2007a; (60) Thoene et al. 2007c; (61) Prochaska et al. 2007b; (62) Cenko et al. 2007b; (63) Jakobsson et al. 2007b; (64) Ledoux et al. 2007; (65) Jakobsson et al. 2007c; (66) Cucchiara et al. 2007b; (67) Jakobsson et al. 2008a; (68) Prochaska et al. 2008a; (69)

Vreeswijk et al. 2008a; (70) Wiersema et al. 2008a; (71) Malesani et al. 2008; (72) Thoene et al. 2008a; (73) Thoene et al. 2008b; (74) Vreeswijk et al. 2008b; (75) de Ugarte Postigo et al. 2008; (76) Jakobsson et al. 2008b; (77) Fynbo et al. 2008a; (78) Wiersema et al. 2008b; (79) Jakobsson et al. 2008c; (80) Prochaska et al. 2008b; (81) Fynbo et al. 2008b; (82) Perley et al. 2008; (83) D'Avanzo et al. 2008; (84) Malesani et al. 2007; (85) Pellizza et al. 2006; (86) Mason et al. 2005; (87) Cobb et al. 2005; (88) Greco et al. 2005; (89) Rol et al. 2005; (90) Schady et al. 2005; (91) Holland et al. 2005; (92) Brown et al. 2005; (93) Rhoads et al. 2005; (94) Poole et al. 2005; (95) Wren et al. 2005; (96) Covino et al. 2005; (97) Poole et al. 2005; (98) Blustin et al. 2005; (99) Blustin et al. 2005; (100) McGowan et al. 2005; (101) Pavlenko et al. 2005; (102) Ramya et al. 2005; (103) Jensen et al. 2005; (104) Chester et al. 2005; (105) Schady et al. 2005; (106) De Pasquale et al. 2005; (107) Hunsberger et al. 2005; (108) Rumyantsev et al. 2005; (109) Blustin et al. 2005; (110) Holland et al. 2005; (111) Poole et al. 2005; (112) Holland et al. 2005; (113) Wozniak et al. 2006; (114) Blustin et al. 2006; (115) Holland et al. 2006; (116) Swan et al. 2006; (117) Cucchiara et al. 2006c; (118) Boyd et al. 2006; (119) Mundell et al. 2006; (120) Blustin et al. 2006b; (121) Schady et al. 2006a; (122) De Pasquale et al. 2006a; (123) Poole et al. 2006; (124) Holland et al. 2006b; (125) Melandri et al. 2006b; (126) De Pasquale et al. 2006b; (127) Brown et al. 2006a; (128) Blustin et al. 2006c; (129) Oates et al. 2006a; (130) Schady et al. 2006b; (131) Schady et al. 2006c; (132) Boyd et al. 2006; (133) Grupe et al. 2006; (134) Pandey et al. 2006; (135) Malesani et al. 2006; (136) Oates et al. 2006b; (137) Cenko et al. 2006c; (138) Morgan et al. 2006; (139) Brown et al. 2006b; (140) Kiziloglu et al. 2006; (141) Schady et al. 2006d; (142) Holland et al. 2006c; (143) Chen et al. 2006; (144) Melandri et al. 2006c; (145) Marshall et al. 2006; (146) Schady et al. 2006e; (147) Roming et al. 2007; (148) Halpern et al. 2007; (149) Marshall et al. 2007a; (150) Kuin et al. 2007; (151) Oates et al. 2007; (152) Landsman & Stamatikos et al. 2007; (153) Schmidt & Mackie et al. 2007; (154) Immler et al. 2007; (155) Landsman & Pagani et al. 2007; (156) Marshall & Grupe et al. 2007; (157) Cucchiara et al.

2007c; (158) Holland et al. 2007; (159) Landsman et al. 2007a; (160) Barthelmy et al. 2007; (161) De Pasquale et al. 2007a; (162) Landsman et al. 2007b; (163) Marshall et al. 2007b; (164) De Pasquale et al. 2007; (165) Malesani et al. 2007; (166) Klotz et al. 2007; (167) Misra et al. 2007; (168) Kocevski et al. 2007; (169) Cenko et al. 2007; (170) Iizuka et al. 2007; (171) Updike et al. 2007; (172) Piranomonte et al. 2007; (173) Williams et al. 2007; (174) Breeveld et al. 2007; (175) Oates et al. 2008a; (176) Breeevld et al. 2008; (177) Xin et al. 2008; (178) Hoversten et al. 2008; (179) Holland et al. 2008a; (180) Holland et al. 2008b; (181) Fatkhullin et al. 2008; (182) Kuin et al. 2008a; (183) Oates et al. 2008b; (184) Oates et al. 2008c; (185) Oates et al. 2008d; (186) Landsman et al. 2008a; (187) Oates et al. 2008e; (188) Fynbo et al. 2008c; (189) Kuin et al. 2008b; (190) Kuin et al. 2008c; (191) Schady et al. 2008; (192) Ward et al. 2008a; (193) Landsman et al. 2008b; (194) Ward et al. 2008b;

We ran a Monte Carlo simulation on a sample of all *Swift* GRBs with z_{spec}. The typical uncertainty of our z_{best} is $\sim 0.69 \times z_{best}$ in the positive direction and $\sim 0.35 \times z_{best}$ in the negative direction. In our simulations, we added random noises on z_{spec}, which were chosen to be normally distributed on both sides, with standard deviations of $0.69 \times z_{best}$ in the positive direction and $0.35 \times z_{best}$ in the negative direction. Whether a positive or a negative uncertainty was added on z_{spec} is also randomly chosen, with the chance half and half. The resultant redshifts were then recorded as $z_{simulated}$. A comparison between the cumulative distribution of the $z_{simulated}$, z_{best} and our z_{best} was then made, as shown in Figure 3.4. A Kolmogorov-Smirnov test was made between z_{best} and $z_{simulated}$, with the maximum difference of 0.06 between these two cumulative distribution function, and a p value of 0.97. From both the comparison plot and the Kolmogorov-Smirnov test, we see that the distribution of $z_{simulated}$ and z_{best} agrees well enough with each other.

From the catalog of our z_{best}, we made a cumulative redshift distribution plot for all *Swift* long GRBs, as shown in Figure 3.5. This is a redshift distribution for *Swift* long GRBs,

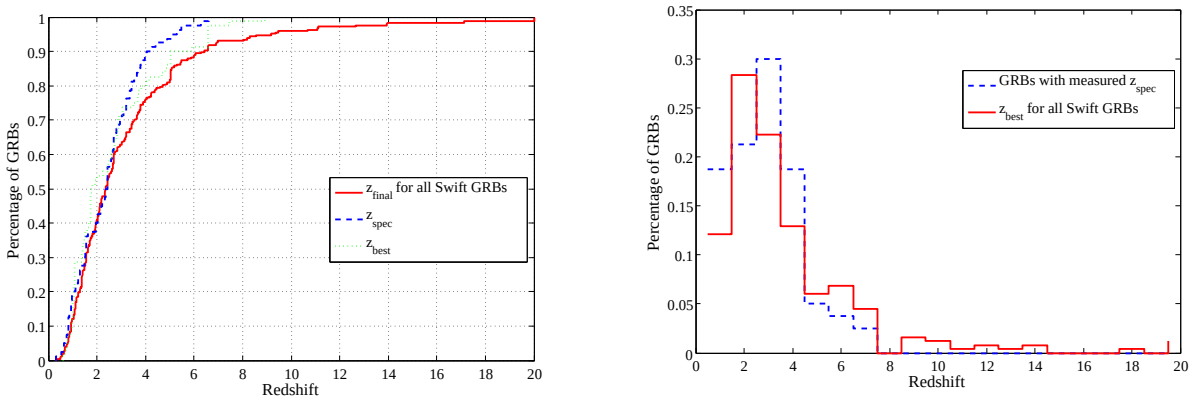

Figure 3.5 Left panel: Cumulative distribution plot of bursts with z_{spec}, z_{best} for bursts with z_{spec} and z_{final} for all *Swift* GRBs. For z_{final} plot, about $\sim$ 20% of the total have their redshift larger than 5. A K-S test is done on bursts with z_{spec} and all *Swift* bursts, a difference of 0.14 is found, and the p value is 0.20. Right Panel: comparison of redshift distribution for GRBs with z_{spec} and all *Swift* GRBs. The bias of the spectroscopic redshift is not as large as expected.

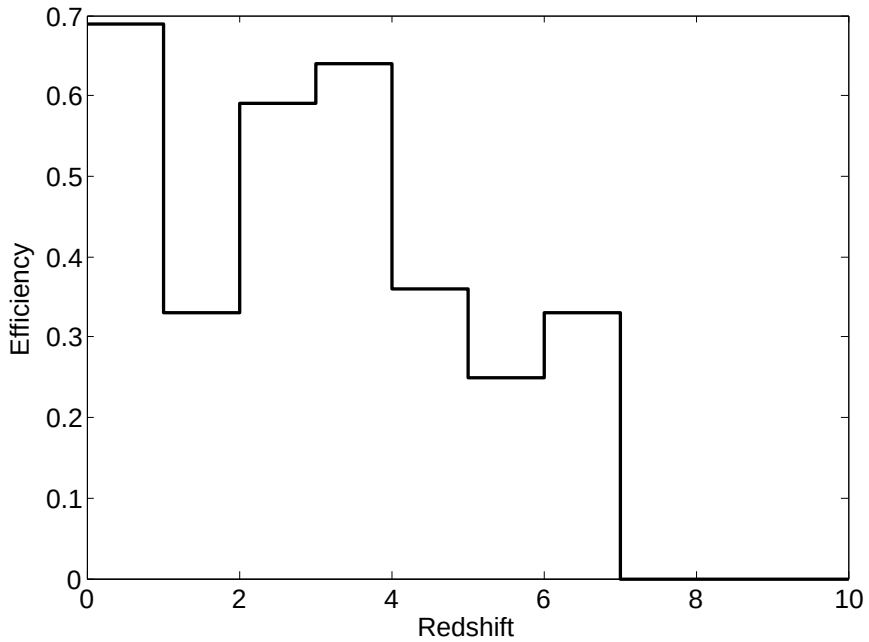

Figure 3.6 Efficiency versus redshift plot, from which we see that the redshift detection efficiency at high redshift is significantly low comparing with that at low redshift.

without any spectroscopic detection threshold effect. However, as stated before, the random noise might cause an offset of our z_{best} distribution from the real GRB redshift distribution. A de-convolution process was then taken to eliminate the noise effect from our z_{best} and to obtain the intrinsic GRB redshift distribution $z_{intrinsic}$. First, take z_{best} distribution as the GRB redshift distribution, by adding a normally distributed random noise on z_{best}, a new distribution of z_I can be calculated. The noise added on z_{best} is randomly selected from a normal distribution of N($0.69\times z_{best}$) in positive direction and N($0.35\times z_{best}$) in the negative direction. The difference between the distributions of z_I and z_{best} is then an estimate of the noise effect on z_{best}. By subtracting the noise effect from z_{best}, a distribution of $z_{best,I}$ was calculated. $z_{best,I}$ can be taken as the first estimated intrinsic distribution. A better estimate of the noise effect can then be obtained by adding random normally distributed noise on the distribution of $z_{best,I}$, where the standard deviation of the noise is $0.69\times z_{best,I}$ in positive direction and $0.35\times z_{best,II}$ in the negative direction. By taking the new noise effect off the distribution z_{best}, the second estimation of the intrinsic redshift distribution, $z_{best,II}$, was then obtained. A Kolmogorov-Smirnov test was then taken between $z_{best,I}$ and $z_{best,II}$ distribution. If the difference between $z_{best,I}$ and $z_{best,II}$ is smaller than 0.10, we then adopt the $z_{best,II}$ as the intrinsic GRB redshift distribution. Otherwise, we will continue from $z_{best,II}$ for a new round of noise effect evaluation and GRB redshift distribution calculation, until we get a $z_{best,i}$ distribution which is within 0.10 from $z_{best,i-1}$ distribution, and $z_{best,i}$ was then the intrinsic redshift distribution that we were looking for. By running this converging process, the intrinsic redshift distribution of our redshift catalog was obtained. The resulting GRB redshift distribution plot is also shown in Figure 3.4. A Kolmogorov-Smirnov test was taken between the cumulative distribution of z_{spec} and $z_{best,i}$, and a 0.14 difference is found, with a p value equals 0.20. A significant difference between these two distributions was found in the high redshift region. The efficiency of redshift detection can be evaluated by taking the ratio of GRBs with spectroscopic redshift versus all GRBs at a given redshift. The

efficiency versus redshift plot is shown in Figure 3.6, from which we see that the efficiency is significantly lower at high redshifts.

In Bromm & Loeb (2006), redshift distributions of all GRBs by different instruments (BATSE and *Swift*) were predicted based on the star formation rate of the universe and the flux-limited detection threshold of these instruments. Their predicted redshift goes up to $z = 17$, and with a fraction f($z > 5$) for *Swift* to be $\sim 10\%$. Our $z_{intrinsic}$ distribution shows a f($z > 5$) $= \sim 10\%$, which is consistent with what Bromm & Loeb (2006) predicted.

3.4 Fermi GRB Redshift Estimation

Fermi, formerly known as GLAST (Gamma-Ray Large Area Space Telescope), launched June 11th, 2008, is another NASA major mission for observations of high energy gamma rays. Its main instrument, the Large Area Telescope (LAT), will provide unprecedented sensitivity to gamma rays in the energy range of $\sim$ 20 MeV to $\sim$ 300 GeV. The GLAST Burst Monitor (GBM) complements the LAT in its observations of transient sources and is sensitive to X-rays and gamma rays with energies between 8 keV and 25 MeV. The combination of the GBM and the LAT provides a powerful tool for studying gamma-ray bursts, particularly for time-resolved spectral studies over a very large energy band. With LAT and GBM, more than 200 bursts per year are expected to be detected by *Fermi*, and near-real-time location information are expected to be distributed to other observatories for afterglow searches. With our success on the *Swift* long GRBs, we are confident to extend our programs on Fermi GRBs. The data pipeline of *Fermi* is able to provide the light curve and spectrum of each GRB, which is all we need for the calculation of our redshifts. One possible option is to import my code into the data analysis software of *Fermi* GRBs, in which case we can make a redshift alert to the community fast ($\sim$ 10 mins after a raw light curve and spectrum are produced). The fast ($\sim$ 10 mins) notification will alert people to possible high-z events (for immediate followup with big telescopes) as the only way that the $> 5\%$ high-z bursts

will likely get looked at with optical and IR spectroscopy. Also, it will alert observers to any low-z bursts for followup by looking for Supernovae.

In Feb. and Mar. 2009, I spent two months visiting the *Fermi* GBM team in Huntsville, AL, and imported my code into the *Fermi* software RMFIT. A few *Fermi* GRBs with known spectroscopic redshifts have been tested. For GRBs detected by GBM, there are four different types of data formats. The TRIGDAT data is produced and transmitted by GBM immediately after the trigger, which consists of a time history of the burst for all detectors with eight channel energy resolution and time resolution varying between 64 ms and 8 s. Three other types of science data packages will be produced half an hour to a few hours later. The CTIME data, consisting of accumulated spectra from each detector with 8 channel pulse height resolution, has an accumulating time interval from 64 to 1024 ms, with a default value of 256 ms. The CSPEC data, consisting of accumulated spectra from each detector with 128 channel pulse height resolution, has an accumulating time interval from 1.024 s to 32.768 s, with a default value of 4.096 s. The TTE data has the same 128 channel boundaries, and the time interval is 0.1 s. With high energy and low temporal resolution, the CSPEC is mostly used for spectral analysis. TRIGDAT data is fast enough for our rapid alert, however, both the energy and temporal resolutions are too low, and the calculated luminosity indicators and redshifts have large uncertainties, which will be shown later. TTE data is the most precise format in our calculation, but it takes much longer to be produced, by which time the follow-up telescopes might not be able to detect the afterglow. As as result, the most ideal case for us is to use CTIME for the temporal analysis to calculate temporal luminosity indicators, CSPEC for the spectral analysis to calculate peak photon energy and fluences, and then combine these results to calculate the redshift.

The software that GBM Burst Advocators have been using is RMFIT. The Graphic User Interface and simple analysis of the software was written in IDL, and the spectral fitting part 'mfit' was programmed in fortran. The Graphical User Interface is shown in Figure 3.7.

All TRIGDAT, CTIME and CSPEC data can be loaded into RMFIT, and the light curves will be depicted in the main frame. Various analysis can be done on these different formats of data. The source can be located by using TRIGDAT data. With a better location of the source, the dynamic response matrix will be generated from the pipeline (which is out of the RMFIT program), and by using the CTIME, CSPEC data and the generated response file, the spectral fit can be done. Various human judgements are needed in the analysis, e.g. choosing the energy range, the time range, and function for the background fitting, double check χ^2 plot, etc. I converted all my calculation of luminosity indicator values and GRB redshift calculation into IDL, and made my own Graphical User Interface, which can be well fitted into the existing User Interface of RMFIT. All my programs are compressed into the 'Redshift Calculation', which includes exporting the original data to the format we need, lag calculation, variability calculation, minimum rise time and number of peak calculation, and the final redshift calculation.

There are a few troubles with the *Fermi* fast alert. One of the troubles is that the only available data format within minutes of the trigger is TRIGDAT. However, both the energy and time accumulated interval are too large in TRIGDAT data. The calculated temporal luminosity indicators (τ_{lag}, Variability, τ_{RT}, and N_{peak}) show uncertainties which are much larger than expected. Without a reliable dynamic response matrix and low energy resolution, the spectral fit cannot be done accurately. As a result, we will not be able to estimate the redshift based upon the TRIGDAT data. Both CTIME and CSPEC data have high resolutions suitable for our calculation. However, it takes half an hour to a few hours before we can obtain the CTIME and CSPEC data, with the delay time varying depending on the pipeline processing and the Burst Advocator. Another trouble which is more important is that the on board localization of *Fermi* GRBs has an accuracy of $10^\circ - 15^\circ$, and the ground localization after delicate calculation is still a few degrees, which is too large for ground optical telescope to follow up. In this case, even if we are able to obtain a CTIME

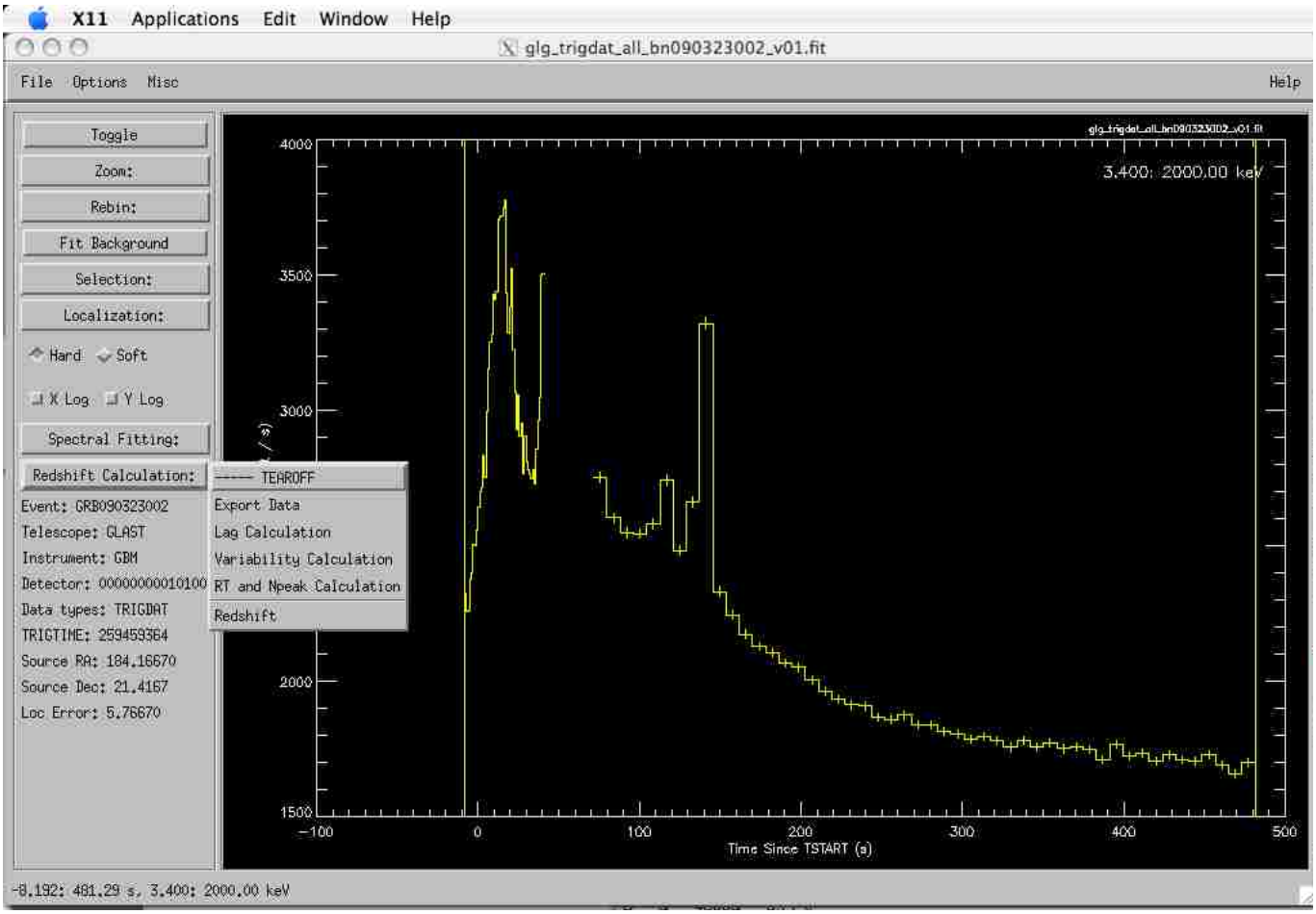

Figure 3.7 Graphical User Interface of GBM software RMFIT. A light curve with format TRIGDAT, CTIME, and CSPEC can be loaded and depicted in the main frame. Various options can be chosen by user, e.g. zoom in and out, change the bin size, choose the time range and function to fit the background, and do spectral fitting. My 'Redshift Calculation' is the program added to do all the temporal analysis and calculate the redshift.

Table 3.8. *Fermi* GRB Redshifts.

GRB	z_{spec}	Ref [a]	z_{best}	z_{min}	z_{max}
080916	0.689	1	1.47	0.81	3.08
081121	2.512	2	1.63	0.98	3.03
081222	2.77	3	0.72	0.49	1.10
090102	1.547	4	1.92	1.16	3.67
090323	3.57	5	8.56	1.88	20
090328	0.736	6	1.13	0.73	1.86
090423	8.26	7	1.72	0.74	5.98
090424	0.54	8	0.45	0.32	0.65
090618	0.54	9	0.32	0.26	0.46

[a]References: —(1) Fynbo et al. (2008d); (2) Berger & Rauch (2008); (3) Cucchiara et al. (2008); (4) de Ugarte Postigo et al. (2009); (5) Chornock et al. (2009a); (6) Cenko et al. (2009a); (7) Tanvir et al. (2009); (8) Chornock et al. (2009b); (9) Cenko et al. (2009b);

and CSPEC light curve and spectrum, our rapid alert cannot be followed by the ground telescopes, and our prediction of high redshift GRBs cannot be confirmed.

However, without the rapid notification service of high redshift GRBs, we can still test our luminosity relations and redshift calculations on this completely independent sample. From the launch of *Fermi* on June, 11, 2008 until August, 2009, there are 13 GRBs with spectroscopic redshift in total. One of the 13 GRBs is a short GRB, which is not applicable in our method, and 3 of the GRBs are so faint and noisy that no useful information can be drawn from either the light curve or the spectrum. I calculated the luminosity indicator values and the redshift value for the remaining 9 GRBs, using my updated version of RMFIT. All my redshift value with comparison to the spectroscopic redshifts are shown in Table 3.8.

Five of the nine GRBs in the table have their spectroscopic redshifts falling into our $1-\sigma$ region, which means that our evaluated error bars are smaller than the real scatters.

The χ^2 value is 4.19, which is significantly larger than unity. However, most of the χ^2 value comes from one GRB, GRB081222, which has a relatively small σ evaluated. As a result, we conclude that due to some reason, the redshift or the uncertainty of GRB081222 does not work well in our method, and if we take it as an outlier, for the remaining 8 GRBs, the redshifts and uncertainties are reasonable. And by excluding GRB081222, the average value of $\log(z_{best}/z_{spec})$ is -0.02, which means our z_{best} is not biased to within the 2% level.

From all above analysis, we conclude that for *Fermi* GRBs, our measured redshifts are uncertainties are reasonable, and the scatter is comparable with the *Swift* GRBs. The improvement on E_{peak} measurement due to better spectrum resolution and larger energy range did not help much in improving the accuracy of our method. With the data and the uncertainty at hand, we are not confident to send out the rapid high redshift notifications to the community yet.

4. Applications of GRB Redshift Catalog

4.1 Long Lag GRBs and the Local Supercluster

The τ_{lag} analysis on BATSE and INTEGRAL samples shows a distribution from $\sim 0-10$ s for long GRBs (Norris , 2002; Foley et al., 2008), with most of these τ_{lag} concentrated in the 0 - 1 s region. According to the $\tau_{lag} - L$ relation, a long τ_{lag} corresponds with a low luminosity, and for a low luminosity GRB to be detected by our instruments, it should be relatively nearby. Norris (2002) pointed out that GRB980425 might represent a subclass of long GRBs, with long τ_{lag}, soft spectrum, ultra-low luminosity, and nearby. In this case, a possible break might exist in the $\tau_{lag}-L$ relation in the long τ_{lag} region, which would indicate that these long τ_{lag} GRBs are even closer than what is predicted by the $L \propto \tau_{lag}^{-1}$ relation. Indeed, two long τ_{lag} bursts are confidently known to be at distances close enough to be inside the Local Supercluster. GRB980425, with $\tau_{lag} = 2.8$ s, had an ultra-low luminosity, and lies in a galaxy only ~ 38 Mpc away (Galama et al., 1998). GRB830801, is the all-time brightest GRB yet has a long τ_{lag} (2.2 ± 0.2 s), so a very low redshift of $z \sim 0.01$ is calculated from the $\tau_{lag} - L$ relation (Schaefer et al., 2001). GRB830801 also happens to be from a direction close to the Virgo Cluster.

Given that these long τ_{lag} GRBs might be nearby, is there any local structure of galaxies to host these GRBs? The Local Supercluster was proposed by de Vaucouleurs (1953), from an investigation of spatial distribution of galaxies. It was first named as 'Supergalaxy', which was later changed to be 'Local Supercluster' (de Vaucouleurs , 1958). More detailed studies show that the main body of the Local Supercluster is a filamentary structure extending over $\sim 40\ h^{-1}$ Mpc, and is centered on the Virgo Cluster (Tully & Fisher , 1987; Karachentsev & Makarov , 1996; Lahav et al., 2000). Around 60% of the luminous galaxies in the volume of

Local Supercluster are within the structure that defines the plane of the Supercluster (20% in Virgo Cluster and 40% in Virgo II Cloud and Canes Venatici Cloud), and most of the remaining 40% lies within five clouds off the plane, which is called a 'halo' (Tully , 1982). Our Local Group is in the outskirt of this region.

Norris (2002) presented a catalog of τ_{lag} values for 1429 BATSE long GRBs, from which a sample of 64 long τ_{lag} GRBs (with $\tau_{lag} > 2$ s) was selected. These τ_{lag} values were calculated in the observer's rest frame, without making the time dilation correction (which should be small for local bursts). By plotting these long τ_{lag} bursts on a sky map in Supergalactic coordinates, a concentration towards the Supergalactic plane was found, with three-fourth of these bursts located in the half of the sky between -30° and 30° of Supergalactic latitude. Quantitatively, the quadrupole moment of these GRBs is roughly -0.10 ± 0.04, which shows a 2.5σ deviation from isotropy. This result implies that long τ_{lag} value will be an indicator for local GRBs. From the solid long GRB-SN connection (e.g. GRB980425 & SN1998bw, GRB030329 & SN2003dh) and the model of massive SN (from the collapsing in highly non-axisymmetric modes), strong gravitational waves can be produced at a rate of $\sim 4\ yr^{-1}$, and these gravitational waves might be able to be detected by LIGO (Norris , 2003).

An independent catalog of long τ_{lag} bursts discovered by INTEGRAL has been created by Foley et al. (2008), with 11 long τ_{lag} ($\tau_{lag} > 0.75$ s) GRBs being pulled out from the whole INTEGRAL sample. They found that 10 of the 11 long τ_{lag} bursts are located within the -30° to 30° Supergalactic latitude region. The quadrupole moment of the 11 GRBs is -0.225 ± 0.090. This result is confirmed by Vianello et al. (2009). By comparing with the simulation based on INTEGRAL sky coverage, the quadrupole moment is $Q = -0.271 \pm 0.089$ for long τ_{lag} GRBs and $Q = -0.007 \pm 0.042$ for the whole sample. The INTEGRAL result is broadly consistent with the conclusion of Norris (2002), however, in Norris (2002), the quadrupole moments for the samples of $\tau_{lag} > 0.5$ s and $\tau_{lag} > 1$ s have a substantially lower significance ($Q = -0.022 \pm 0.020$ for the $\tau_{lag} > 0.5$ s sample and $Q = -0.043 \pm 0.026$

for the $\tau_{lag} > 1$ s sample). With three results on two independent samples (pointing to a concentration towards the Supergalactic plane), another sample is needed to test the Local Supercluster hypothesis.

The accurate localizations of *Swift* GRBs make possible the search for hosts of long τ_{lag} bursts in Local Supercluster galaxies. The GRB redshift will also directly tell us the distances of these GRBs. From our *Swift* GRB redshift and luminosity indicators catalog (ranging from Dec. 2004 (GRB041220) to Jul. 2008 (GRB080723A)), 18 GRBs with long τ_{lag} values ($\tau_{lag} > 1$ s) are pulled out. Data for these 18 GRBs are listed in Table 4.1. Column 1 gives the six digit identification numbers of each GRB. Column 2 lists our measured τ_{lag} values with their $1-\sigma$ uncertainties. Column 3 gives the spectroscopic redshifts for 6 of these GRBs and our calculated redshifts z_{ind} with $1-\sigma$ uncertainties for the remaining 12. The references for these redshifts are listed in column 4. The celestial right ascension and declination of these GRBs from BAT localizations are listed in columns 5 and 6, and the corresponding latitude and longitude in Supergalactic coordinate systems are listed in columns 7 and 8. The conversion from celestial coordinate system to the Supergalactic coordinate system is done by using the online tools provided on a NASA website[1]. Column 9 lists the galaxy information within the field of the GRBs, with all the references given in column 10. All information of the galaxies are drawn from the reports on GCN Circulars and the Digital Sky Survey[2]. The sky distribution of these long τ_{lag} GRBs in Supergalactic coordinates are plotted in Figure 4.1. At first glance, there is no tendency of concentration either towards the Supergalactic plane or towards the Virgo or Coma Cluster. More detailed analysis is presented below.

[1]http://lambda.gsfc.nasa.gov/toolbox/tb_coordconv.cfm
[2]http://archive.stsci.edu/cgi-bin/dss_form

Table 4.1. Information of Swift GRBs

GRB	τ_{lag}	Redshift	Ref[a]	RA[b]	Dec[b]	Longitude[c]	Latitude[c]	Galaxy In the Field?	Ref[a]
041228	4.02 ± 0.15	$2.3^{+4.2}_{-1.2}$	1	22:26:34	05:01:55	290:50:01	37:02:09	no galaxy with $m < 20.8$	10
050126	2.41 ± 0.08	1.29	2	18:32:27	42:23:02	35:37:03	62:53:07	host z = 1.29	2
050219A	2.39 ± 0.17	$0.6^{+0.2}_{-0.1}$	1	11:05:39	- 40:40:51	154:49:21	-30:46:32	no galaxy with $m < 20.8$	10
050410	3.32 ± 0.30	$1.04^{+5.15}_{-0.32}$	1	05:59:01	79:36:18	23:56:45	05:36:23	no galaxy with $m < 20.8$	10
050716	4.09 ± 0.31	$1.4^{+1.1}_{-0.5}$	1	22:34:22	38:40:58	333:24:23	37:00:24	no galaxy with $m < 20.8$	10
051021B	1.53 ± 0.06	$2.1^{+1.3}_{-0.7}$	1	08:24:14	- 45:32:02	178:59:49	-54:47:23	no galaxy with $m < 20.8$	10
051111	1.74 ± 0.07	1.55	3	23:12:32	18:22:01	309:07:18	28:42:13	no galaxy with $m < 20.8$	10
060218	177 ± 16[d]	0.03	4	03:21:31	16:54:36	325:57:54	-28:05:07	host z = 0.0331, $M_V \sim 15.8$ mag	4, 11
060319	1.19 ± 0.13	$2.0^{+1.1}_{-0.6}$	1	11:45:31	60:02:16	55:03:16	05:13:06	no galaxy with $m < 20.8$	10
060403	1.15 ± 0.02	$1.3^{+0.7}_{-0.4}$	1	18:49:21	08:19:37	195:41:24	82:29:38	no galaxy with $m < 20.8$	10
060501	1.55 ± 0.25	$1.8^{+1.0}_{-0.5}$	1	21:53:29	44:00:07	342:50:10	42:54:49	no galaxy with $m < 20.8$	10
060502A	4.65 ± 0.16	1.51	5	16:03:44	66:36:14	44:59:56	31:55:36	no galaxy with $m < 20.8$	10
060607A	1.34 ± 0.05	3.08	6	21:58:49	-22:29:45	257:13:41	30:59:00	no galaxy with $m < 20.8$	10
060607B	2.98 ± 0.27	$1.3^{+0.6}_{-0.4}$	1	02:48:10	14:45:18	319:54:06	-21:51:22	no galaxy with $m < 20.8$	10
070330	2.48 ± 0.07	$2.4^{+1.5}_{-0.8}$	1	17:58:07	-63:47:56	200:08:29	09:44:18	no galaxy with $m < 20.8$	10
070506	2.28 ± 0.08	2.31	7	23:08:48	10:42:39	300:21:59	28:14:04	no galaxy with $m < 20.8$	10
070621	2.75 ± 0.37	$1.5^{+0.7}_{-0.4}$	1	21:35:13	-24:48:32	251:04:31	33:43:47	no galaxy with $m < 21.5$	9
071101	1.45 ± 0.01	$3.7^{+2.9}_{-1.5}$	1	03:12:43	62:31:26	04:05:20	-00:37:40	no galaxy with $m < 20.8$	10

[a]References:——(1) Xiao & Schaefer 2009b; (2) Berger et al. 2005; (3) Hill et al. 2005; (4) Mirabal et al. 2006; (5) Cucchiara et al. 2006; (6) Ledoux et al. 2006; (7) Thoene et al. 2007; (8) Jakobsson et al. 2008; (9) Bloom et al. 2007; (10) Digital Sky Survey: http://archive.stsci.edu/cgi-bin/dss_form (11) Modjaz et al. 2006;

[b]The Right scension and declination values are in the celestial coordinate system.

[c]The longitude and latitude values are in the supergalactic coordinate system.

[d]Value obtained from Liang et al. (2006).

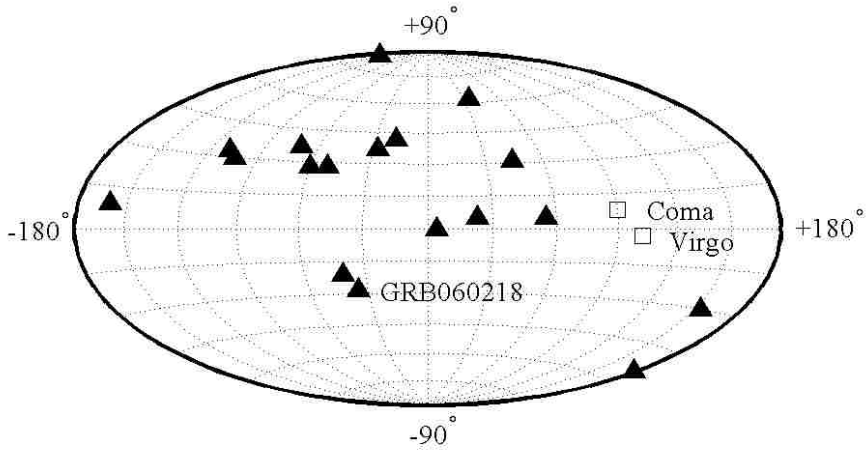

Figure 4.1 Sky distribution of the 18 long τ_{lag} *Swift* GRBs, the Virgo Cluster, and the Coma Cluster. The GRBs are marked as filled triangles, and the Virgo and Coma Clusters are marked as empty squares (upper: Coma, lower: Virgo). GRB060218, the Virgo and Coma Clusters are all marked on the right. From this figure we do not see any tendency either towards the Supergalactic plane (the horizontal line running through the middle) or towards the Virgo or Coma Clusters.

4.1.1 Concentration Towards Supergalactic Plane

Our Local Supercluster has a flattened distribution, with 60% of its luminous galaxies in the structure which is called the plane of the Local Supercluster, and the other 40% lies in five clouds off the plane, called the 'halo'. If long τ_{lag} GRBs reside in galaxies in our Local Supercluster, they will show a tendency of concentration towards the Supergalactic plane.

To quantitatively measure the tendency of the concentration, a quadrupole moment of the distribution can be calculated, with $Q =< \sin^2 b - 1/3 >$ and $\sigma_Q = \sqrt{4/(45N_{GRB})}$ (Briggs et al., 1996), where b is the latitude of GRBs in Supergalactic coordinate and N_{GRB} is the number of GRBs. A significant concentration towards the plane will result in a negative Q value, while an isotropic distribution will result in a near-zero Q value. Both the quadrupole moments of Norris (2002) ($Q \sim -0.10 \pm 0.04$) and of Foley et al. (2008) ($Q = -0.225 \pm 0.090$) show low-moderate significance (with $|Q| = 2.5\sigma_Q$ in both cases) of a concentration towards the Supergalactic plane.

For our long τ_{lag} burst sample from *Swift*, by simply counting the number of GRBs, we get only 8 of a total of 18 ($\sim$ 44%) lying between -30° and 30° in Supergalactic latitude, which covers 50% of the whole sky. The calculated quadrupole moment of this distribution is $Q = -0.02 \pm 0.07$. It is not significantly negative. Instead, the Q value equals zero within $1 - \sigma$ uncertainty and this is an indication of a homogeneous distribution. We also raised the lower limit of the 'long τ_{lag}' criteria to $\tau_{lag} > 1.5$ s and $\tau_{lag} > 2$ s, and calculated the quadrupole moment for these subsamples. The results of $Q = -0.02 \pm 0.08$ for $\tau_{lag} > 1.5$ s and $Q = -0.06 \pm 0.09$ for $\tau_{lag} > 2$ s also show no tendency towards the Supergalactic plane. The samples and our results are shown in Table 4.2. A real-time sky map of *Swift* GRBs[3] shows a nearly isotropic sky distribution for *Swift* bursts, and the quadrupole moment for all short τ_{lag} ($\tau_{lag} < 1$ s) long duration GRBs ($Q = -0.03 \pm 0.02$) also shows an isotropic sky distribution, with no tendency either towards or away from the Supergalactic plane. With this, we see that *Swift* has a uniform sky coverage for the purpose of this paper, and so our quadrupole moment of the long τ_{lag} bursts needs no correction for sky coverage. As such, we find no concentration towards the Supergalactic plane, and the Supergalactic hypothesis fails our first test.

4.1.2 Concentration Towards Virgo or Coma Cluster

The majority of the mass in our Local Supercluster is towards the Virgo Cluster and the Coma Cluster (which is in about the same direction as the Virgo Cluster, but with much larger distance from the Earth). So if these long τ_{lag} GRBs are from the Local Supercluster, there should be a tendency of concentration towards the Virgo and Coma Clusters. A dipole moment can be calculated to quantitatively measure the concentration, with $D =< \cos\theta >$ and $\sigma_D = \sqrt{1/(3N_{GRB})}$ (Briggs et al., 1996), in which θ is the angle between the GRB and the Virgo or Coma Cluster. A concentration towards the Virgo or Coma Cluster will result

[3]http://grb.sonoma.edu/

Table 4.2. Dipole and quadrupole Statistics

Sample	N_{GRB}	Q[a]	D for Virgo[b]	D for Coma[b]
$\tau_{lag} < 1$ s	331	-0.03 ± 0.02	-0.03 ± 0.03	-0.01 ± 0.03
$\tau_{lag} > 1$ s	18	-0.02 ± 0.07	-0.25 ± 0.14	-0.14 ± 0.14
$\tau_{lag} > 1.5$ s	14	-0.02 ± 0.08	-0.30 ± 0.15	-0.20 ± 0.15
$\tau_{lag} > 2$ s	11	-0.06 ± 0.09	-0.28 ± 0.17	-0.18 ± 0.17

[a]The quadrupole moment is sensitive to measuring a concentration towards the Supergalactic plane ($Q \ll 0$), while an isotropic distribution yields $Q \simeq 0$.

[b]The dipole moment is sensitive to measuring a concentration towards either the Virgo Cluster or the Coma Cluster ($D \gg 0$), while an isotropic distribution yields $D \simeq 0$.

in a positive dipole moment, while an isotropic distribution would result in a near-zero dipole moment. D values for a majority of long *Swift* GRBs (331 bursts with $\tau_{lag} < 1$ s) shows no tendency towards or away from Virgo and Coma Clusters, as shown in Table 4.2. The fact that the dipole for the $\tau_{lag} < 1$ s bursts is closely zero tells us that the *Swift* sky coverage is sufficiently uniform for the purpose of this paper and no correction to our measured D values is needed.

We calculated the dipole moment of our long τ_{lag} GRBs, towards both the Virgo and Coma Clusters. For the Virgo Cluster, the dipole moments are -0.25 ± 0.14 for $\tau_{lag} > 1$ s sample, -0.30 ± 0.15 for the $\tau_{lag} > 1.5$ s subsample, and -0.28 ± 0.17 for the $\tau_{lag} > 2$ s subsample. While for Coma Cluster, the calculated dipole moments are respectively -0.14 ± 0.14, -0.20 ± 0.15, and -0.18 ± 0.17 for the three cuts on τ_{lag}. With the *negative* dipole moments, *Swift* long τ_{lag} bursts are showing a tendency *away from* the Virgo and Coma clusters. Hence the hypothesis that these GRBs are from the Local Supercluster fails our second test. By checking Figure 5 in Norris (2002) and Figure 3 in Foley et al. (2008), we do not see any tendency towards the Virgo or Coma Cluster.

4.1.3 Host Galaxy of These GRBs

As long GRBs are formed by the collapsing of fast-rotating massive stars, they should be located in the star forming region of galaxies (e.g. in the spiral arms of the spiral galaxies), and these galaxies should appear within the small *Swift*-XRT 90% error circles. If these galaxies are members of the Local Supercluster, given the scale of the Local Supercluster ($\sim 40\ h^{-1}$ Mpc), they should be rather nearby, and hence relatively bright. If we adopt the R-band Schechter luminosity function with $M^* = -21.2$ (for a Hubble constant of 65 km s^{-1} Mpc^{-1}; Lin et al. (1996)), a galaxy in our Local Supercluster with luminosity of $L^*/10$ will have its absolute magnitude of $M = -18.7$. This limit of $L^*/10$ is somewhat arbitrary, but it does include 90% of the mass in a standard luminosity function. Such a galaxy on the far edge of Local Supercluster (for which we adopt a distance of ~ 56 Mpc) will have an apparent magnitude of $m = 15.0$ or brighter. An increasing of Hubble constant from 65 km s^{-1} Mpc^{-1} to 72 km s^{-1} Mpc^{-1} will cause a slightly decrease of the distance, and hence a brighter apparent magnitude for the threshold. As a result, if the long τ_{lag} GRBs reside in our Local Supercluster, we should be able to find their host galaxies with $m \leq 15$. That is, any GRB from our Local Supercluster should be immediately obvious by having its bright host galaxy in the *Swift*-XRT error circle.

We checked all the GCN reports regarding to these long τ_{lag} GRBs, and all these 18 GRBs have follow up observations reported except for GRB060607B (which was too close to the Sun). Possible host galaxies are found for GRB050126 and GRB060218, with redshifts of 1.29 and 0.0331. With accurate positions reported by XRT, no galaxies are found to be within the XRT 90% error circles for the remaining 16 GRBs. We also searched through the Digital Sky Survey for the fields of these GRBs, and no galaxies are found to be within the XRT error circle for all of the 18 GRBs in POSS II-F archive, the limit magnitude of which is 20.8. Hence the Supergalactic hypothesis fails this test also.

GRB060218 is a very long and smooth burst with a very long lag (Liang et al., 2006). An optical transient was speedily discovered with UVOT (Marshall et al., 2006) and with ROTSE (Quimby et al., 2006). The burst position is coincident with a nearby galaxy at z = 0.0331 (Mirabal et al., 2006). Later, a supernova (SN2006aj) was found at the same position (Masetti et al., 2006; Soderberg et al., 2006). The position is on the edge of the constellation Taurus, with $\theta = 128^\circ$ to the Virgo Cluster and $\theta = 125^\circ$ to the Coma Cluster. For the redshift and a Hubble constant of $H_0 = 72$ km s^{-1} Mpc^{-1}, the burst is ~ 140 Mpc distant from the Earth. This is close, but certainly outside our Local Supercluster. As such, this long τ_{lag} burst is an example of an extremely under-luminous event, but is not associated with any concentration towards the Supergalactic plane.

4.1.4 Redshifts

Given that the distance of galaxies in Local Supercluster are less than 56 Mpc from the Earth (for the Hubble constant $H_0 = 72$ km s^{-1} Mpc^{-1}), the corresponding upper limit on the redshift is $z < 0.013$. If the long τ_{lag} GRBs are from the Local Supercluster, they should be at redshift $z < 0.013$ or so.

Of our 18 long τ_{lag} GRBs, 5 have their spectroscopic redshift reported, ranging from 1.29 to 3.08 (as listed in Table 4.1). These bursts are certainly far outside the Local Supercluster. The redshift of GRB050126 is measured from the spectrum of its host galaxy, while the other 4 are all from multiple absorption lines in the optical afterglow spectra, hence these redshift values have high confidence. The sixth GRB with a spectroscopic redshift is GRB060218, with z = 0.0331, which is also too far to be inside our Local Supercluster (see previous section). With six out of six long τ_{lag} GRBs having their spectroscopic redshift much larger than the upper limit redshift of Local Supercluster (0.013), we are very confident to make the conclusion that the Supergalactic hypothesis fails this test also for the *Swift* sample. While for the remaining 12 GRBs lack spectroscopic redshifts, our redshift calculated from

luminosity indicators z_{ind} are within the range of 0.6 to 5.0 (Xiao & Schaefer, 2009), and the $1-\sigma$ lower limit of redshifts for all these GRBs are $z > 0.5$. In summary, all these *Swift* long τ_{lag} bursts are certainly outside the Local Supercluster, with 17 out of 18 at $z > 0.5$. Hence the Supergalactic hypothesis fails the fourth test for all of 18 long τ_{lag} GRBs.

Moreover, if we check the whole *Swift* GRB catalog (with long and short τ_{lag} values), it is easy to see that only one of all the GRBs (GRB980425) with reported spectroscopic redshift are close enough to be in our Local Supercluster. The lack of low redshift GRBs in the catalog also indicates that it is impossible to have a large fraction of long τ_{lag} of GRBs in Local Supercluster.

4.1.5 Implications

The Local Supercluster hypothesis strongly failed all of our four tests. Although some small fraction of long τ_{lag} GRBs can still be local (e.g. GRB980425, GRB830801), our analysis on *Swift* data puts a limit of $< 5\%$ on the fraction of long τ_{lag} GRBs to be in our Local Supercluster.

Both the results of Norris (2002) and Foley et al. (2008) show a tendency of concentration towards the Supergalactic plane (with a significance of $|Q| = 2.5\sigma_Q$ in both cases), which is not significantly convincing. Given that BATSE positions have had many selections of GRBs examined for anisotropies in many directions (Briggs et al., 1996), with this large number of trials, we can expect that some will be significant at this level.

From our analysis, only a small fraction of long τ_{lag} GRBs (less than one out of eighteen or so) could be in the Local Supercluster. Hence, the rate of long τ_{lag} GRBs in the Local Supercluster is greatly smaller than what has been reported by Norris (2003), and should not be included in the calculation of LIGO's detection rate.

From Table 4.1 we see that redshifts for these long τ_{lag} GRBs ($< z >= 1.61$) are not greatly lower than for other GRBs ($< z > \sim 2.3$). From the logic that long τ_{lag} corresponds

with low luminosity, one might be curious as to how we can detect a $\tau_{lag} > 1$ s GRB at redshift as high as $z = 3$? GRB980425 is an example of long τ_{lag} and low redshift ($z \sim 0.008$) GRB, and it is *very* under-luminous (with its γ-ray peak luminosity $L = 5.5 \pm 0.7 \times 10^{46}\ erg\ s^{-1}$ according to Galama et al. (1998)). Of course if we put GRB980425 to the redshift of $z = 3$, its luminosity distance will be increasing by a factor of ~ 730, and its peak flux will be decreasing by a factor of 5.3×10^5. With such a low peak flux, we will definitely not be able to detect it. However, GRB980425 is not a typical GRB. Its energy is much lower than a 'normal' GRB, and it falls far below the $\tau_{lag} - L$ relation curve by a factor of several hundred. GRB980425 might represent a subclass of long GRBs with long τ_{lag}, soft spectrum and low luminosity, as suggested by Norris (2002), but with only one example, it is unreasonable for us to take all long τ_{lag} GRBs as ultra-low luminosity bursts.

Consider a 'normal' long GRB that has $\tau_{lag} = 1$ s and redshift $z = 3$. Its $\tau_{lag,rest}$ in the GRB rest frame would be 0.25 s. Assuming that it fits well with the $\tau_{lag} - L$ relation from Table 2.1, its luminosity value L would be 8.40×10^{51} erg s^{-1}. From the concordance cosmological model (Equation (3.6)), the luminosity distance d_L at a given redshift is calculated, with $H_0 = 72$ km s^{-1} Mpc^{-1}, $c = 3 \times 10^5$ km s^{-2}, $\Omega_M = 0.27$ and $\Omega_\Lambda = 0.73$. The luminosity distance for $z = 3$ is $d_L \sim 2.5 \times 10^4$ Mpc. Then from the inverse square law for light, $P = L/(4\pi d_L^2)$, the bolometric peak flux would be $P_{bolo} = 1.12 \times 10^{-7}$ erg cm^{-2} s^{-1}. From the luminosity and the $E_{peak} - L$ relation from Table 2.1, a low E_{peak} value $E_{peak} \sim 57$ keV can be adopted. From the E_{peak} and average values of the low-energy power law index $\alpha = -1.1$ and high-energy power law index $\beta = -2.2$ (Band et al., 1993), a peak flux value in the energy range 15 keV to 150 keV can be calculated, with the result of $P = 4.93 \times 10^{-8}$ erg cm^{-2} s^{-1}, which is ~ 0.54 ph cm^{-2} s^{-1}. It is significantly higher than the trigger threshold of *Swift*. As a result, there is no doubt that we can detect long τ_{lag} GRBs at a high redshift (z=3). Indeed, the long τ_{lag} GRBs at $z > 1$ are consistent with the unbroken $\tau_{lag} - L$ relation. Thus, it appears that the ultra-low luminosity 'class' of bursts is quite rare (roughly fewer

than one-in-eighteen), and the usual $L \propto \tau_{lag}^{-1}$ relation should be used for normal long τ_{lag} bursts with reasonable confidence.

4.2 GRB Luminosity Function Evolution

Another important application from my redshift catalog and catalog of luminosity indicators is the evaluation of the luminosity function evolution. A luminosity function is a measure of the number of objects per unit luminosity, and it is therefore connected with the energy budget and the physical parameters determining the emission mechanism. As many GRBs (especially long GRBs) are associated with star-forming regions according to observations, and long GRBs are generated from the collapse of fast-rotating massive stars according to the current model, the measurement of GRB luminosity function will help us not only in understanding GRBs themselves, but also in other astrophysical problems, e.g. the massive star formation rate at high redshifts. One of the questions in the GRBs luminosity function studies is whether the luminosity function varies with redshift, for which a test of correlation between luminosity and redshift should be performed. With our catalog, we have redshift values for all *Swift* long GRBs calculated, with or without a spectroscopic redshift.

With our catalog, we have a bivariate GRB distribution of luminosity and redshift $\Psi(L, z)$. An estimation of $\Psi(L)$ depending on z would be an measurement of the luminosity function evolution. In Fenimore & Ramirez-Ruiz (2000), an evaluation of the luminosity function evolution was made using the luminosity and redshift values calculated from the L-V relation. They first assumed the independence between variables L and z, and then constructed z-L bins which are parallel to the L and z axis. A luminosity function $\Psi(L)$ was estimated within each redshift bin, and an evolution function of $\Psi(L)$ was found, shown as $\rho(z) \propto (1+z)^{3.3\pm0.3}$. However, this evaluation is based on the assumption of 'no luminosity function evolution'. As a result, although the result proved that there is evolution of luminosity function, the exact function form is not well evaluated.

There is a better statistical method to evaluate a strongly truncated sample (by the flux threshold of *Swift*), which was proposed by Efron & Petrosian (1992). A few tests have been done with this method, as applied to redshift surveys. In Lloyd-Ronning et al. (2002), this method was used for the specific problem of luminosity function evolution. However, the redshift and luminosity values that Lloyd-Ronning et al. (2002) used were totally calculated from the Luminosity-Variability relation, which has been shown to be the least-constrained luminosity relation among all the proved ones, and the data sample they have been using is all BATSE GRBs. Now with a completely independent *Swift* sample and a much better calculated redshift catalog (with accurately measured uncertainties on each redshift), we will be able to make an improved, independent test of the luminosity function evolution.

The idea of this method is simple. If there is no evolution of the GRB luminosity function, for an nontruncated data sample (GRBs), the GRBs would be uniformly distributed in the two dimensional L-z space. If there is a truncation function of the flux threshold, for each given redshift, GRBs with luminosity smaller than some specific value (defined by the truncation function, say L(z, truncated)) will not be detected. If we separate the variables z and L, for a given redshift z_i, all GRBs with L larger than L(z, truncated) would have the same possibility to be with redshift of z_i, and the luminosity of the real GRB with redshift z_i would tend to be near the median value of all possible luminosity values. The offset between the real luminosity value and the median value of all possible luminosity values varies, however, for a large sample of hundreds of GRBs, the weighted average of the offset would be near zero. A few functions and variables are used to evaluate the offset, the details of which are referred to Efron & Petrosian (1992).

This method provides an effective evaluation of whether there is an evolution of the luminosity function. To exactly measure the function of the evolution, we need to construct a new variable $\Psi(L, Z) = \rho(Z)\phi(L/\lambda(Z))$, where $Z = (1 + z)$, $\phi(L/\lambda(Z))$ is the luminosity function and $\lambda(Z)$ parameterizes the correlation between L and (1+z). Assuming $\lambda(Z)$

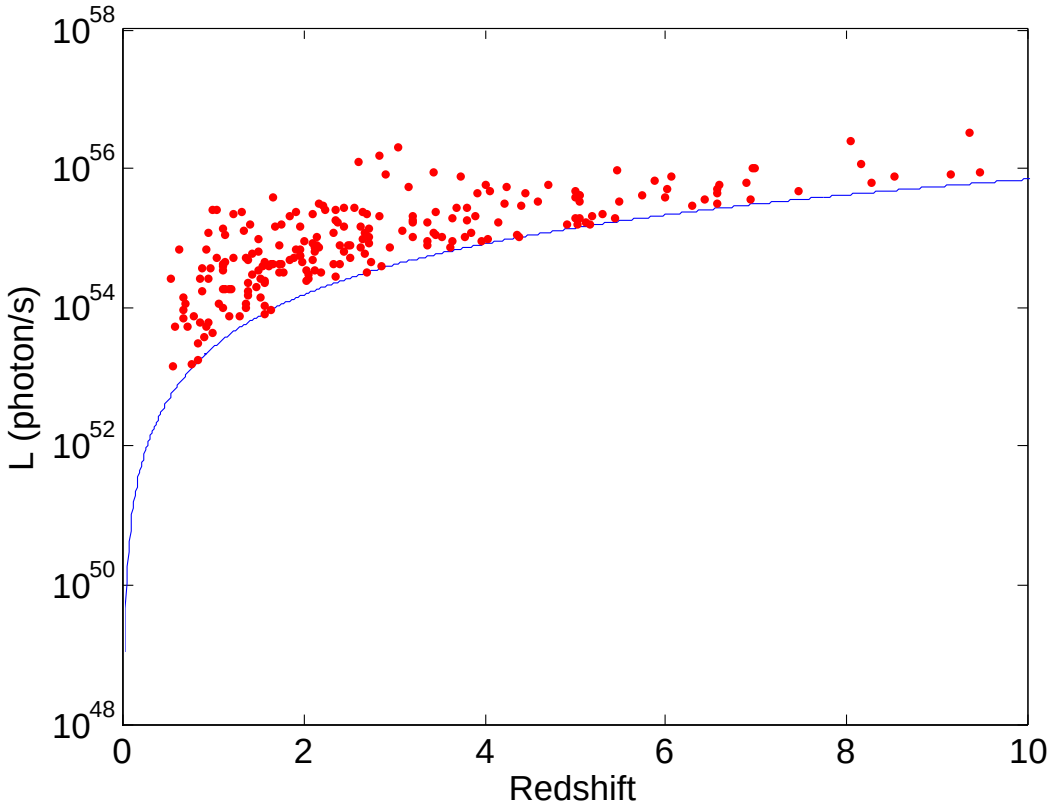

Figure 4.2 Luminosity function evolution with a strong truncation. The L_{limit} is the truncation caused by the flux threshold of our sample, and each of the red solid dots is a GRB with a measured redshift z and luminosity L. An evolution is found from the statistic method proposed by Efron & Petrosian (1992), and the function for the evolution is evaluated to be $\lambda(Z) = (1+z)^{1.7\pm0.3}$.

can be written as $\lambda(Z) = (1+z)^{\alpha}$, by varying the value of α, we will be able to find a $\Psi(L, Z)$, which shows no correlation between redshift z and luminosity L, and this $\lambda(Z)$ with $\lambda(Z) = (1+z)^{\alpha}$ would be the evolution function we are trying to measure. The details of this measurement are in to Lloyd-Ronning et al. (2002).

By running this method on our *Swift* sample of GRBs, we are able to evaluate the α value with no correlation between Z and L for variable $\Psi(L, Z)$. The corresponding evolution function is $\lambda(Z) = (1+z)^{1.7\pm0.3}$, which agrees well with the result of Lloyd-Ronning et al. (2002), $\lambda(Z) = (1+z)^{1.4\pm0.2}$, to within error bars. Our result confirms the claim of Fenimore

& Ramirez-Ruiz (2000) and Lloyd-Ronning et al. (2002) that the evolution of the luminosity function with redshift exists, and our result with an improved and independent data set confirms the result of Lloyd-Ronning et al. (2002) at the $1 - \sigma$ level.

5. Conclusions

We developed a method to calculate the redshifts for long GRBs, using their light curves and spectra. We applied our method to bursts with known spectroscopic redshifts, detected by BATSE, HETE, Konus and *Swift*. By comparing our calculated redshifts with their spectroscopic redshifts, we are able to examine the accuracy of our method.

We compared each of the luminosity relations for pre-*Swift* and *Swift* bursts by making a F-test. With the F values close to unity, we have significant evidence against any claim that the relations are caused by the detection threshold effects or any other artificial effects of the instruments.

We compared our results with the spectroscopic redshifts. We find that our z_{best} are not biased (with the average value of $log_{10}(z_{best}/z_{spec})$ equal to 0.01), and our reported $1-\sigma$ error bars are good (with $\chi^2_{red} = 0.86$, and 70% of the z_{spec} fall into the $1-\sigma$ region of z_{best}). Our accuracy on the redshifts are not as accurate as those from spectroscopy, yet nevertheless have a reasonable accuracy for demographical and statistical studies, with the RMS of $log_{10}(z_{best}/z_{spec})$ is 0.26. The RMS value is about twice what was found in Schaefer (2007). One of the reasons is, in Schaefer (2007), the accuracy is calculated assuming a known z_{spec}, and in this paper, as we are treating the unknown-redshift case, so extra degrees of freedom have been brought in the calculation, which caused the accuracy to get worse by about a factor of 2. Another reason is that the large RMS is dominated by faint and noisy bursts, and for a subsample with $\sigma_{z_{minus}/z_{best}} < 0.5$ and $\sigma_{z_{plus}/z_{best}} < 1$, we get the RMS of $[log(z_{best}/z_{spec})]$ of 0.19, which is much smaller. As our z_{best} are from the light curves, the spectra and the concordance cosmological model, it is independent of the spectroscopic redshift. As a result, our method can be applied to all long GRBs.

For *Swift* bursts, as we are measuring over a relatively narrow energy band (15 keV - 350

keV), the uncertainties in the calculation of peak energy E_{peak} is large, and it becomes one of the main restrictions on our accuracy.

We applied the same method to all the *Swift* long bursts. This method has been developed and tested on bursts with spectroscopic redshift in Xiao & Schaefer (2009). We calculated the values for all the luminosity indicators and our z_{best} with $1-\sigma$ uncertainties for 263 *Swift* long GRBs (out of a total number of 277 in our sample). By combining z_{best} with the spectroscopic redshifts and the photometric redshift limits from multi-wavelength detections of UVOT and some ground telescopes, a nearly complete *Swift* GRB redshift catalog is constructed.

We compared the redshift distribution for those bursts with spectroscopic redshift (z_{spec}) between our redshift z_{best} and the reported z_{spec}. The Kolmogorov-Smirnov test result shows a maximum difference of 0.15 and p value of 0.30. The differences between these two distributions mostly appeared in the high redshift tail in our redshift distribution. The existence of the high redshift tail is caused by the intrinsic distribution of GRB redshifts, and that our uncertainties are not following the distributions. A Monte Carlo simulation is made, with a difference between the intrinsic distribution and noise the result showing the same high redshift tail.

From these values, we made a redshift distribution plot for all the *Swift* long GRBs. A de-convolution process was taken to get rid of the noise effect on the high redshift tail, and an intrinsic *Swift* GRB redshift distribution was made. The distribution shows a significant offset from the distribution of z_{spec}, especially in the high redshift region. About 10% of all *Swift* GRBs shows a redshift larger than 5. This percentage is consistent with what is predicted by Bromm & Loeb (2006).

Our program was also imported in the *Fermi* GBM data analysis software RMFIT. The combination of our temporal analysis and the original spectral analysis as well as our redshift calculation works well. However, due to the constraint of the GRB localization and the long

time delay of the *Fermi* pipeline product, we are not able to send out reliable fast alerts on high redshift GRBs. However, the program has been tested on a few *Fermi* GRBs with known spectroscopic redshift, with the results showing that the accuracy of our redshift values is reasonable, but not as high as expected to be used in the rapid high redshift alert.

Our catalog is then used to test the hypothesis that a large fraction of long-lag GRBs are from the Local Supercluster. With four independent test failed, this hypothesis is disproved. Hence these long-lag GRBs can not be counted in the calculation of LIGO detection rates. An explanation of why we can detect long-lag GRBs at high redshift is presented.

Our catalog is also used to make an evaluation of the GRB luminosity function evolution. By using a non-parametric statistic method on the truncated sample of GRBs, we find a significant evolution of the GRB luminosity function at different redshift. A power law function of z is then constructed to parameterize the evolution. Our result is consistent with the result of Lloyd-Ronning et al. (2002) using the BATSE sample and luminosity-Variability relation only.

Bibliography

Amati, L. et al. 2002, A&A, 390, 81.

Amati, L. et al. 2007, GCN 6017.

Aurière, M. 1982, A&A, 109, 301.

Bagoly, Z., Balázs, L. G., Horváth, I., Kelemen, J., Mészáros, A., Veres, P., & Tusnády, G., 2008, in AIP Conf. Proc. 1065, 2008 Nanjing Gamma-Ray Burst Conference, ed. Y. F. Huang, Z.-G. Dai, & B. Zhang (Melville, NY: AIP), 119.

Band, D. et al. 1993, ApJ, 413, 281.

Band, D. L. 1997, ApJ, 486, 928.

Barbier, L. et al. 2006a, GCN 4518.

Barbier, L. et al. 2008, GCN 6810.

Barthelmy, S. D. et al. 2007, GCN 6522.

Barthelmy, S. D. et al. 2007, GCN 6811.

Barthelmy, S. D. et al. 2008, GCN 7606.

Bellm, E. et al. 2006, GCN 5867.

Berger, E. 2006, GCN 5962.

Berger, E. et al. 2005a, GCN 3088.

Berger, E. et al. 2005b, GCN 3368.

Berger, E. et al. 2005c, GCN 3088.

Berger, E. et al. 2006a, GCN 4815.

Berger, E. et al. 2006b, GCN 5568.

Berger, E., Fox, D. B. & Cucchiara, A. 2007, GCN 6470.

Berger, E. & Gladders, M. 2006, GCN 5170.

Berger, E. & Shin, M.-S. 2005, GCN 5283.

Berger, E. & Rauch, M., 2008, GCN 8542.

Bloom, J. S., Chen, H.-W., Perley, D. A. & Pollack, L. 2007, GCN 6568.

Bloom, J. S., Perley, D. A. & Chen, H. W. 2006, GCN 5826.

Blustin, A. J. et al. 2005, GCN 3717.

Blustin, A. J. et al. 2005, GCN 3733.

Blustin, A. J. et al. 2005, GCN 4107.

Blustin, A. J. et al. 2006b, GCN 4824.

Blustin, A. J. et al. 2006c, GCN 5228.

Blustin, A. J. et al. 2006, GCN 4482.

Boyd, P. et al. 2006b, GCN 5357.

Boyd, P. et al. 2006, GCN 4722.

Breeevld, A. A. et al. 2008, GCN 7360.

Breeveld, A. A. et al. 2007, GCN 7028.

Briggs, M. S. et al. 1996, ApJ, 459, 40.

Bromm, V. & Loeb, A. 2006, ApJ, 642, 382.

Brown, P. et al. 2005, GCN 3516.

Brown, P. et al. 2006a, GCN 5172.

Brown, P. et al. 2006b, GCN 5565.

Butler, N. R. et al. 2007, ApJ, 671, 656.

Campana, S., Guidorzi, C., Tagliaferri, G., Chincarini, G., Moretti, A., Rizzuto, D., & Romano, P. 2007, A&A, 472, 395.

Castro-Tirado, A. J. et al. 2006, GCN 5218.

Cenko, S. B. et al. 2005, GCN 3542.

Cenko, S. B. et al. 2006a, ApJ, 652, 490.

Cenko, S. B. et al. 2006b, GCN 5155.

Cenko, S. B. et al. 2006c, GCN 5529.

Cenko, S. B. et al. 2007a, GCN 6322.

Cenko, S. B. et al. 2007b, GCN 6888.

Cenko, S. B. et al. 2007c, GCN 6895.

Cenko, S. B. et al. 2009a, GCN 9053.

Cenko, S. B. et al. 2009b, GCN 9518.

Chen, H. W. et al. 2005, GCN 3709.

Chen, Y. C. et al. 2006, GCN 5797.

Chester, M. et al. 2005, GCN 3838.

Chornock, R. et al. 2009a, GCN 9028.

Chornock, R. et al. 2009b, GCN 9243.

Cobb, B. E. et al. 2005, GCN 3104.

Collazzi, A. C. & Schaefer, B. E., 2008, ApJ, 688, 456.

Costa, E. et al. 1997, Nature, 387, 783.

Covino, S. et al. 2005, GCN 3657.

Cucchiara, A. et al. 2006a, GCN 4729.

Cucchiara, A. et al. 2006b, GCN 5052.

Cucchiara, A. et al. 2006c, GCN 4674.

Cucchiara, A. et al. 2007a, GCN 6083.

Cucchiara, A. et al. 2007b, GCN 7124.

Cucchiara, A. et al. 2007c, GCN 6419.

Cucchiara, A. et al. 2008, GCN 8713.

Curran, et al. 2007, MNRAS, 381, L65.

Dai, X. et al. 2008, ApJ, 682, L77.

Dai, X. & Stanek, Z. 2006, GCN 5147.

D'Avanzo, P. et al. 2008, GCN 7997.

De Pasquale, M. et al. 2005, GCN 3960.

De Pasquale, M. et al. 2006a, GCN 5035.

De Pasquale, M. et al. 2006b, GCN 5130.

De Pasquale, M. et al. 2007a, GCN 6557.

De Pasquale, M. et al. 2007b, GCN 6650.

De Pasquale, M. et al. 2007, MNRAS, 377, 1638.

De Ugarte Postigo, A. et al. 2008, GCN 7650.

de Ugarte Postigo, A., Jakobsson, P., Malesani, D., Fynbo, J. P. U., Simpson, E. & Barros, S. 2009, GCN 8766.

de Vaucouleurs, G. 1953, AJ, 58, 30.

de Vaucouleurs, G. 1958, AJ, 63, 253.

Dupre, A. K. et al. 2006, GCN 4969.

Efron, B & Petrosian, V. 1992, ApJ, 399, 345.

Eichler, D. & Levinson, A. 2004, ApJ, 614, L13.

Fatkhullin, T. A. et al. 2008, GCN 7534.

Fenimore, E. E. & Ramirez-Ruiz, E. 2000, astro-ph/0004176.

Fenimore, E. et al. 2007, GCN 6237.

Fenimore, E. et al. 2008, GCN 7726.

Ferrero, P. et al. 2008, A&A, 497, 729.

Filgas, R. et al. 2008, GCN 7747.

Firmani, C., Ghisellini, G., Avila-Reese, V., & Ghirlanda, G., 2006, MNRAS, 370, 185.

Foley, R. J. et al. 2005, GCN 3483.

Foley, S., McGlynn, S., Hanlon, L., McBreen, S. & McBreen, B. 2008, A & A, 484, 143.

Frail, D. et al. 1997, Nature, 389, 261.

Frail, D. et al. 1998, Nature, 395, 663.

Fugazza, D. et al. 2005, GCN 3948.

Fugazza, D. et al. 2006, GCN 5513.

Fynbo, J. P. U. et al. 2005a, GCN 3176.

Fynbo, J. P. U. et al. 2005b, GCN 3874.

Fynbo, J. P. U. et al. 2006a, GCN 4692.

Fynbo, J. P. U. et al. 2006b, GCN 5651.

Fynbo, J. P. U. et al. 2006c, GCN 5809.

Fynbo, J. P. U. et al. 2008a, GCN 7797.

Fynbo, J. P. U. et al. 2008b, GCN 7949.

Fynbo, J. P. U. et al. 2008c, GCN 7770.

Fynbo, J. P. U. et al. 2008d, GCN 8254.

Galama, T. J., et al. 1998, Nature, 395, 670.

Gehrels, N. et al. 2004, ApJ, 611, 1005.

Gehrels, N. et al. 2004, ApJ, 611, 1005.

Ghirlanda, G., Ghisellini, G., & Lazzati, D. 2004, ApJ, 616, 331.

Ghirlanda, G., Nava, L., Ghisellini, G. & Firmani, C. 2007, A&A, 466, 127.

Golenetskii, S. et al. 2005a, GCN 3152.

Golenetskii, S. et al. 2005b, GCN 3619.

Golenetskii, S. et al. 2005c, GCN 3640.

Golenetskii, S. et al. 2005d, GCN 4078.

Golenetskii, S. et al. 2005e, GCN 4238.

Golenetskii, S. et al. 2006a, GCN 4439.

Golenetskii, S. et al. 2006b, GCN 4542.

Golenetskii, S. et al. 2006c, GCN 4989.

Golenetskii, S. et al. 2006d, GCN 5113.

Golenetskii, S. et al. 2006e, GCN 5446.

Golenetskii, S. et al. 2006f, GCN 5460.

Golenetskii, S. et al. 2006g, GCN 5518.

Golenetskii, S. et al. 2006h, GCN 5722.

Golenetskii, S. et al. 2006i, GCN 5748.

Golenetskii, S. et al. 2006j, GCN 5837.

Golenetskii, S. et al. 2006k, GCN 5984.

Golenetskii, S. et al. 2007a, GCN 6124.

Golenetskii, S. et al. 2007b, GCN 6230.

Golenetskii, S. et al. 2007c, GCN 6344.

Golenetskii, S. et al. 2007d, GCN 6459.

Golenetskii, S. et al. 2007e, GCN 6798.

Golenetskii, S. et al. 2007f, GCN 6849.

Golenetskii, S. et al. 2007g, GCN 6879.

Golenetskii, S. et al. 2007h, GCN 6960.

Golenetskii, S. et al. 2007i, GCN 7114.

Golenetskii, S. et al. 2008a, GCN 7482.

Golenetskii, S. et al. 2008b, GCN 7487.

Golenetskii, S. et al. 2008c, GCN 7548.

Golenetskii, S. et al. 2008d, GCN 7589.

Golenetskii, S. et al. 2008e, GCN 7784.

Golenetskii, S. et al. 2008f, GCN 7812.

Golenetskii, S. et al. 2008g, GCN 7854.

Golenetskii, S. et al. 2008h, GCN 7862.

Golenetskii, S. et al. 2008i, GCN 7884.

Golenetskii, S. et al. 2008j, GCN 7983.

Golenetskii, S. et al. 2008k, GCN 7995.

Graham, J. F. et al. 2007, GCN 6836.

Grazian, A. et al. 2006, GCN 4545.

Greco, G., Bartolini, C., Guarnieri, A., Piccioni, A., Pizzichini, G., Bernabei, S., & Marinoni, S., 2005, GCN 3319.

Grupe, D. et al. 2006a, ApJ, 645, 464.

Grupe, D. et al. 2006b, GCN 5432.

Grupe, D. et al. 2007, ApJ, 662, 443.

Guidorzi, C. et al. 2007, A&A, 463, 539.

Halpern, J. P. & Mirabal, N. et al. 2006, GCN 5982.

Halpern, J. P. & Mirabal, N. et al. 2007, GCN 6082. .

Hill, G., Prochaska, J. X., Fox, D., Schaefer, B. & Reed, M., 2005, GCN 4255.

Holland, S. et al. 2005a, GCN 3475.

Holland, S. et al. 2005b, GCN 4235.

Holland, S. et al. 2005c, GCN 4300.

Holland, S. et al. 2006b, GCN 5116.

Holland, S. et al. 2006c, GCN 5745.

Holland, S. et al. 2006, GCN 5820.

Holland, S. et al. 2007, GCN 6466.

Holland, S. T. et al. 2008a, GCN 7496.

Holland, S. T. et al. 2008b, GCN 7497.

Hoversten, E. A. et al. 2008, GCN 7398.

Hunsberger, S. D. et al. 2005, GCN 4041.

Hurkett, C. P. et al. 2006, MNRAS, 368, 1101.

Iizuka, R. et al. 2007, GCN 6886.

Immler, S. et al. 2007, GCN 6336.

Jakobsson, P. et al. 2005, GCN 4029.

Jakobsson, P. et al. 2006a, AIPC, 836, 552.

Jakobsson, P. et al. 2006b, GCN 5298.

Jakobsson, P. et al. 2006c, GCN 5320.

Jakobsson, P. et al. 2006d, A&A, 447, 897. .

Jakobsson, P. et al. 2007a, GCN 6283.

Jakobsson, P. et al. 2007c, GCN 7117.

Jakobsson, P. et al. 2008a, GCN 7286.

Jakobsson, P. et al. 2008b, GCN 7757.

Jakobsson, P. et al. 2008c, GCN 7832.

Jakobsson, P., Malesani, D., Fynbo, J. P. U., Hjorth, J. & Milvang-Jensen, B., 2008d, in AIP Conf. Proc. 1133, Gamma-Ray Bursts, 6th GRB Huntsville Symposium, ed. C. Meegan, N. Gehrels & C. Kouveliotou (Huntsville, AL: AIP), 455.

Jakobsson, P., Vreeswijk, P. M., Hjorth, J., Malesani, D., Fynbo, J. P. U. & Thoene, C. C. 2007b, GCN 6952.

Jaunsen, A. O. et al. 2007a, GCN 6010.

Jaunsen, A. O. et al. 2007b, GCN 6216.

Jaunsen, A. O. et al. 2008, ApJ, 681, 453.

Jensen, B. L. et al. 2005, GCN 3809.

Kaneko, Y., Preece, R. D., Briggs, M. S., Paciesas, W. S., Meegan, C. A., & Band, D. L., 2006, ApJSupp, 166, 298.

Kann, D. A. et al. 2007, GCN 6935.

Kann, D. A., Laux, U. & Ertel, S. 2008, GCN 7865.

Karachentsev, I. D. & Makarov, D. A. 1996, AJ, 111, 794.

Kawai, N. et al. 2005, GCN 3937.

Kelson, D. & Berger, E. 2005, GCN 3101.

Kiziloglu, U. et al. 2006, GCN 5618.

Klebesadel R, Strong I, & Olson R. 1973. ApJ. 182, L85.

Klotz, A., Boer M. & Atteia J. L., 2007, GCN 6787.

Kocevski, D., Perley, D. A., & Modjaz, M. 2007, GCN 6885.

Krimm, H. 2005, private communication.

Krimm, H. 2006, private communication.

Krimm, H. A. et al. 2007, ApJ, 665, 554.

Krimm, H. et al. 2006a, in Gamma-Ray Bursts in the Swift Era, eds S. S. Holt, N. Gehrels, and J. A. Nousek (AIP Conf. Proc. 836), pp. 145-148.

Krimm, H. et al. 2006b, GCN 4864.

Krimm, H. et al. 2008, GCN 7325.

Krimm, H. et al. 2009, ApJ, 704, 1405.

Kuin, N. P. M. et al. 2007, GCN 6238. .

Kuin, N. P. M. et al. 2008a, GCN 7552.

Kuin, N. P. M. et al. 2008b, GCN 7808.

Kuin, N. P. M. et al. 2008c, GCN 7844.

Lahav, O., Santiago, B. X., Webster, A. M., Strauss, M. A., Davis, M., Dressler, A., & Huchra, J. P. 2000, MNRAS, 312, 166.

Landsman, W. B. et al. 2008a, GCN 7660.

Landsman, W. B. et al. 2008b, GCN 7965.

Landsman, W. et al. 2007a, GCN 6504.

Landsman, W. et al. 2007b, GCN 6591.

Landsman, W. & Pagani, C. et al. 2007, GCN 6378.

Landsman, W. & Stamatikos, W. et al. 2007, GCN 6340.

Ledoux, C. et al. 2006, GCN 5237.

Ledoux, C. et al. 2006. GCN 5247.

Ledoux, C. et al. 2007, GCN 7023.

Levinson, A. & Eichler, D. 2005, ApJ, 629, L13.

Li, L. 2007, MNRAS, 374, L20.

Li, W., Jha, S., Filippenko, A. V., Bloom, J. S., Pooley, D., Foley, R. J., & Perley, D. A. 2005, GCN 4095.

Liang, E.-W., Racusin, J. L., Zhang, B., Zhang, B.-B., &Burrows, D. N. 2008, ApJ, 675, 528.

Liang, E.-W., Zhang, B.-B., Stamatikos, M., Zhang, B., Norris, J., Gehrels, N., Zhang, J. & Dai, Z.-G., 2006, ApJ, 653, L81.

Lin, H. et al. 1996, ApJ, 464, 60.

Lloyd-Ronning, N. M., Fryer, C. L. & Ramirez-Ruiz, E. 2002, ApJ, 574, 554.

Malesani, D. et al. 2006, GCN 5422.

Malesani, D. et al. 2007, GCN 6700.

Malesani, D. et al. 2008, GCN 7544.

Malesani, D., Jakobsson, P., Fynbo, J. P. U., Hjorth, J. & Vreeswijk, P. M. 2007, GCN 6651.

Marshall, F. E. et al. 2006, GCN 5833.

Marshall, F. E. et al. 2007a, GCN 6213.

Marshall, F. E. et al. 2007b, GCN 6676.

Marshall, F. E. & Grupe, D. et al. 2007, GCN 6392.

Marshall, F. et al. 2006, GCN 4779.

Masetti, N. et al. 2008, GCN 4803.

Mason, K. et al. 2005, GCN 3037.

McGowan, K. et al. 2005, GCN 3745.

McLean, K. et al. 2008, GCN 7306.

Melandri, A. et al. 2006a, GCN 4539.

Melandri, A. et al. 2006b, GCN 5103.

Melandri, A. et al. 2006c, GCN 5804.

Mirabal, N. et al. 2006, GCN 4792.

Misra, K. et al. 2007, GCN 6840.

Modjaz, M. et al. 2006, ApJ, 645, L21.

Molinari, E. et al. 2007, A&A, 469, L13.

Morgan, A. N. et al. 2006, GCN 5553.

Mundell, C. G. et al. 2006, GCN 4726.

Nakagawa, Y. et al. 2005, GCN 3053.

Norris, J. P. 2002, ApJ, 579, 386.

Norris, J. P. 2003, in AIP Conf. Ser. 686, The Astrophysics of Gravitational Wave Sources, ed. J. M. Centrella (College Park: AIP), 74.

Norris, J. P. & Bonnell, J. T. 2006, ApJ, 643, 266.

Norris, J. P., Marani, G. F., & Bonnell, J. T. 2000, ApJ, 534, 248.

Norris, J. P., Share, G. H., Messina, D. C., Matz, M., Kouveliotou, C., Dennis, B. R., Desai, U. D. & Cline, T. L. 1986, Adv. Space Rev., 6, 19.

Oates, S. R. et al. 2006a, GCN 5243.

Oates, S. R. et al. 2006b, GCN 5519.

Oates, S. R. et al. 2007, GCN 6291.

Oates, S. R. et al. 2008a, GCN 7253.

Oates, S. R. et al. 2008b, GCN 7592.

Oates, S. R. et al. 2008c, GCN 7607.

Oates, S. R. et al. 2008d, GCN 7611.

Oates, S. R. et al. 2008e, GCN 7693.

Ohno, M. & Sakamoto, T. et al. 2007, GCN 6638.

Ohno, M. & Tueller, J. et al. 2008, GCN 7630.

Page, et al. 2007, ApJ, 663, 1125.

Panaitescu, A. 2007, MNRAS, 380, 374.

Pandey, S. B. et al. 2006, GCN 5397.

Pavlenko, E. et al. 2005, GCN 3783.

Pellizza, L. J., et al. 2006, GCN 5269.

Perley, D. A., Chornock, R. & Bloom, J. S. 2008, GCN 7962.

Peterson, B. et al. 2006, GCN 5223.

Piranomonte, S. et al. 2006a, GCN 4520.

Piranomonte, S. et al. 2006b, GCN 5626.

Piranomonte, S. et al. 2007, GCN 6985.

Podsiadlowski, Ph., Mazzali, P. A., Nomoto, K., Lazzati, D. & Cappellaro, E. 2004, ApJ, 607, L17.

Poole, T. et al. 2005a, GCN 3596.

Poole, T. et al. 2005b, GCN 3698.

Poole, T. et al. 2005c, GCN 4263.

Poole, T. et al. 2006, GCN 5068.

Price, P. A. et al. 2003, ApJ, 589, 838.

Price, P. A. et al. 2006, GCN 5104.

Prochaska, J. X., Bloom, J. S., Wright, J. T., Butler, R. P., Chen, H. W., Vogt, S. S., & Marcy, G. W. 2005b, GCN 3833.

Prochaska, J. X. et al. 2007b, GCN 6864.

Prochaska, J. X. et al. 2008a, GCN 7388.

Prochaska, J. X. et al. 2008b, GCN 7849.

Prochaska, J.X., Thoene, C.C., Malesani, D., Fynbo, J.P.U. & Vreeswijk, P.M. 2007a, GCN 6698. .

Quimby, R. et al. 2006, GCN 4782.

Quimby, R., Fox, D., Hoeflich, P., Roman, B., & Wheeler, J. C. 2005, GCN 4221.

Ramya, S. et al. 2005, GCN 3774.

Riess, A. G., et al, 2004, ApJ, 607, 665.

Rees, M. J. & Mészáros, P. 2005, ApJ, 628, 847.

Rhoads, J. et al. 2005, GCN 3531.

Rol, E. et al. 2005, GCN 3186.

Rol, E. et al. 2006, GCN 5555.

Roming, P. et al. 2007, GCN 6009.

Ruiz-Velasco, A. E. et al. 2007, ApJ, 669, 1.

Rumyantsev, V. et al. 2005, GCN 4081.

Rykoff, et al. 2006, ApJ, 638, L5.

Sakamoto, T. et al. 2006, ApJ, 636, L73.

Sakamoto, T. et al. 2007, ApJS, 175, 179.

Sari, R., Piran, T, & Halpern, J. P., 1999, ApJ, 519, L17.

Schady, P. et al. 2005a, GCN 3280.

Schady, P. et al. 2005b, GCN 3880.

Schady, P. et al. 2006a, GCN 4978.

Schady, P. et al. 2006b, GCN 5294.

Schady, P. et al. 2006c, GCN 5296.

Schady, P. et al. 2006d, GCN 5719.

Schady, P. et al. 2006e, GCN 5861.

Schady, P. et al. 2006f, ApJ, 643, 276.

Schady, P. et al. 2007, MNRAS, 380, 1041.

Schady, P. et al. 2008, GCN 7858.

Schaefer, B. E. 2002, Gamma-Ray Bursts: The Brightest Explosions in the Universe (Harvard).

Schaefer, B. E. 2003a, ApJ, 583, L67.

Schaefer, B. E. 2003b, ApJ, 583, L71.

Schaefer, B. E. 2003b, ApJ, 583, L71.

Schaefer, B. E. 2004, ApJ, 602, 306.

Schaefer, B. E. 2007, ApJ, 660, 16.

Schaefer, B. E. & Collazzi, A. C. 2007, ApJ, 656, L53.

Schaefer, B. E., Deng, M. & Band, D. L. 2001, ApJ, 563, L123.

Schaefer, B. E. et al. 1994, ApJSupp, 92, 285.

Schmidt, B. & Mackie, G. et al. 2007, GCN 6325.

Soderberg, A., Berger, E. & Schmidt, B, 2006, IAUC, 6784.

Soderberg, A. M. et al. 2005, GCN 4186.

Stanek, K. Z. et al. 2003, ApJ, 591, L17.

Swan, H. et al. 2006, GCN 4568.

Rees, M. J. & Mészáros, P. 1992, MNRAS, 258, 41.

Rees, M. J. & Mészáros, P. 1994, ApJ, 430, L93.

Rees, M. J. & Mészáros, P. 2005, ApJ, 628, 847.

Tagliaferri, G. et al. 2005, A&A, 443, L1.

Tanvir, N. et al. 2009, Nature, in press, arXiv: astro-ph/0906.1577.

Thoene, C. C., Cia, A. D., Malesani, D. & Vreeswijk, P. M. 2008a, GCN 7587.

Thoene, C. C. et al. 2006a, GCN 5373.

Thoene, C. C. et al. 2006c, GCN 5812.

Thoene, C. C. et al. 2007a, GCN 6379.

Thoene, C. C. et al. 2007b, GCN 6499.

Thoene, C. C. et al. 2008b, GCN 7602.

Thoene, C. C. et al. 2008c, astro-ph/0806.1182.

Thoene, C. C., Jaunsen, A. O., Fynbo, J. P. U., Jakobsson, P. & Vreeswijk, P. M. 2007, GCN 6379.

Thoene, C. C., Perley, D. A. & Bloom, J. S. 2006b, GCN 6663.

Thoene, C. C., Perley, D. A., Cooke, J., Bloom, J. S., Chen, H.-W. & Barton, E. 2007c, GCN 6741.

Tully R. B. 1982, ApJ, 257, 389.

Tully, R. B. & Fisher, J. R. 1987, Atlas of Nearby Galaxies (Annales de Geophysique).

Uehara, T. et al. 2007, GCN 6396.

Uemura, M. et al. 2007, GCN 7037.

Updike, A. C. et al. 2007, GCN 6979.

Usov, V. V. 1992, Nature, 357, 472.

Usov, V. V. 1994, MNRAS, 267, 1035.

van Paradijs, J. et al. 1997, Nature, 386, 686.

Vaughan, S. et al. 2006, ApJ, 638, 920.

Vianello, G., Götz, D. & Mereghetti, S. 2009, A&A, 495, 1005.

Vreeswijk, P. et al. 2006, GCN 5535.

Vreeswijk, P. et al. 2008a, GCN 7444.

Vreeswijk, P. M. et al. 2008b, GCN 7601.

Ward, P. et al. 2008a, GCN 7941.

Ward, P. et al. 2008b, GCN 7996.

Wiersema, K. et al. 2008a, GCN 7517.

Wiersema, K. et al. 2008b, GCN 7818.

Williams, G. G. et al. 2007, GCN 6995.

Wozniak, P.R., Vestrand, W.T., Wren, J., White, R., & Evans, S., 2006, GCN 4474.

Wren, J. et al. 2005, GCN 3604.

Xiao, & Schaefer, B. E., 2009, ApJ, 707, 387.

Xiao, L. & Schaefer, B. E., 2010, to be submitted.

Xin, L. P. et al. 2008, GCN 7371.

Yamazaki, R., Ioka, K., & Nakamura, T. 2004, ApJ, 606, L33.

Yost, S. A. et al. 2007, ApJ, 657, 925.

Zhang, B., Zhang, B.-B., Liang, E.-W., Gehrels, N., Burrows, D. N., & Mészáros, P. 2007, ApJ, 655, L25.

Zhang, B-B, Liang, E-W, & Zhang, B, 2007, ApJ, 666, 1002.

Zhuchkov, R. et al. 2008, GCN 7803.

Appendix A

Letter of Permission

Before your article can be published in an American Astronomical Society (AAS) journal, we require you to grant and assign the entire copyright in it to the AAS. The copyright consists of all rights protected by the copyright laws of the United States and of all foreign countries, in all languages and forms of communication, including the right to furnish the article or the abstracts to abstracting and indexing services, and the right to republish the entire article in any format or medium. In return, the AAS grants to you the non-exclusive right of republication, subject only to your giving appropriate credit to the journal in which your article is published. This non-exclusive right of republication includes your right to allow reproduction of parts of your article wherever you wish, and permits you to post the published (PDF) version of your article on your personal web site.

(http://www.iop.org/EJ/journal/-page=extra.3/APJ)

Vita

Limin Xiao was born in Linqing, China, in March, 1986. She earned her bachelor's degree in applied physics in 2005 from University of Science and Technology of China. The degree of Doctor of Philosophy will be awarded to Ms. Xiao at the August 2010 Commencement.